

R-10-59

The Greenland Analogue Project

Yearly Report 2009

Svensk Kärnbränslehantering AB

December 2010

Svensk Kärnbränslehantering AB

Swedish Nuclear Fuel
and Waste Management Co

Box 250, SE-101 24 Stockholm
Phone +46 8 459 84 00



ISSN 1402-3091

SKB R-10-59

The Greenland Analogue Project

Yearly Report 2009

Svensk Kärnbränslehantering AB

December 2010

Contents

1	Introduction	5
1.1	Overview of the GAP Sub-projects	7
2	Sub-project A activities 2009	9
2.1	Remote sensing: Overview	10
2.1.1	MODIS data	16
2.1.2	Preliminary results of NERC Airborne Research and Survey Facility LiDAR survey and analysis	22
2.2	Climate, Automatic Weather Station (AWS) and surface run-off mapping	26
2.2.1	Automatic weather station placement	27
2.2.2	Automatic weather station set-up	28
2.2.3	Observations	28
2.2.4	Modelling the mass balance budget	31
2.3	Geodetic quality GPS acquisition across the Russell Glacier Catchment	32
2.3.1	GPS data collection	32
2.3.2	Data processing	34
2.3.3	Results	35
2.3.4	Future processing	38
2.4	Geophysics: radar sounding trials (Spring 2009)	38
2.4.1	Radar data acquisition	38
2.4.2	Data processing	39
2.4.3	Results	40
2.4.4	Data acquisition issues	41
2.4.5	Ice thickness and bed elevation	43
2.4.6	Radar operations in 2010	44
2.5	Geophysics: passive seismic trials	45
2.5.1	2009 field trial program, equipment and installation	46
2.5.2	Preliminary data analysis	47
2.5.3	Future work	49
2.6	Tracer experiments	49
2.6.1	SF ₆ and dye tracing	49
2.6.2	Electronic tracers	51
3	Sub-project B activities 2009	53
3.1	Field reconnaissance of drilling sites	53
3.1.1	Ice penetrating radar	54
3.1.2	Surface drilling conditions	56
3.2	Radar reconnaissance of drilling sites	57
3.3	Transport of Alaskan drill	58
3.4	Deep-Ice hot water drill design and fabrication	58
3.5	Sensor design and testing	60
3.6	Modelling	61
3.7	Logistics planning	63
4	Sub-project C activities 2009	65
4.1	Objectives of diamond drilling and drilling site selection	68
4.2	Diamond drilling	69
4.2.1	Drilling technique	69
4.2.2	Flushing water	69
4.2.3	Supervision and monitoring measurements	70
4.2.4	Orientation of the boreholes based on geological mapping	70
4.2.5	Drilling schedule	73
4.3	Preliminary core loggings	78

4.4	Fracture mineral investigations	81
4.5	Instrumentation of DH-GAP01 and DH-GAP03	83
4.5.1	DH-GAP01 P/T/EC sensors	88
4.5.2	DH-GAP03 P/T/EC sensors	92
4.6	Distributed temperature sensing (DTS)	94
4.6.1	DTS measurements in DH-GAP01 and DH-GAP03	95
4.6.2	Modelling of the temperature observations in DH-GAP01 and DH-GAP03	99
4.7	Hydrogeochemistry of DH-GAP01 and surface waters	100
4.7.1	Preliminary preparations of DH-GAP01	100
4.7.2	Instrumentation of the Pingo Spring area	101
4.7.3	Sampling and analysing methods	102
4.7.4	Drill hole and surface water sampling	102
4.7.5	Drill hole DH-GAP01 and surface water results	104
4.8	Concluding remarks and the plans for 2010	106
4.9	Supporting modelling: Regional groundwater flow model	108
5	Summary	111
5.1	Sub-project A activities	111
5.2	Sub-project B activities	112
5.3	Sub-project C activities	113
6	References	115

1 Introduction

A deep geological repository for spent nuclear fuel needs to be designed to keep used nuclear fuel isolated from mankind and the environment for a million years. Within this time frame glacial conditions are expected in regions that have been glaciated in the past two to ten million years. Climate induced changes such as the growth of ice sheets and permafrost will influence and alter the ground surface and subsurface environment, including its hydrology, which may impact repository safety. Glaciation impact assessments have to-date used over-simplified models and conservative assumptions, for example in the representation of ice sheet hydrology, that do not reflect the complexity of natural systems and processes. This is largely due to lack of direct observations of such processes from existing ice sheets, which if more readily available could help reduce uncertainties and provide a strong scientific basis for the treatment of glacial impacts in safety assessments. Our current understanding of the hydrological, hydrogeological and hydrogeochemical processes associated with glacial cycles and their impact on the long-term performance of deep geological repositories for spent nuclear fuel will be significantly improved by studying a modern analogue.

To advance the understanding of processes associated with glaciation and their impact on the long-term performance of a deep geological repository, the Greenland Analogue Project (GAP), a four-year field and modelling study of the Greenland ice sheet and sub-surface conditions, has been initiated collaboratively by SKB, Posiva and NWMO. The study site encompasses a land terminus portion of the Greenland ice sheet east of Kangerlussuaq and is in many ways considered to be an appropriate analogue of the conditions that are expected to prevail in much of Canada and Fennoscandia during future glacial cycles. The project is planned to run from 2009 until 2012. The GAP will conduct the first *in situ* investigations of some of the parameters and processes needed to achieve a realistic understanding of how an ice sheet may impact a deep repository, and will provide measurements, observations and data that may significantly improve our safety assessments and risk analyses of glaciation scenarios. The project includes three sub-projects (A–C) with specific individual objectives, which collectively aim at contributing knowledge and input to the overall project aim. Figure 1-1 gives an overview of the different aspects of the three GAP sub-projects. The purpose of subdividing the project is that insights and data obtained from the different sub-projects constitute self-consistent data sets, which will be tested and implemented within the individual sub-projects. The overall idea is that the results of all sub-projects used and analyzed together will result in large synergistic effects for the understanding of hydrological conditions during glacial periods. That is also the reason why all sub-projects are performed within the same geographical area (see Figure 1-2). Finally, the GAP project will contribute to a three dimensional process understanding of a glaciated environment by obtaining an integrated view of ice sheet hydrology and groundwater flow and chemistry (Figure 1-1).

This report was produced by the GAP team members and presents the outcome of the activities within the GAP during 2009.

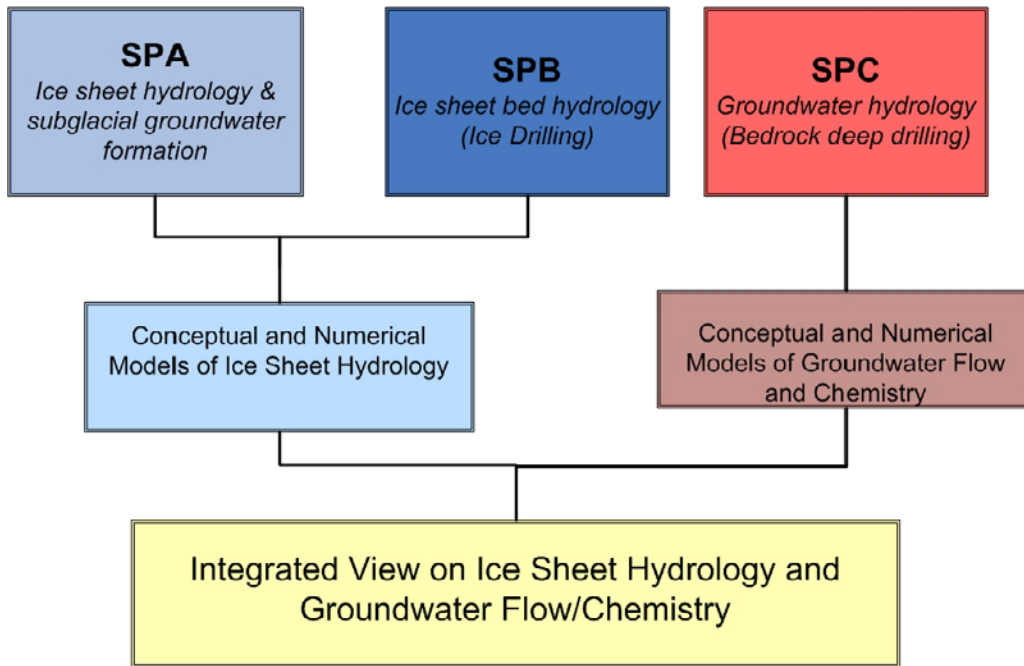


Figure 1-1. Chart illustrating how the expected output from the individual GAP sub-projects will feed into joint modelling work, which will aid and improve our current understanding of ice sheet hydrology and groundwater flow and chemistry, and how this impacts the safety of geological repositories for spent nuclear fuel. The obtained data from each sub-project will: 1) be incorporated into modelling work in the safety assessments carried out by SKB, NWMO and Posiva; and 2) will be utilised by the researchers involved in the complementary sub-projects.

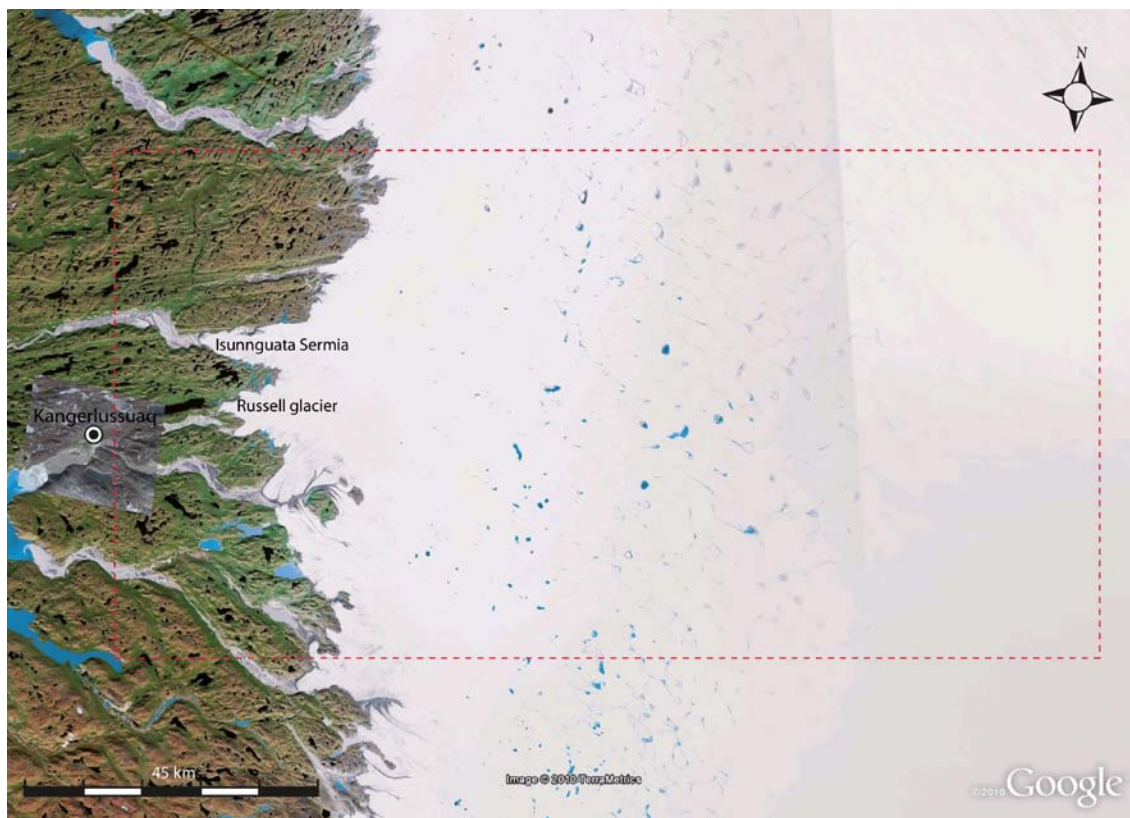


Figure 1-2. The area within the red dashed rectangle represents the GAP field area, where the three sub-projects carry out field investigations and monitoring work.

1.1 Overview of the GAP Sub-projects

Sub-project A (SPA): Ice sheet hydrology and subglacial groundwater formation

Sub-project A aims to improve the understanding of ice sheet hydrology in order to assess how an ice sheet impacts groundwater circulation and chemistry around a deep geological repository. The data collected in SPA will be utilised in numerical ice sheet flow and hydrological modelling. SPA focuses on *indirect* observations of the properties of the hydrological system at the base of the ice sheet and on what parts of the ice sheet that contribute water for groundwater infiltration. The latter includes quantification of ice sheet surface water production and how the water is routed from the surface to the base of the ice. This will be done through studies of ice velocity variations and surface melt water production. Main activities within SPA involve the installation and monitoring of GPS receivers and automatic weather stations on the ice sheet, and air borne/ and ground-based radar studies.

SPA contributors: Alun Hubbard (sub-project manager), Dirk van As, Jason Box, Sam Doyle, Andrew Fitzpatrick, Ian Joughin, Bernd Kulesa, Adrian Luckman, Adrian McCallum, Peter Nienow, Duncan Quincey, Rickard Pettersson, Chrisitan Helanow and Jemma Wadham.

Sub-project B (SPB): Subglacial ice sheet hydrology

SPB, like SPA, aims at improving the understanding of ice sheet hydrology. SPB aims at doing *direct* observations and measurements of the characteristics of the hydrological system at the base of the ice sheet. The data collected in SPB will be utilised in numerical ice sheet flow and hydrological modelling. The main activity for SPB is drilling through the ice sheet at a number of locations, where the ice sheet has been found to be wet-based from the radar surveys in SPA, in order to observe water pressures at the interface between the ice and bedrock. In addition to the ice drilling, collection of remote sensing data of surface conditions will be carried out. SPB is the core of the larger ice sheet hydrology and groundwater formation project (i.e. SPA and SPB) and will provide pioneering measurements of sub glacial water pressures beneath an ice sheet. This information will give important input to the conceptualization of hydraulic gradients during glacial conditions, including their spatial and temporal variation, for ground water models applicable in Fennoscandia and Canada. Data and results from SPA serve as necessary information for finding suitable locations for the ice drilling.

SPB contributors: Joel Harper (sub-project manager), Neil Humphrey, Jesse Johnson, Toby Meierbachtol, Douglas Brinkerhoff, Clair Landowski and Chris Cox.

Sub-project C (SPC): Bedrock drilling, hydrogeochemistry and hydrogeology

SPC aims at studying the penetration of glacial melt water into the bedrock, groundwater flow and the chemical composition of water when and if it reaches repository depth (around 500 m down in the bedrock). Main activities for SPC involve deep bedrock drilling in front of the ice sheet for subsequent down hole surveys and hydrogeological/hydrogeochemical instrumentation, sampling and monitoring. The deep drilling requires a detailed understanding of the geology of the area, including fracture frequencies and composition of rock types and hydrogeochemical information (i.e. chemistry of different water end-members). Before selecting a site for the deep drilling, test drilling of two shallow holes (100–300 metres) have been carried out. Besides giving important information on geology and hydrology, the test drilling has also given useful information on the permafrost extent. In order to study if taliks may act as discharge points for deep groundwater formed under the ice sheet, one of the test holes has been drilled into a talik. Data and understanding of the ice sheet hydrology from SPA provide necessary information for selecting the location of the deep borehole. Data on water formation and chemistry at the base of the ice sheet from SPB will be important when analyzing the results of SPC.

SPC contributors: Timo Ruskeeniemi (sub-project manager), Ilmo Kukkonen, Jyrki Liimatainen, Jon Engström, Shaun Frapé, Emily Henkemans, Mike Makahnouk, Barry Freifeld, Knud Erik Klint, Tomi Laakso, Anne Lehtinen, Ismo Aaltonen, KATI Oy, and Lillemor Claesson Liljedahl.

2 Sub-project A activities 2009

Since its inception, Sub-project A (SPA) of the Greenland Analogue Project (GAP) has been concerned with the direct and remote measurement of all processes linking melt forcing at the surface to the bed and its related ice motion (both vertical and horizontal) response across the Russell Glacier Catchment (RGC), a land-terminating outlet glacier draining the western margin of the Greenland Ice Sheet (GrIS) (Figure 2-1). The aim of SPA is to determine to what extent spatial and temporal variations in glacier dynamics are linked to changes in supraglacial hydrological inputs on the Greenland Ice Sheet and to establish to what extent perturbations in ice velocity at the margin can effect inland ice drawdown through basal hydrodynamic coupling. This project is utilizing a broad range of data sources in order to complete the aims and objectives. Catchment wide velocity field variations over daily, seasonal and annual timescales have been calculated using geodetic GPS and repeat TerraSAR-x surveys acquired throughout 2009. Repeat MODIS and SPOT satellite imagery are being used to monitor the evolution and drainage patterns of supraglacial lakes on the Russell Outlet glacier, providing large scale measurements of supraglacial lake area and volume. Results from repeat high resolution LIDAR surveys which extend 100 km up-glacier over the Russell glacier, acquired during July 2007 and August 2009, are being used calculate large scale changes in surface elevation. The results from this survey are helping to determine if the recent observed velocity acceleration at the glacier margins is causing drawdown of ice from further up-glacier via longitudinal coupling. This project will assist in providing more information to allow for better prediction of the dynamic response of the Greenland Ice Sheet to future climate change.

SPA dovetails with a number of UK and internationally-funded projects led by Hubbard and many collaborators involved in understanding ice dynamics, and response to climate change at the margin of the GrIS. The aim of this chapter is to present insight into the breadth and scope of activities and research conducted within SPA (and its collaborators) in 2009.

Work for SPA in 2009 occurred from April to October (three seasons) on the RGC to continue previously established activities and trial new field techniques. Throughout 2009 an intensive remote-sensing acquisition and processing project was carried out in parallel with field activities. In total, five separate field campaigns were conducted on the ice sheet:

The spring campaign, conducted during 10 days in April and 4 days in May, was concerned with deployment and maintenance of AWS and GPS stations and a safety and feasibility trial of skidoo-based deep-look radar. Personnel included: Hubbard, van As, Petterson, Doyle, McCallum.



Figure 2-1. Location map of Camp at SGL-Ice T, geodetic-GPS and Automatic Weather Stations (AWS) across the Russell Glacier catchment.

The summer campaign, conducted over 14 days in June/July, focused on processes around a targetted supra-glacial lake (SGL-IceT, located at IceT-Camp see Figure 2-1) in order to investigate hydrological processes and feedbacks and to trial passive seismics equipment. Personnel included: Hubbard, Kulessa, Luckman, Doyle, Helanow & 3 assistants.

The autumn campaign, conducted during 3 days in September and 4 days in October, included downloading AWS and GPS data and over-winterising equipment. Personnel included: Hubbard, Doyle & 1 assistant.

The following field data sets were collected in Sub-project A during 2009:

- Automatic Weather Station (AWS) data (e.g. air pressure, temperature, wind speed, solar radiation) to study the melting of the ice sheet.
- Geodetic Positioning System (GPS) data to monitor ice velocity across the Russell Glacier Catchment.
- Ground based radar data to study ice thickness and bed elevation.
- Passive seismic data to study glacio-hydrological processes.
- Tracer test data (dye and electronic tracers) to study englacial and subglacial drainage.

2.1 Remote sensing: Overview

The project has accessed a combination of archive and real-time satellite remote sensing datasets to better constrain the surface elevation and dynamics to basal hydrological mechanisms (Table 2-1). The recently launched TerraSAR-X satellite provided partial (11-day repeat) coverage of the 2009 field season at spatial resolutions ranging from 1 to 16 m. The Synthetic Aperture Radar sensor is not affected by inclement weather conditions, making it the ideal tool for capturing RGC-wide motion patterns throughout the evolution of the melt-season and as individual supraglacial lakes develop and drain. Standard satellite radar feature tracking (SRFT), speckle tracking (SRST) and radar interferometry (InSAR) procedures have been employed to provide composite patterns of surface speed (Figure 2-2).

Archive and real-time SPOT, ASTER and Landsat TM/ETM+ datasets (Table 2-1) have been collated and processed to provide RGC-wide constraints on annual, seasonal and specific temporal snapshots of surface speed, initial lake and moulin distribution, drainage and network connections along with the temporal-development and drainage characteristics of the lakes (Figure 2-3). A high resolution (40 m) SPOT DEM (Figure 2-4) has provided catchment-wide elevation data to model surface hydrology, aiding the identification of preferential flow pathways, channels and supra glacial lake (SGL) systems for example. Figure 2-5 to Figure 2-8 present examples of the remote sensing data archive.

Table 2-1. Remote sensing datasets acquired for the Russell Glacier catchment (RGC).

Sensor	Spatial resolution	Temporal coverage
TerraSAR-X	1–16 m	Summer 2009
SPOT	5 m	Summer 2008
ASTER	15 m	2002 – present
Landsat TM/ETM+	15–30 m	1999 – present (SLC on/off)
MODIS	250–500 m	Summer 2007 – summer 2009
Aerial Photography	~ 1 m	July 2007 and August 2009
LiDAR	~ 1 m	July 2007 and August 2009

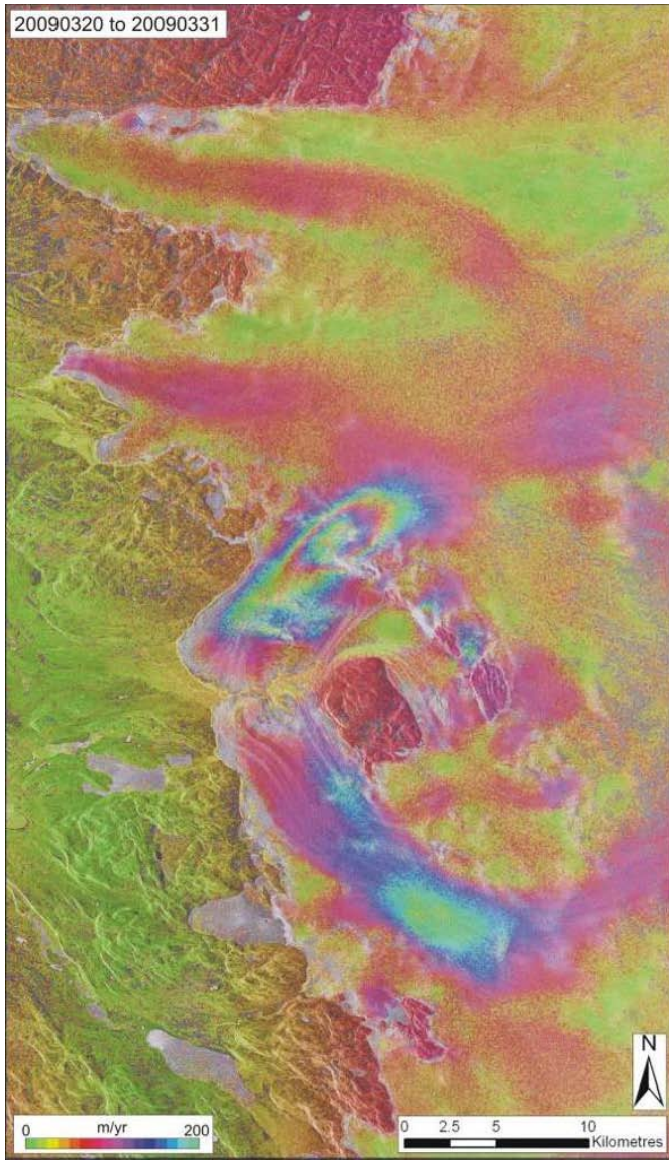


Figure 2-2. SRFT surface velocity data calculated from TerraSAR-X 1 m resolution SAR imagery.

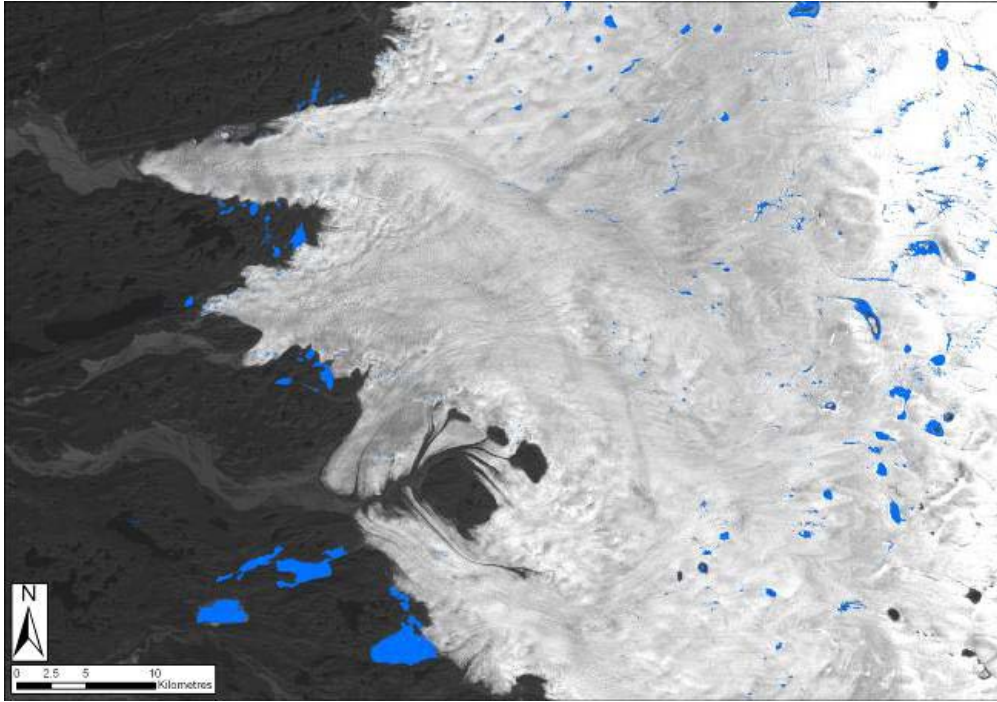


Figure 2-3. Automatic lake and drainage network classification from ASTER satellite data.

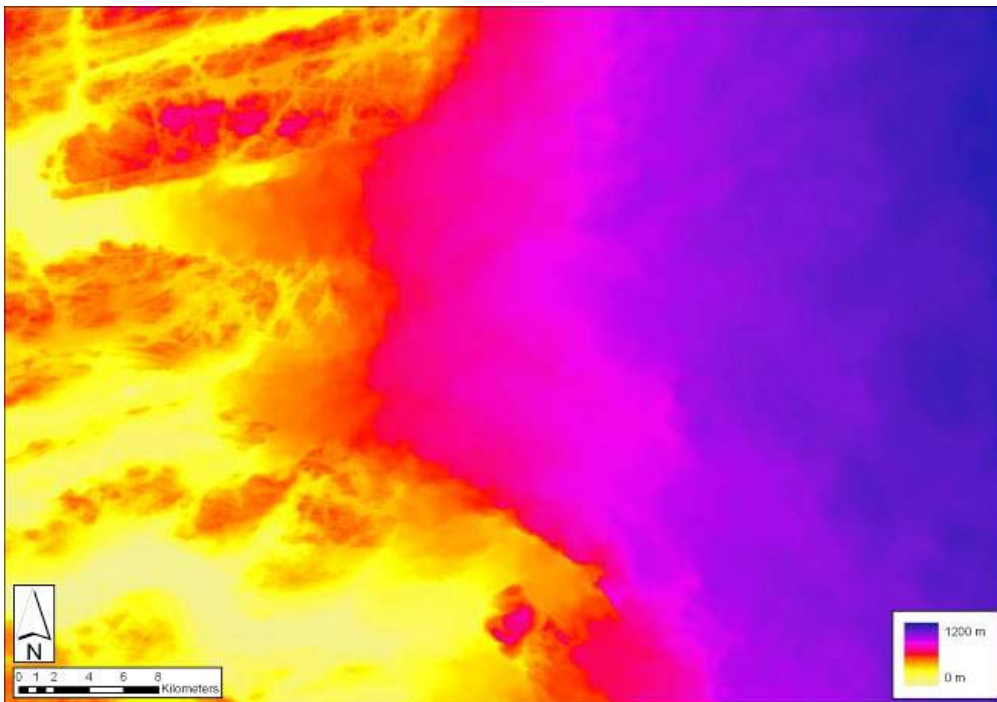


Figure 2-4. Digital Elevation Model derived from SPOT-5 HRS data and extracted at 40 m spatial resolution.

Remote sensing data examples (with archive length in brackets):

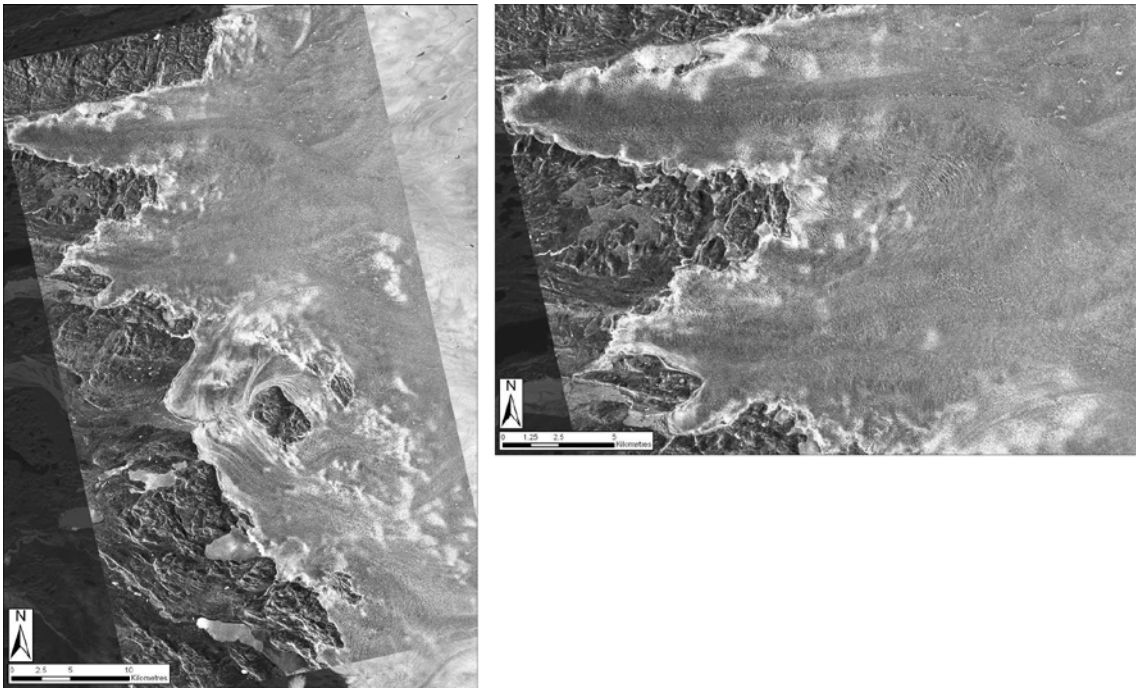


Figure 2-5. TerraSAR-X images showing the area covered by the TSX sensor swath over RGC, and more detail at the front of Russell and Isunnguata Sermia outlets (summer 2009).

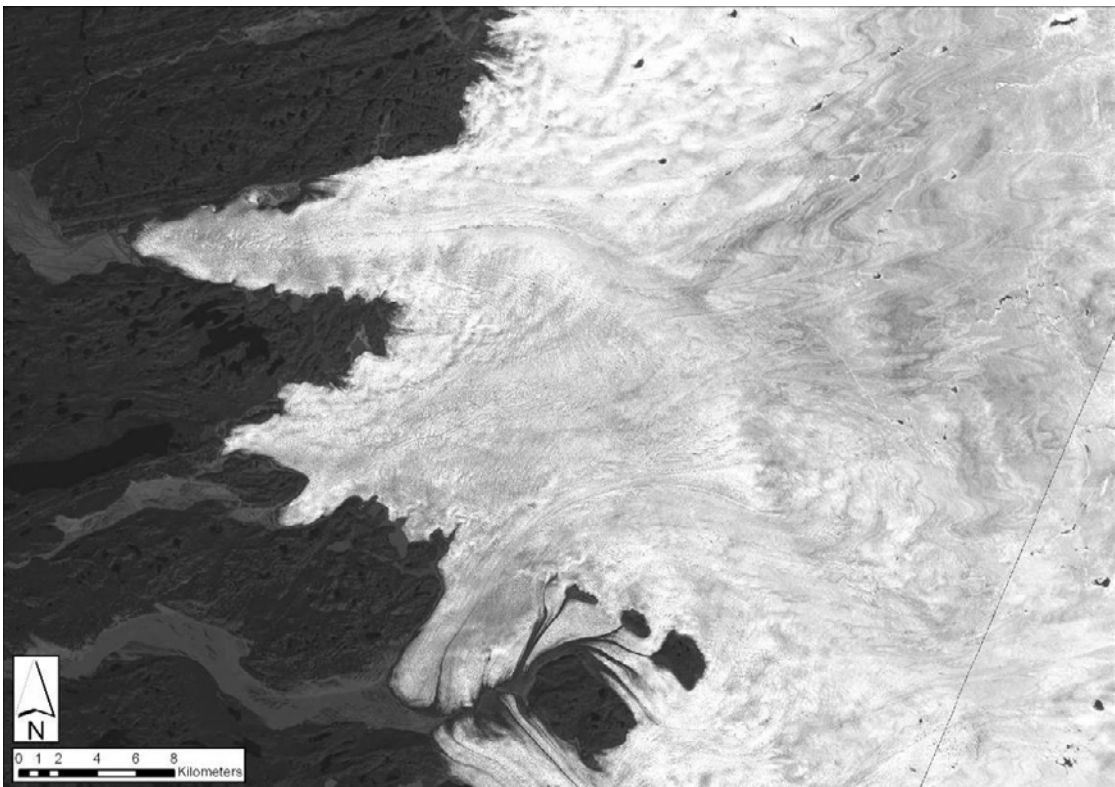


Figure 2-6. SPOT image (summer 2008 – summer 2010).



Figure 2-7. Landsat TM/ETM+ image (1999–present).

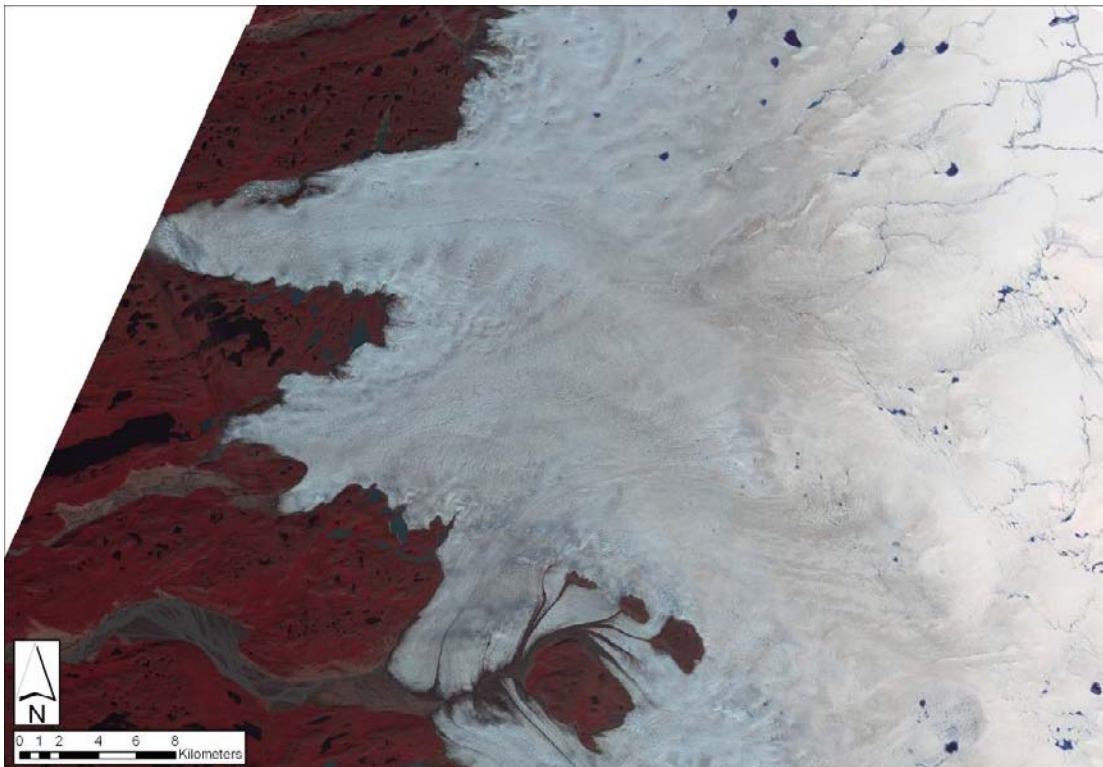


Figure 2-8. ASTER image (2002–present).

Image comparisons – TerraSAR-X (TSX) radar data yield different (and more detailed) information compared to SPOT and ASTER optical imagery (Figure 2-9). The TSX sensor is an active system, emitting energy at microwave wavelength and recording the backscatter received at the sensor. The microwave energy is able to penetrate cloud cover, and the sensor measures backscatter at very fine spatial resolution in one single band, making it ideal for multitemporal surface velocity calculations; SPOT, Landsat and ASTER are passive optical sensors, which are unable to penetrate cloud cover, but provide multispectral data (i.e. at multiple wavelengths), which are ideal for detailed surface structural analyses and also the automatic identification and monitoring of SGLs.

Velocity comparisons (Figure 2-10) – TSX data are ideally suited to feature and speckle tracking because the extremely fine resolution facilitates matching of even the smallest surface features and backscatter patterns; Landsat 15 m data are adequate to give a broad overview of velocities but melt is problematic higher up in the catchment; SPOT has good potential for providing additional velocities where there are gaps with TSX or for historical datasets.

The SGL Ice-T, location of summer 2009 base camp, imaged in SPOT 5 m data – the most detailed optical satellite data we have available for Russell Glacier Catchment at present is shown in Figure 2-11. We have an on-going application for IKONOS imagery that yields very fine spatial resolution (< 1 m) for selected sites over 2010.

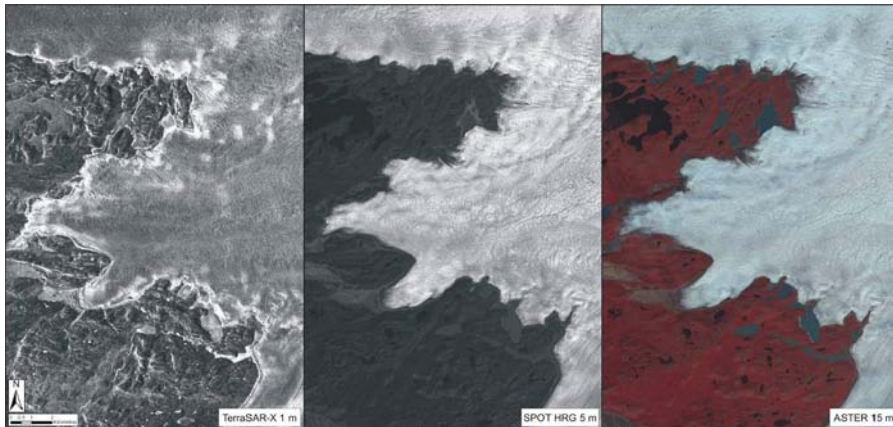


Figure 2-9. Image comparisons between TerraSAR-X, SPOT and ASTER.

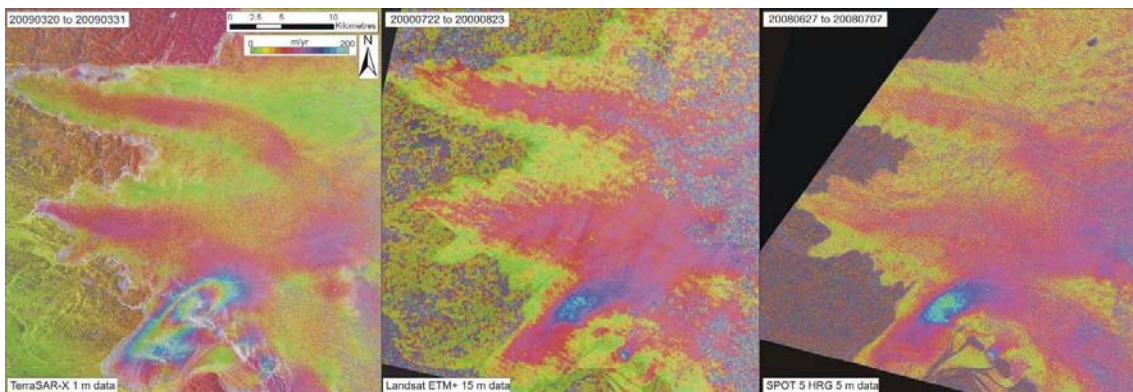


Figure 2-10. Velocity comparisons between TerraSAR-X, Landsat ETM and SPOT.

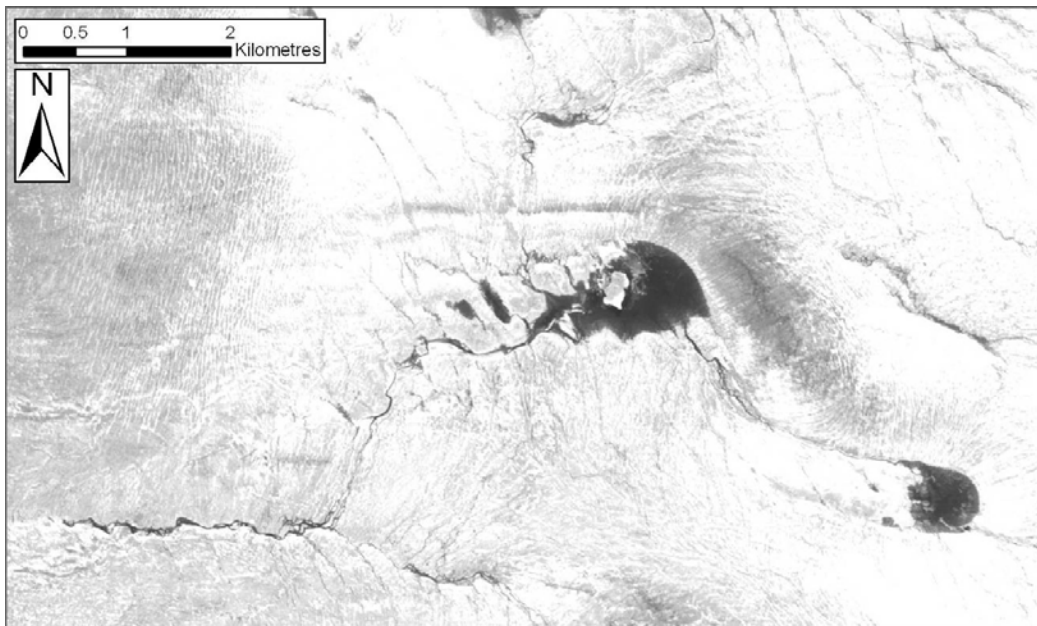


Figure 2-11. SPOT image of the supraglacial lake Ice-T.

Future work

In 2010 the current data acquisition strategy will be continued and intensified. A new order has been placed to obtain SPOT 1 m data images (at 7-day repeat interval) over RGC. 11-day repeat TSX 3 m data will be repeated and MODIS, ASTER and LandsAT products will be downloaded and processed in real-time. As the Summer campaign commences from June 2010 onwards, we wish to be supplied with daily updates of the state of SGL filling/drainage. Imagery and vital statistics will be processed at Aberyswyth University and compressed and made available for appropriate download at our 'on-ice' camp at our discretion, so that field-campaign can be best informed for optimal field-sites. We will also carry out a terrestrial based LiDAR survey of the front of Russell, Leveret and Isunnkata Sermia outlet glaciers and we wish to continue analysis of elevation change using new IceBridge and other potential airborne data.

2.1.1 MODIS data

The MODerate-Resolution Imaging Spectroradiometer (MODIS) is an optical sensor onboard the Terra and Aqua satellites collecting spectral reflectance data in 36 spectral bands at 250 m, 500 m and 1 km spatial resolutions. MODIS is well-suited to the study of catchment-scale SGL dynamics as the 2,330 m wide swath allows repeat imaging of the Russell Glacier every 1–2 days. For the analysis on SGL evolution, three bands within the visible spectrum (0.46–0.67 μm) are of greatest use: Band 1 (red, 250 m resolution), Band 3 (blue, 500 m resolution) and Band 4 (green, 500 m resolution). These bands are derived from Level 1B calibrated and geolocated products: MOD02QKM (bands 1–2 in 250 m resolution); and MOD02HKM (containing bands 1–7 in 500 m resolution). To maximise the available data resolution Bands 3 and 4 were initially oversampled to a pixel spacing of 250 m using Equation 2-1:

$$\frac{B_{500}}{(B_{500}/B_{250})} = B_{250} \quad \text{Equation 2-1}$$

where B is the band to be oversampled, $B1$ is band 1, and subscript values refer to the band spatial resolution. True colour images were derived for thirty-seven cloud free images acquired between May and September 2009 (Figure 2-12) using the 250 m resolution composite of Bands 1, 3 and 4. (Figure 2-12) and subset to cover the Russell Glacier Catchment. Even a basic visual analysis of these data shows SGL evolution and subsequent drainage over the summer season and their variability with altitude, with lakes at lower elevations developing and draining in the early to mid-season, and lakes at higher elevations developing and draining in the mid to late-season.

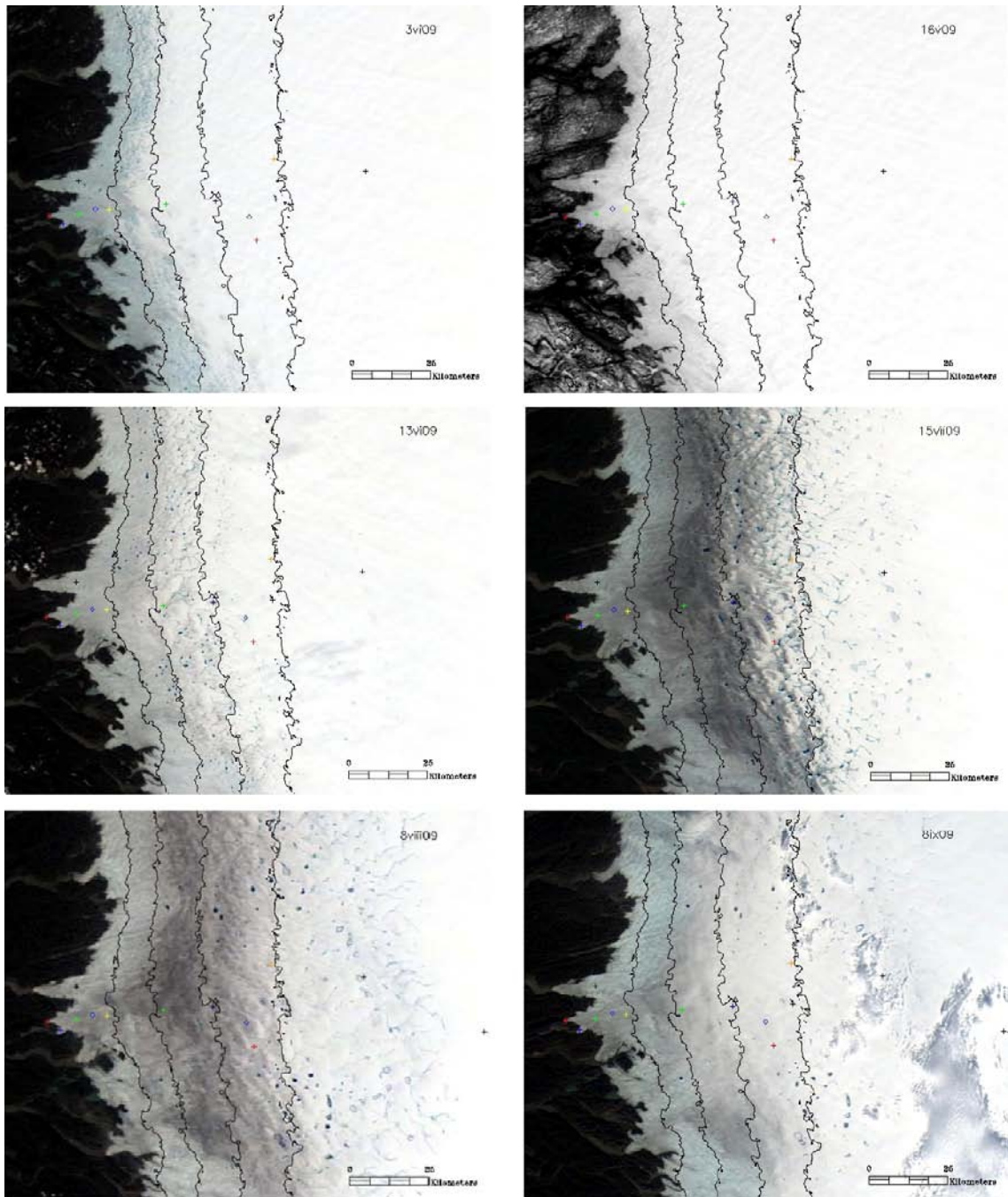


Figure 2-12. A selection of MODIS images between May and September 2009 highlighting the spatial changes in lake distribution throughout the melt season. Contours spaced at 250 m. The location of GPS and AWS sites are indicated by coloured dots on the image.

Position and size information were extracted for each SGL by using a semi-automated classification approach (Equation 2-2). The Normalised Difference Water Index (NDWI) exploits the distinct spectral response of water bodies in visible and near-infrared wavelengths:

$$NDWI = \frac{B_{NIR} - B_{BLUE}}{B_{NIR} + B_{BLUE}} \quad \text{Equation 2-2}$$

where B_{NIR} and B_{BLUE} represent the near infra-red and blue bands respectively. Raw lake classification data were refined to include areas in shadow and those lakes with partially frozen surfaces. Data relating to total SGL area change through time (Figure 2-13), change with elevation (Figure 2-14) and change through time with elevation (Figure 2-15) were extracted from the final classification results.

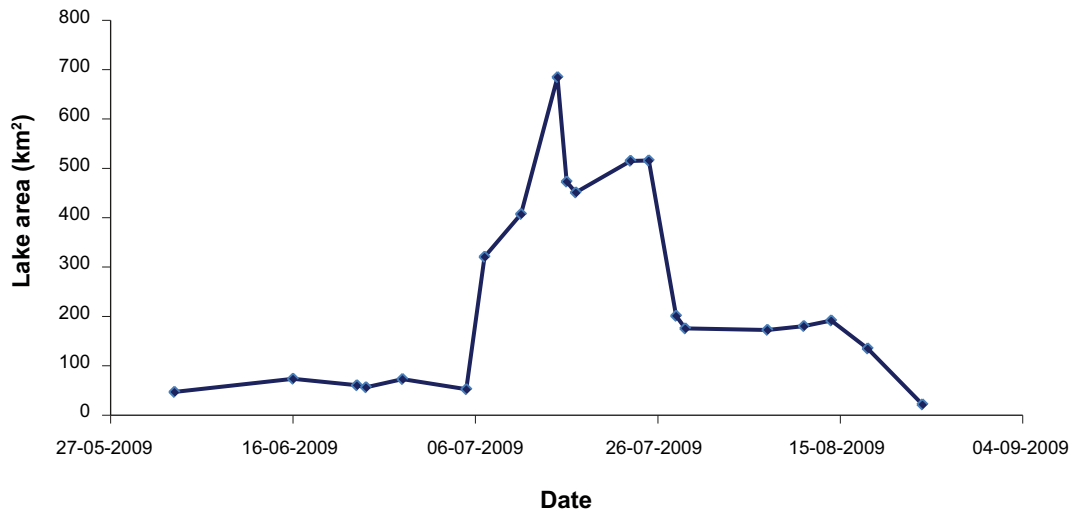


Figure 2-13. Change in SGL area over the entire RGC during the 2009 melt season.

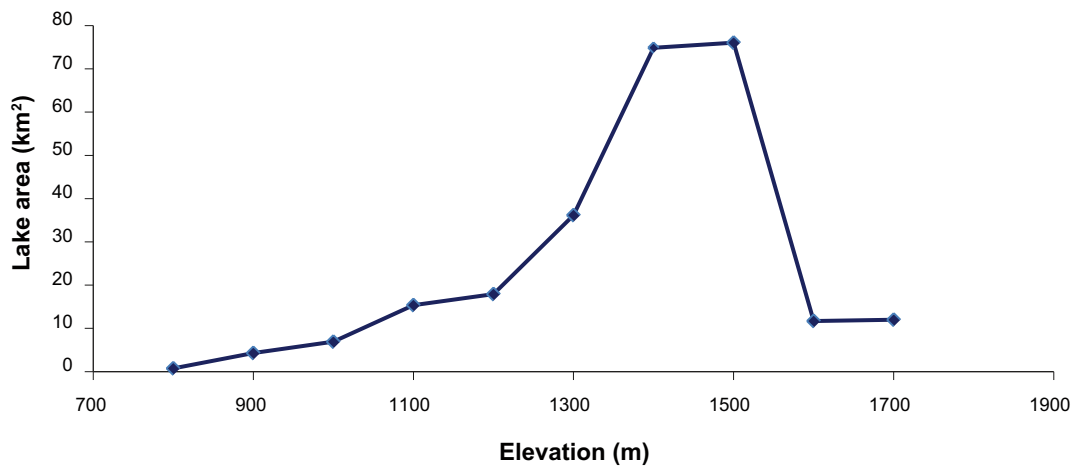


Figure 2-14. Mean SGL area over the entire RGC, bracketed at different elevations throughout the 2009 melt season.

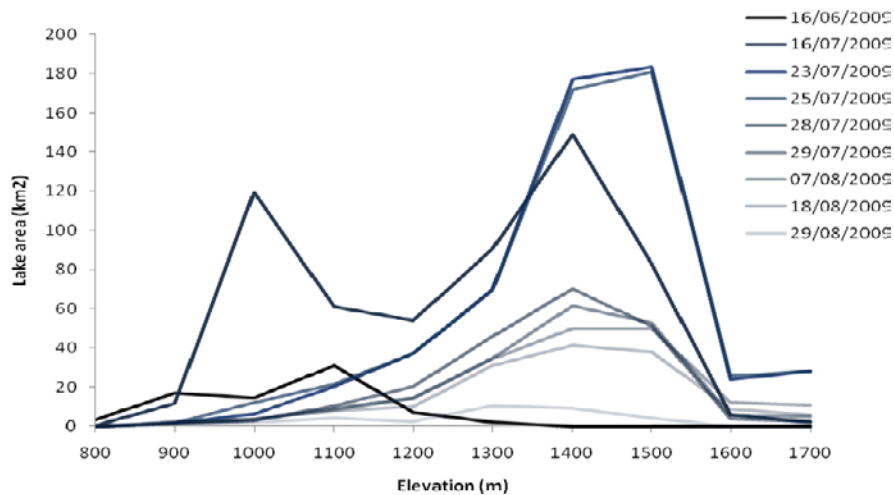


Figure 2-15. SGL area-elevation distribution throughout the 2009 melt season.

Velocity Analysis

Studies of glacier velocity require the identification of displaced features or image speckle across two time-separated images. There is an optimal window in which these patterns have moved sufficiently to be detected, but not destroyed by deformation. The 11-day revisit time of the TSX sensor provides this optimal window for the Russell Glacier Catchment. Surface velocity fields were derived for each 11-day interval during the period March to November (Figure 2-16) using a combined feature and speckle tracking approach.

The highly consistent imaging geometry and repeat-pass reliability of satellite imaging systems allow glacier surface feature patterns to be tracked, sometimes over considerable distances, by cross-correlation of image patches between repeat-pass pairs of images. Images are first co-registered to sub-pixel accuracy using stable areas within the image, before cross-correlation between image patches is performed on both stable and non-stable terrain. Matches are accepted or rejected based on their signal-to-noise ratio, which is a measure of the height of the cross-correlation peak in comparison to surrounding correlation estimates, and transformed from SAR co-ordinates to map co-ordinates using a digital elevation model (DEM).

Speckle tracking works on similar principles, but instead of tracking real surface features defined by the radar backscatter, speckle produced by constructive and destructive interference between multiple returns of the narrow bandwidth incident radiation can be matched between images, even where displacement has occurred. The process chain is similar to that of feature tracking, with sub-pixel co-registration of the two images being a critical first step. Matching of speckle between the two images is done on a very fine scale and can therefore supply very precise displacement measurements.

Velocity distributions from Figure 2-16 were subset and masked according to RGC area and a summary of their vital statistics is given in Table 2-2 and plotted in Figure 2-17. Table 2-2 and Figure 2-17 indicate the magnitude of surface speed change between March and November, 2009 across RGC. Longitudinal profiles of surface speed were also extracted along the approximate RGC flowline up to 55 km from the ice margin (Figure 2-18). Maximum and mean recorded velocities peak in July. March and November indicate faster mean and maximum flow than August, 2009.

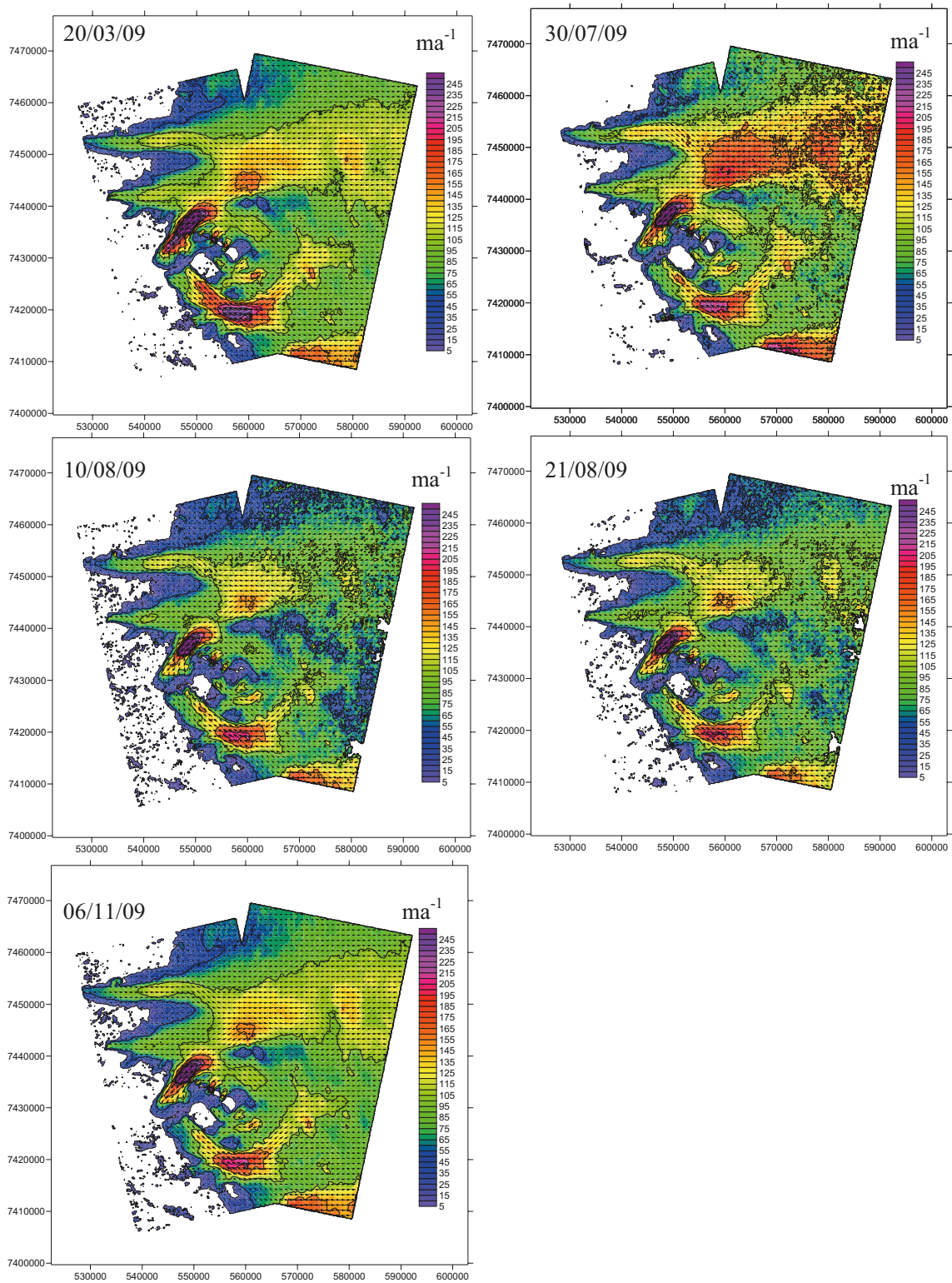


Figure 2-16. Surface speed maps (ma^{-1}) across the Russell Glacier Catchment (RGC) derived from feature tracking of TSX imagery at 11 day repeat intervals between March and November in 2009.

Table 2-2. RGC velocity statistics from optical image feature tracking.

Date	Max (ma ⁻¹)	Mean (ma ⁻¹)	St. Dev.
20/03/2009	437.1	45.5	54.7
30/07/2009	1,250.6	48.5	59.3
10/08/2009	832.9	36.3	45.4
21/08/2009	369.7	37.9	46.5
06/11/2009	396.5	42.8	51.3

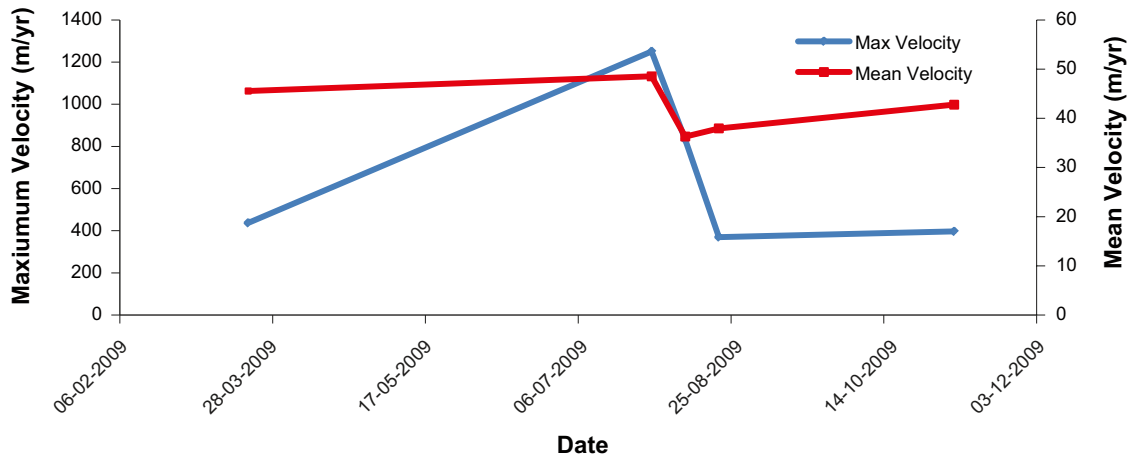


Figure 2-17. Time-series indicating maximum and mean velocity (m a⁻¹) of RGC.

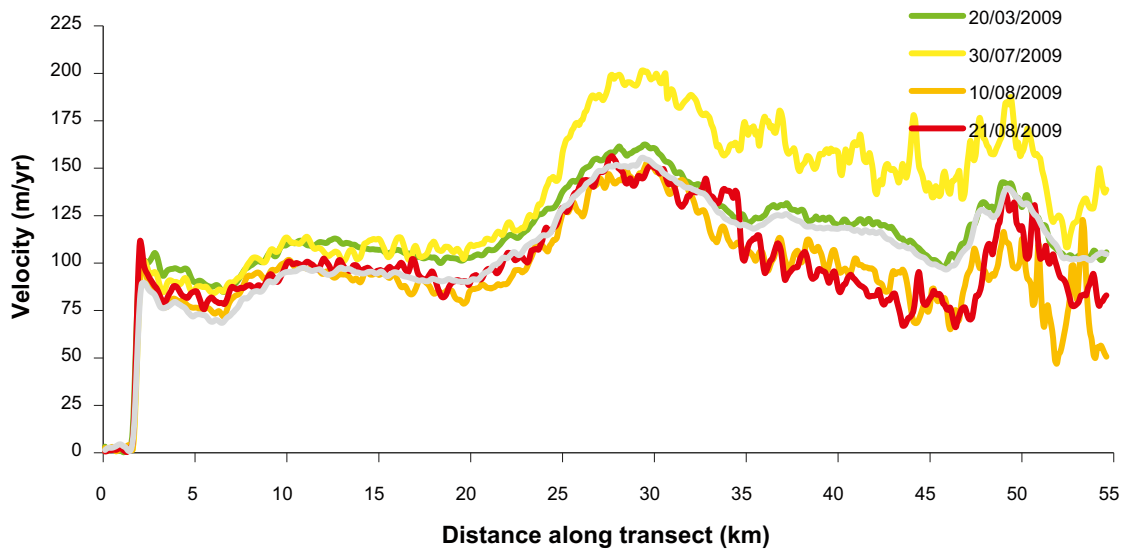


Figure 2-18. Temporal change in velocity along a long-profile up RGC during 2009.

2.1.2 Preliminary results of NERC Airborne Research and Survey Facility LiDAR survey and analysis

In July 2007 and August 2009 the UK Natural Environmental Research Council (NERC) Airborne Research and Survey Facility (ARSF) acquired data over numerous flightlines across RGC (Figure 2-19). The survey recorded: (1) LiDAR (Light Image Detection And Ranging); and (2) multispectral data sets using a Leica ALS50 Airborne laser scanner and a Daedalus 1268 Airborne Thematic Mapper (ATM) respectively. Georeferenced products, corrected against our geodetic-GPS were supplied by ARSF. Methods of initial processing and an overview of preliminary analysis of the LiDAR data set is provided. The LIDAR survey extends 100 km up Russell glacier covering an elevation range of 200–1,600 m.a.s.l. Twenty flight lines were surveyed and repeated between the 20th and the 23rd July 2007, and the area covered is shown in blue in Figure 2-19. Twenty-two lines were surveyed on the 5th August 2009 (two additional lines across SGL Ice-T were requested) (Figure 2-19).

The LIDAR data was supplied as point-cloud data in space-delimited ASCII format. The individual files contain GPS time data, UTM Easting, UTM Northing, height and intensity values for both the first pulse and last pulse of the radar. Python scripts were used to parse and extract Easting, Northing and elevation value from each line. Geographic Resources Analysis Support System (GRASS), an open source GIS software run on a Linux operating system was subsequently used to process the ASCII files. A new region was created in GRASS covering the Russell catchment and a command was run to read the data for each flight line to determine the minimum and maximum North and Easting. Once these parameters were set, each flight line was imported into GRASS and interpolated into an appropriate raster format. Flight lines which were repeated in 2009 were processed together with 2007 data so that they could be combined allowing their spatial boundaries to cover the same mutual region. Finally, individual files were exported as digital elevation models (DEMs) for analysis with a pixel resolution of 1 to 25 m. Each DEM (representative of one flight line) was imported in ENVI software and header files were created containing their spatial extent. In order to calculate the change in elevation for each pixel at its appropriate resolution between 2007 and 2009, a mask was created by overlaying the images and then applying the mask back onto the original DEMs. By doing this only areas that were surveyed in both 2007 and 2009 would be processed. The top panel of Figure 2-20 shows the areas of overlap from the 2007 and 2009 LIDAR surveys.

The band math function in ENVI was finally used to calculate the change in elevation for each pixel, and background values were given a null value (NaN) to blank out off-swath zones and differentiate them from zones of no surface-elevation change. To calculate the average change in height at regular intervals along each line the files were rotated until the strips were parallel to the x-axis. Individual LIDAR strips were then saved in an ENVI standard format and a python script was applied to each file to extract the average of each line (x-axis) of data, excluding null values. The average change in height at 20 m intervals (the pixel resolution) along each transect was then plotted in Excel as shown in the examples of Figure 2-20 and Figure 2-21.

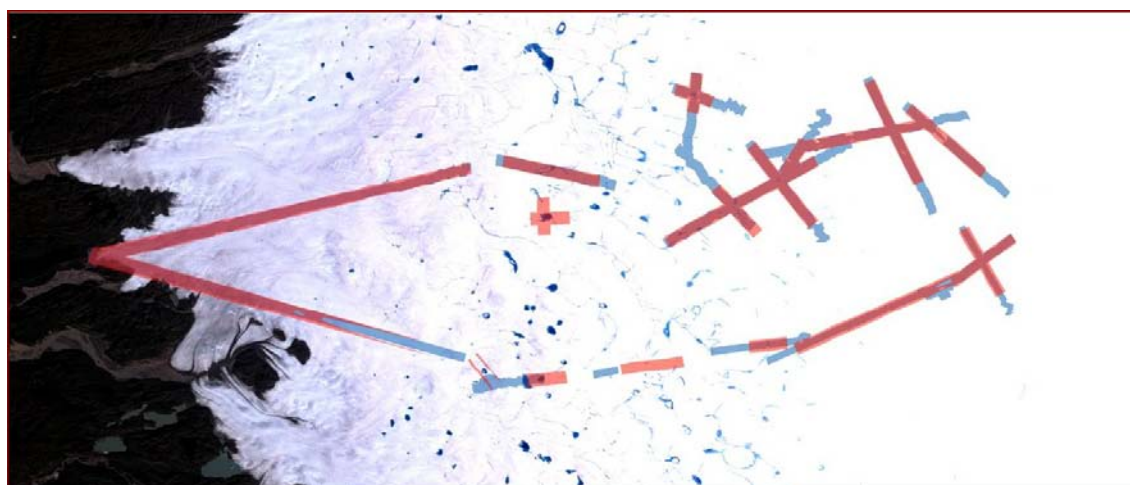


Figure 2-19. Swath flight lines covered by the LIDAR surveys in 2007 (blue) and 2009 (red).

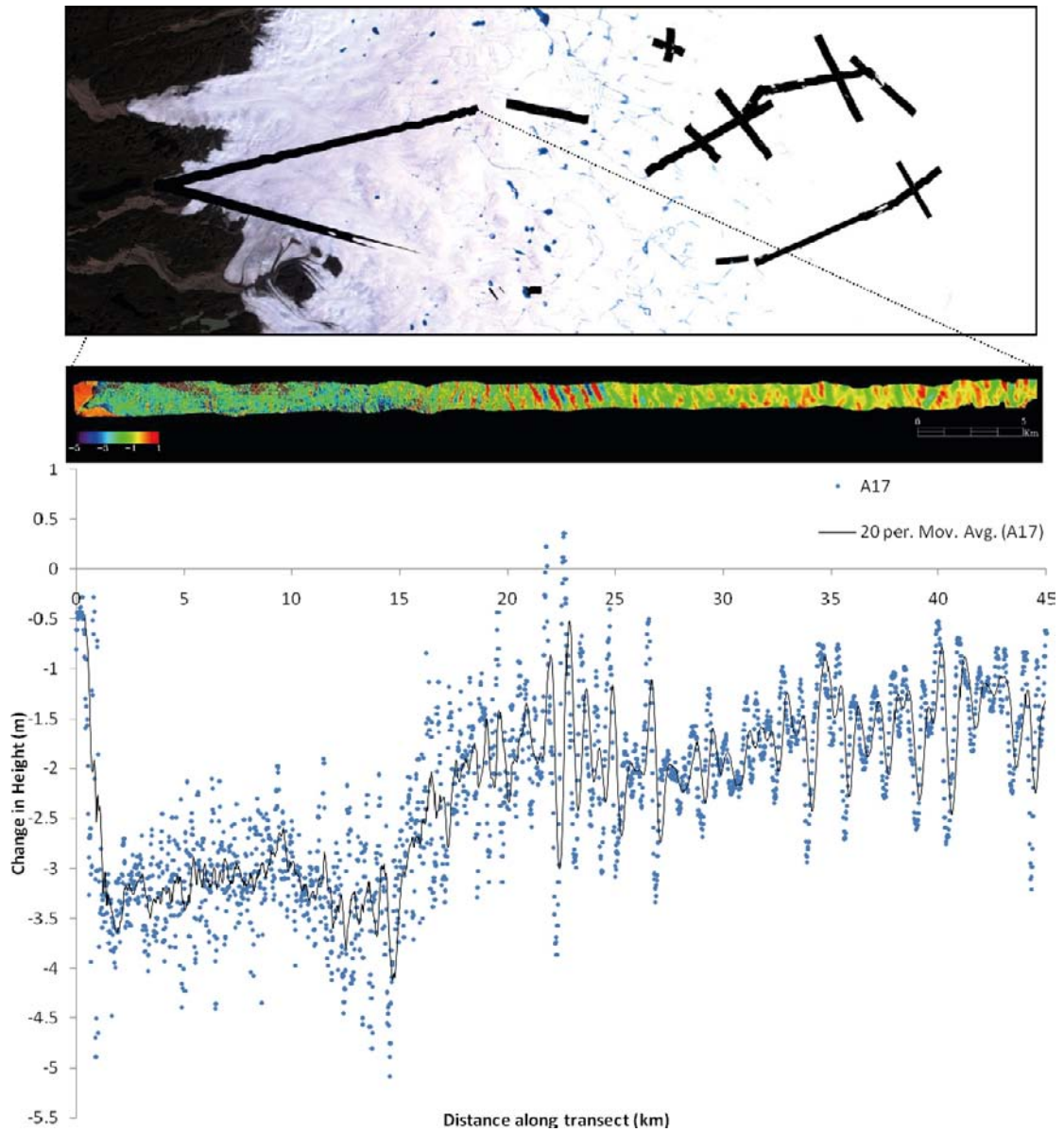


Figure 2-20. Lowermost LiDAR strip extending 45 km from the front of Russell showing the change in elevation (m) between 2007 and 2009. The lower panel illustrates the mean surface elevation change between 2007–2009 against distance along transect.

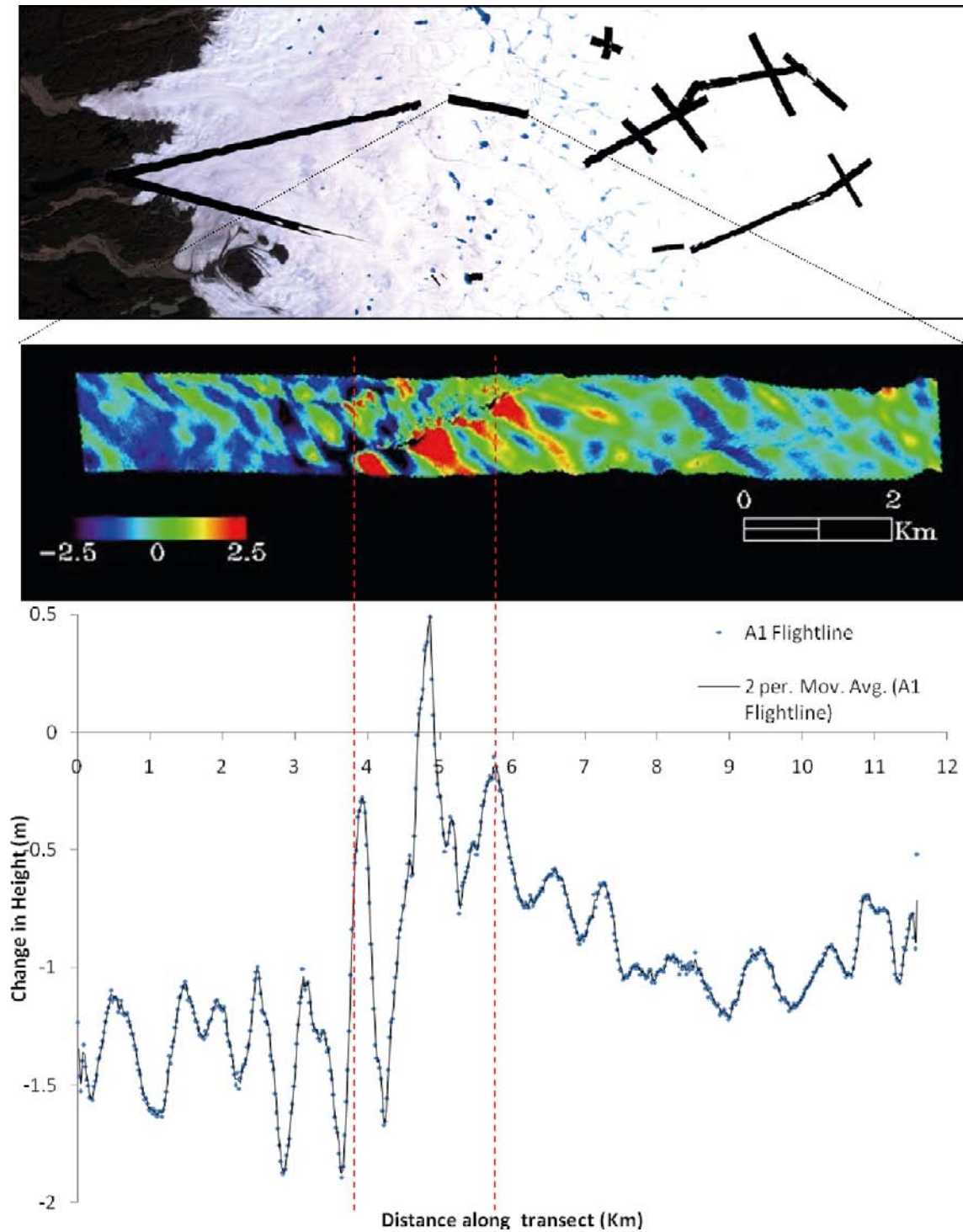


Figure 2-21. A single strip (~ 1,200 m.a.s.l.) of change in surface elevation (m) between 2007 and 2009. The graph beneath the image illustrates the mean change in elevation of the ice surface along this flight line against distance along transect. The dashed red lines on the graph represent the extent of a band of stored supra-glacial water.

This process was repeated to extract the 2007 elevation data for every column along each flight line. Change in surface height (m) is plotted against elevation for each flight line (Figure 2-22).

Figure 2-22 yields a reasonably strong relationship between change in surface height between 2007 and 2009 and elevation. At low elevations an average height difference of -3.5 m was recorded between the 2007 and 2009 surveys and that lowering of the ice surface extends to as high as 1,500 m.a.s.l. Despite this, the trends are noisy and there is still significant processing and analysis of these data to be performed. Large fluctuations in the data at lower elevations are due to the large number of transverse crevasses located in this region, as shown on the hill shade images in Figure 2-23. Crevasses migrate down-glacier as the ice moves. Due to the two year interval between LIDAR surveys individual crevasses were therefore not located in the same positions thus resulting in the large fluctuations observed. The peaks in the data set at higher elevations are where the LIDAR strips intersect SGLs. Lakes at different stages of filling and drainage significantly alter the surface topography yielding systematic differences between 2007 and 2009. For example, a SGL that was empty during the 2007 survey and full in 2009 would result in a positive change in height value illustrated as a peak on the graph.

Data Accuracy

The ARSF reported that the LIDAR data contain a mean error magnitude of 3.9 cm with a standard deviation of 4.5 cm at the time the surveys were undertaken. Additionally the ARSF reported a problem with the roll boresight angle varying between flight lines with no definite trend being observed in the variations. Calibration flights undertaken by the ARSF recorded an error magnitude of 25 cm across the LIDAR swath. This error has been manually corrected for by the ARSF for flight lines which have overlapping areas.

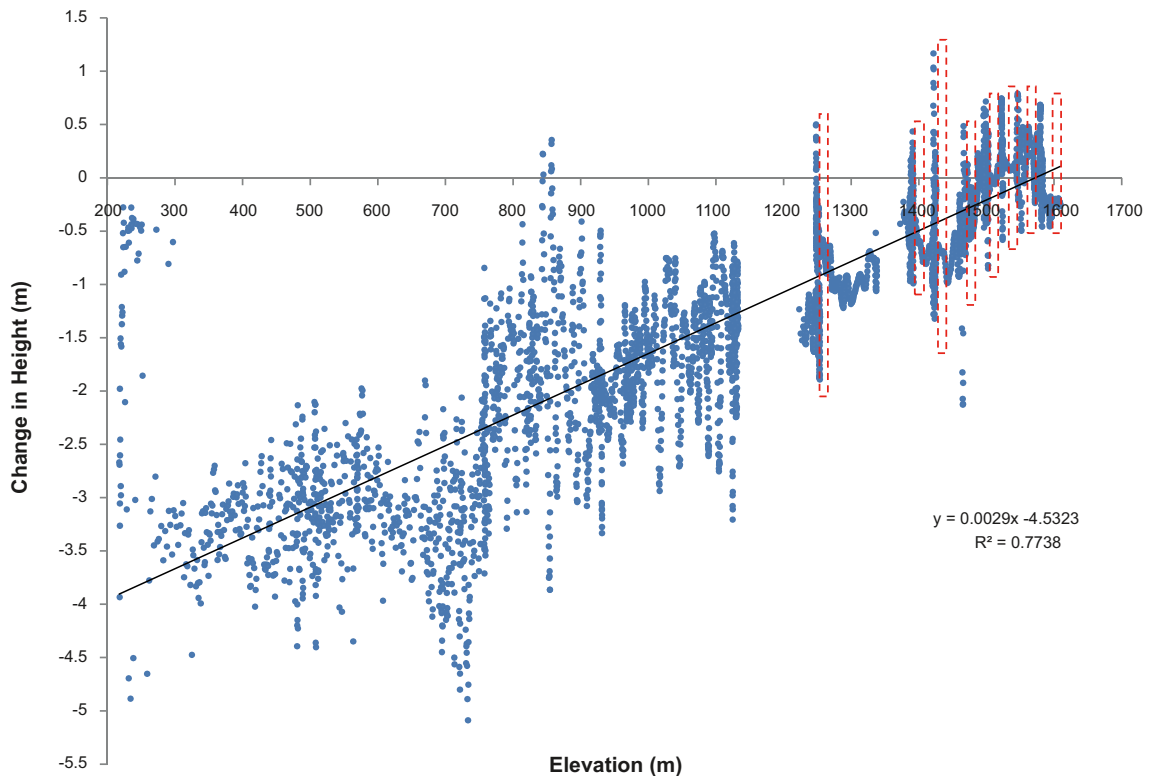


Figure 2-22. Scattergram of change in ice surface elevation against elevation across all LiDAR flight lines acquired over RGC. The dashed red lines represent the extent of supraglacial lakes.

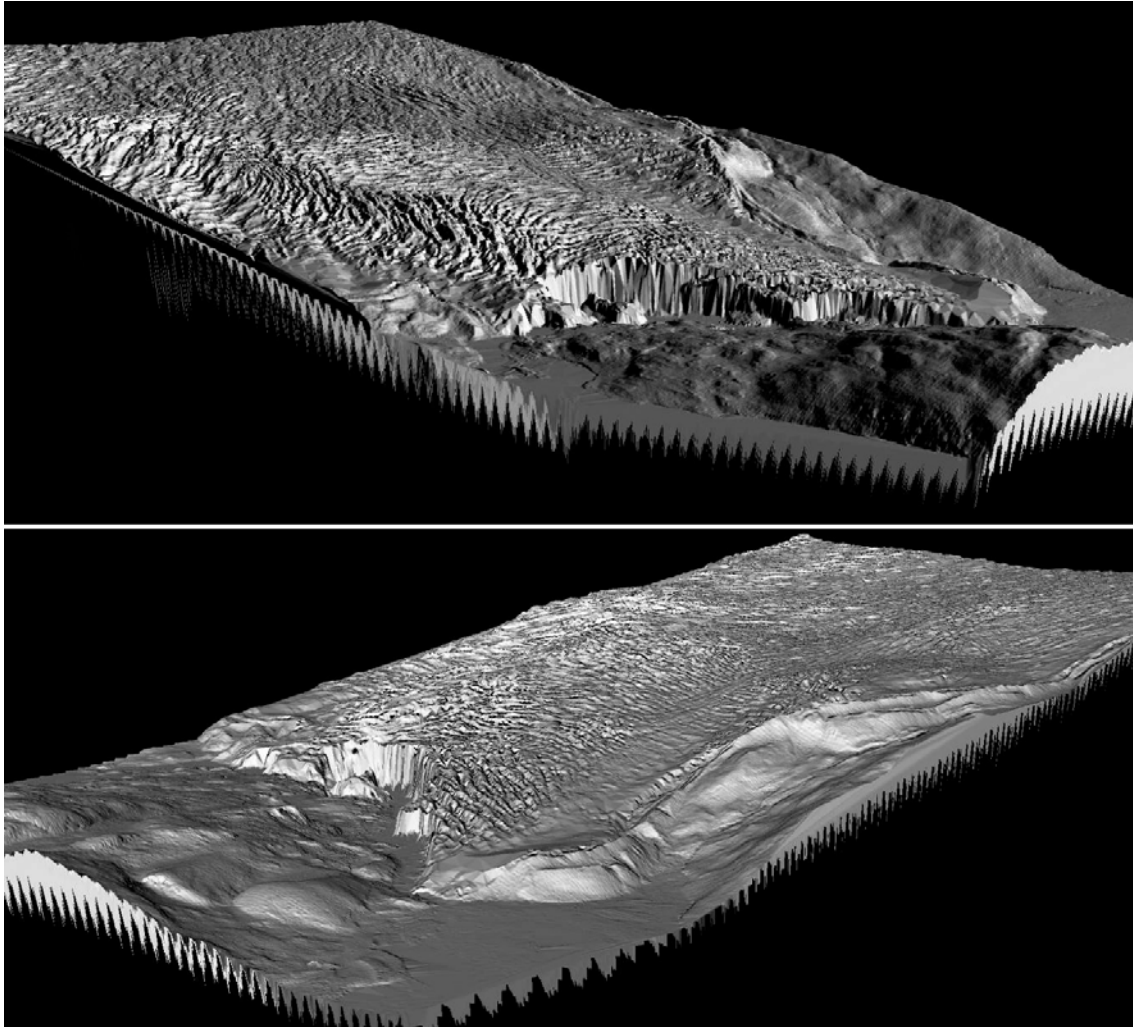


Figure 2-23. Hill shade renders of a single LIDAR flight line at 1 m resolution indicating nature of the surface topography at the terminus and pro-glacial zone of Russell Glacier.

Multispectral data

The multispectral data sets recorded by the ATM were supplied as level 1b HDF (Hierarchical Data Format). These were georeferenced with azgcorr and azexhdf software which runs on LINUX, supplied by the ARSF. Bands 5, 3 and 2 were mapped to Universal Transverse Mercator coordinate system (UTM), using the WGS84 datum to create a georeferenced RGB image with 5 m resolution.

2.2 Climate, Automatic Weather Station (AWS) and surface run-off mapping

One of the important activities in GAP is to study the drainage patterns of the meltwater produced at the ice sheet's surface. In order to obtain accurate ablation rates from the ice sheet, automatic weather stations (AWSs) are recording surface accumulation and ablation and the meteorological parameters that directly or indirectly govern the surface mass budget of the ice sheet. These point measurements of local meteorology serve as input for distributed melt modelling and are validated by the independently obtained ablation records. The resulting regional melt maps are then used in the study of meltwater routing through the ice, and the impact of meltwater flux variability on ice dynamics and characteristics of the basal hydrological system.

2.2.1 Automatic weather station placement

The Geological Survey of Denmark and Greenland (GEUS) placed three AWSs in the melt zone directly due east of Kangerlussuaq in the south-western section of Greenland. These stations supplement the transect already in place by the Institute for Marine and Atmospheric Research in Utrecht, The Netherlands (IMAU), consisting of three additional AWSs. As a result, the Kangerlussuaq region has the highest density of AWSs on the Greenland Ice Sheet, enabling a study of unprecedented detail in spatial and temporal surface mass budget variability. Figure 2-24 shows that the stations transects are interwoven, where the IMAU station S5 is the one at the lowest elevation, and the GEUS station KAN_U is the highest, well above the equilibrium line altitude which is located approximately at station S9.

Table 2-3 lists the coordinates and date of placement of the GEUS AWSs funded by GAP. The lower and middle stations (KAN_L and KAN_M) were placed during the first field campaign early September 2008 when shared logistics between Aberystwyth University, IMAU (Institute for Marine and Atmospheric Research Utrecht), and GEUS proved to be a successful method to reduce helicopter expenses. The upper station (KAN_U) was constructed during the second field campaign conducted using snowmobiles early April 2009. The construction of an AWS takes roughly three hours for two to three people. The installation of all stations was a full success, with the exception of the thermistor string at KAN_M, which could not be installed in 2008 due to losing a number of Kovacs drill flights to the ice.

Table 2-3. Automatic weather station metadata.

Station name	Latitude (°N)	Longitude (°W)	Elevation above sea level (m)	Date of placement
KAN_L	67.097	49.933	680	1 Sept, 2008
KAN_M	67.066	48.818	1,270	2 Sept, 2008
KAN_U	67.000	47.017	1,850	4 April 2009



Figure 2-24. Google Earth satellite image of the automatic weather station transect near Kangerlussuaq. GEUS stations are in red, IMAU stations in orange.

2.2.2 Automatic weather station set-up

The GEUS AWS has been developed to fulfil the following requirements:

- The measurements should be of high quality.
- The instruments must be able to survive harsh climatic conditions and ongoing freezing and thawing cycles over an extended period of time.
- The station must have low power consumption.
- The station must be easy to construct.
- All equipment should be able to fit in a Bell AS350 helicopter or onto a sledge to minimize logistical expenses.

The frame of a station consists of a custom-made aluminium tripod held upright by thick steel wire. The tripod is not drilled into the ice, but stands loosely on it to be able to melt down with the surface. Wooden boards are attached to the feet of the tripod to prevent the legs from melting into the ice, which could build strain and would alter the measurement height of the sensors (for instance introducing a false signal in the surface height measurements). This relatively lightweight set-up is kept in place during strong-wind events by the heavy battery box that is mounted underneath the mast. In wintertime, when winds over the ice sheet are stronger, the accumulation covers part of the tripod, giving it extra stability until the snowpack has melted off in spring (Figure 2-25).

2.2.3 Observations

Since installation, all three AWSs have performed excellently with 100% temporal data coverage, seen both in transmitted data and data downloaded in field. Figure 2-26 presents time-series of key data for the three AWS over their entire deployment period which can be analyzed in detail. For example, Figure 2-27 shows the temperature record for the 2009 melt season, running from May to September. Whereas above-freezing temperatures prevailed continuously at KAN_L, sub-freezing temperatures occurred over longer periods of time at the higher elevations. At KAN_U, in the accumulation zone, melting conditions occurred only during three periods (early June, mid-July and mid-August), and temperatures never exceeded +3°C. Here night-time temperatures occasionally dropped to below -15°C, in spite of the nights being short.

Note the lack of a daily cycle in temperatures at the lower station. Here, the surplus of energy from solar radiation, terrestrial radiation emitted by a warm atmosphere, and turbulent heat exchange between atmosphere and ice kept the ice surface at the melting point at all times, and prohibited the near-surface atmospheric temperature to deviate by more than a few degrees.

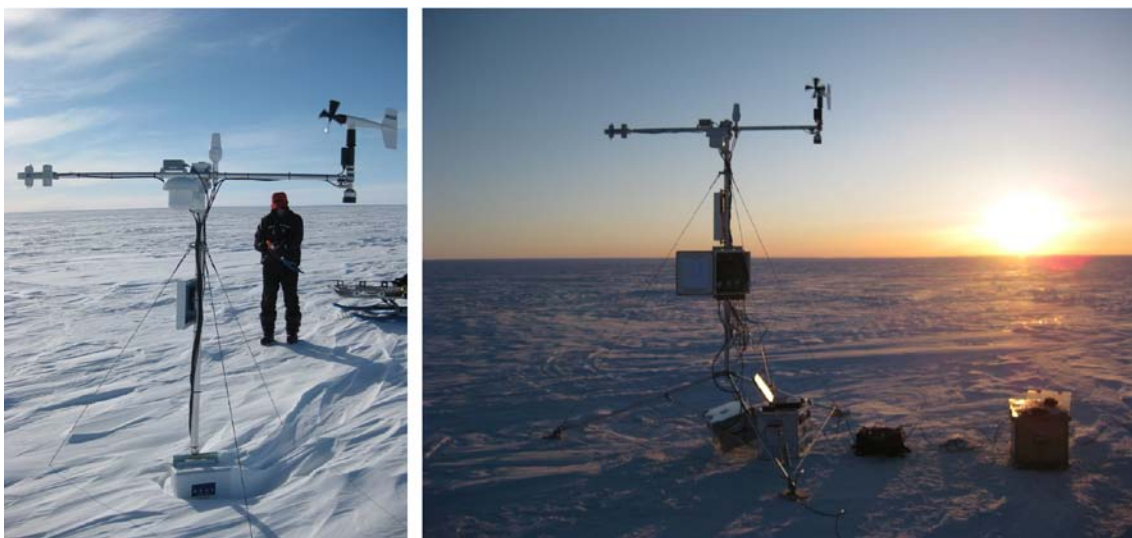


Figure 2-25. Left – the middle AWS (Kan_M) partially covered by a wintertime snowpack in April 2009. Right – assembly and calibration of the upper AWS (Kan_U) in April, 2009. Photo by Dirk Van As.

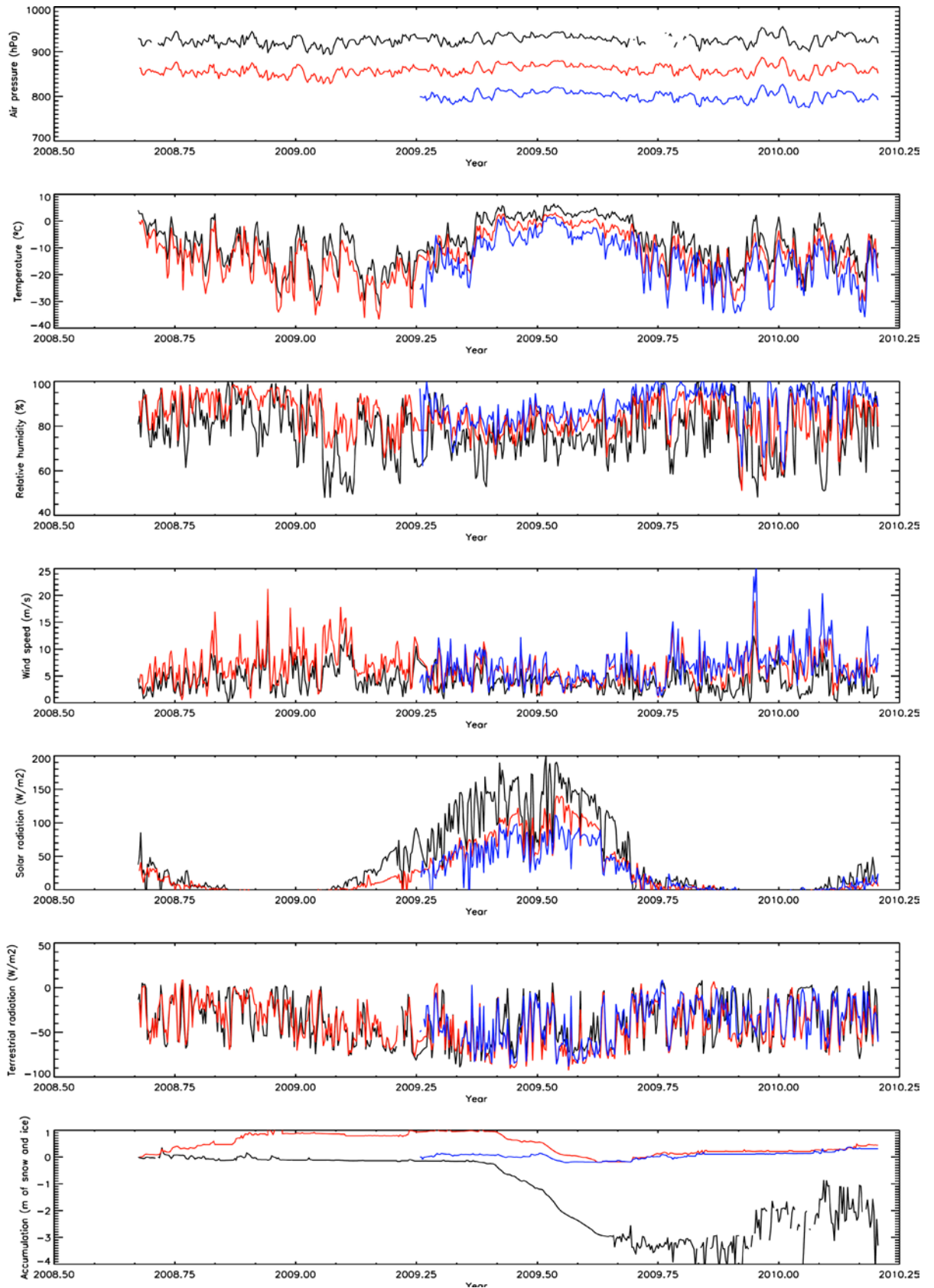


Figure 2-26. Summary output of main meteorological parameters for the three AWS on RGC over entire deployment period (Key: Black = KAN_L, Red = KAN_M, Blue = KAN_U).

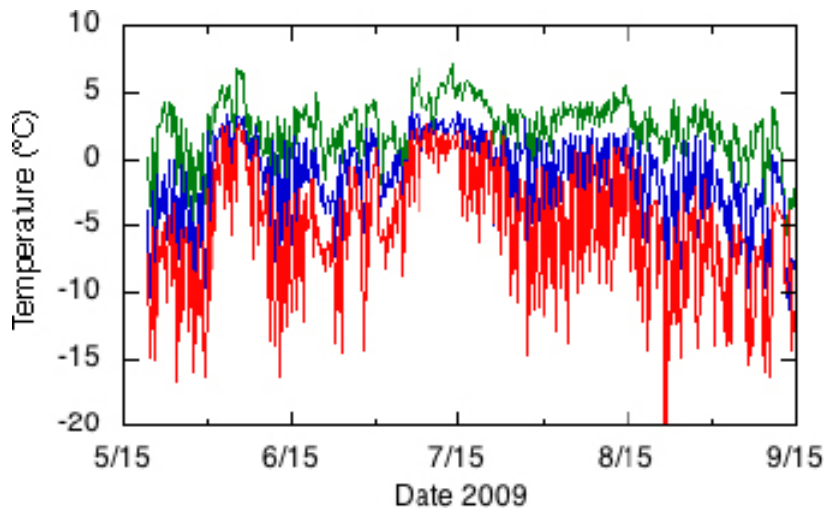


Figure 2-27. Near-surface air temperature at the lower (green), middle (blue) and upper (red) automatic weather station during the 2009 melt season.

The second data sample is given in Figure 2-28, which shows the surface height at the three GEUS AWSs over the 2009 melt season as measured by sonic rangers mounted on stake assemblies drilled into the ice. At KAN_U a relatively small amount of surface lowering due to ablation and compaction of the surface snow takes place (0.25 m). The largest surface lowering occurs during the second period of positive temperatures at the station in mid-July. A few minor snowfall events can be identified, most notably in mid-September. The September precipitation also shows up in the KAN_M record. The middle station located in the upper ablation zone experiences more ablation than accumulation over a year. The figure shows that total ablation is 1.2 m in 2009. Since wintertime accumulation added up to roughly 0.8 m prior to the melt season, net ablation over 2009 was about 0.4 m of ice at KAN_M. This is a small amount in contrast to the ablation at KAN_L (≥ 2.7 m of ice), where ablation rates are large and no wintertime accumulation was recorded.

There is a great resemblance in the temporal variability of the ablation records of all three stations, which indicates that in spite of the large distances between the AWSs, the regional meteorology impacts variability in ablation rates similarly over a wide range of elevations. Though temperature is not an exact measure of ablation, we can tell by comparing Figure 2-26 and Figure 2-27 that periods of positive air temperatures coincide with periods of (melt-dominated) ablation.

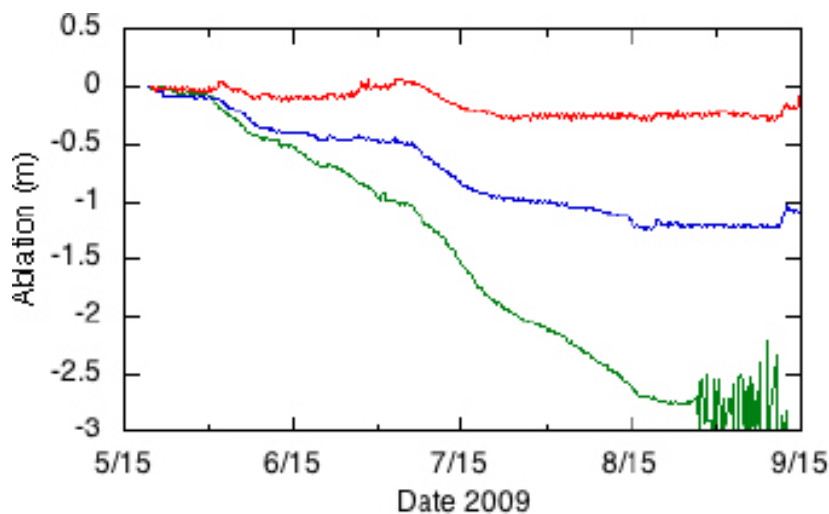


Figure 2-28. Surface height change due to ablation and accumulation at the lower (green), middle (blue) and upper (red) automatic weather station during the 2009 melt season.

Current problems with the AWSs as seen from the transmissions are minor. At the lower station, all sensors are functional, though the stake assembly came partially apart at the end of summer 2009, causing inaccurate sonic ranger measurements (Figure 2-28, green line). At KAN_M, the 2009 newly installed thermistor string measuring sub-surface temperatures stopped functioning. The sensors at the upper station seem fine, but high tilt values are recorded since a storm event in October 2009. The extent of the wind damage to the station is unknown.

2.2.4 Modelling the mass balance budget

To be able to calculate the surface meltwater produced on the ice sheet, we will make use of a physically-based surface energy and mass budget model. The model will use the meteorological measurements from the AWSs to estimate the surface heat fluxes (radiative, turbulent, sub-surface conductive, and rain) to determine the impact on the mass budget through melt and sublimation. The model includes iterative turbulent heat flux calculations, solar radiation penetration in snow and ice, meltwater refreezing, etc. Results will be validated for the AWS locations by comparing modelled and measured changes in surface height. The model will be run for elevation bins between sea level and 2,000 m altitude, distributing input parameters with altitude by inter-/extrapolating the measurements from the six AWSs in the region, which is a common practice in these types of studies. The result of this exercise will be maps of the surface energy and mass fluxes that can be used for studying meltwater channelling on top of, through and beneath the ice sheet.

We will also explore the possibility to refine an important input parameter for the melt modelling: surface albedo. Using MODIS satellite maps of surface reflectivity could provide us with a more accurate spatial variability in surface melt. Figure 2-29 shows an example of such an albedo map for a particularly cloudless day in the Kangerlussuaq region (16 July 2009). But before implementing MODIS-derived albedo in our melt model we will need to take a few necessary steps, such as the validation of the satellite data with our AWS observations, the interpolation over clouded areas/periods, and the removal of artefacts (e.g. the specks of 'land' on ice and the stretch lines on the right hand side of Figure 2-29).

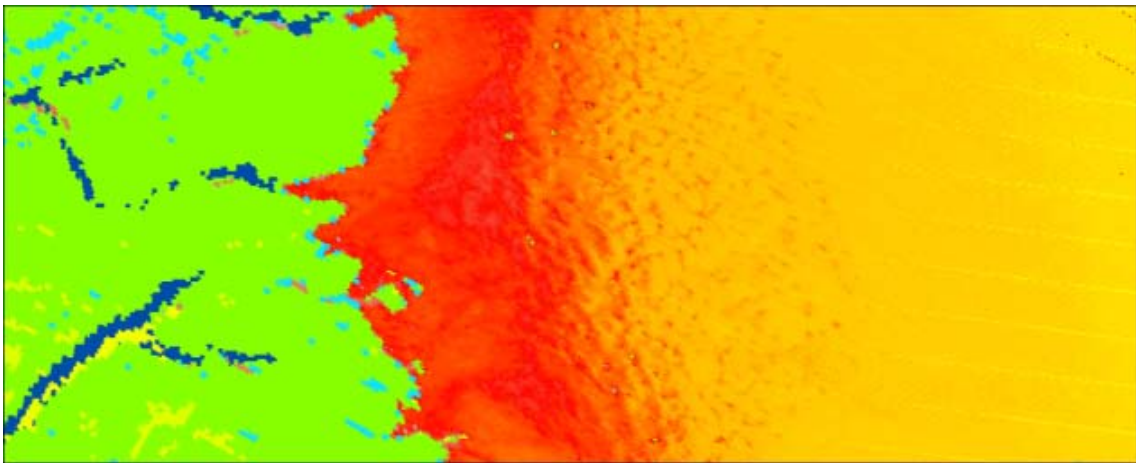


Figure 2-29. MODIS snow and ice albedo map of 16 July 2009 for the approximate area shown in Figure 2-24. High albedo is shown in orange, low values in red. Green indicates bare land, dark blue is water and light blue are clouds.

2.3 Geodetic quality GPS acquisition across the Russell Glacier Catchment

In simple terms, GPS receivers measure the travel-time for a radio signal emitted from a satellite. Computing three of these measurements from different satellites, with known orbital positions, gives a 2D position and four or more measurements give a 3D position. In practice, GPS receivers make many measurements from multiple satellites and use complex mathematics to minimize the errors caused by variations in the radio signal propagation through the troposphere and ionosphere. The ability of relative (or differential) positioning to achieve cm to mm scale accuracy is due to the GPS system's ability to measure carrier phases to about 1/100th of a cycle – which equals about 2 mm in linear distance /Leick 2004/. In addition, the high frequency L1 and L2 frequencies penetrate the ionosphere relatively well and as the time delay caused by the ionosphere is inversely proportional to the square of the frequency its effects can be effectively reduced using interferometry between carrier phase observations at both frequencies. Dual frequency observations are especially important for long base lines where synchronised satellite observation may be lower and the differential ionospheric delay is likely greater.

2.3.1 GPS data collection

Data collection commenced in July 2007 with the installation of seven geodetic GPS receivers (Trimble NetRS) across RGC. Four new GPS receivers (Trimble R7s) were installed in September 2008 and a further two in 2009 (Trimble 5700s) adding to the network (Figure 2-30). Power and memory capacity problems have led to some interruptions in the data acquisition. Solutions to these issues are constantly being developed in order to optimise data-acquisition against logistical limitations. In 2010 these problems will be addressed through larger capacity solar-panels, upgrading all permanent stations with Forgen wind-generators and through bespoke intelligent power management and regulation. Also in the 2010 season all receivers will be serviced (with new batteries where required) and in total 15 new receivers will be installed (four permanent and 12 temporary for the melt season). Table 2-4 lists the GPS site locations and Table 2-5 summarises the data acquired.

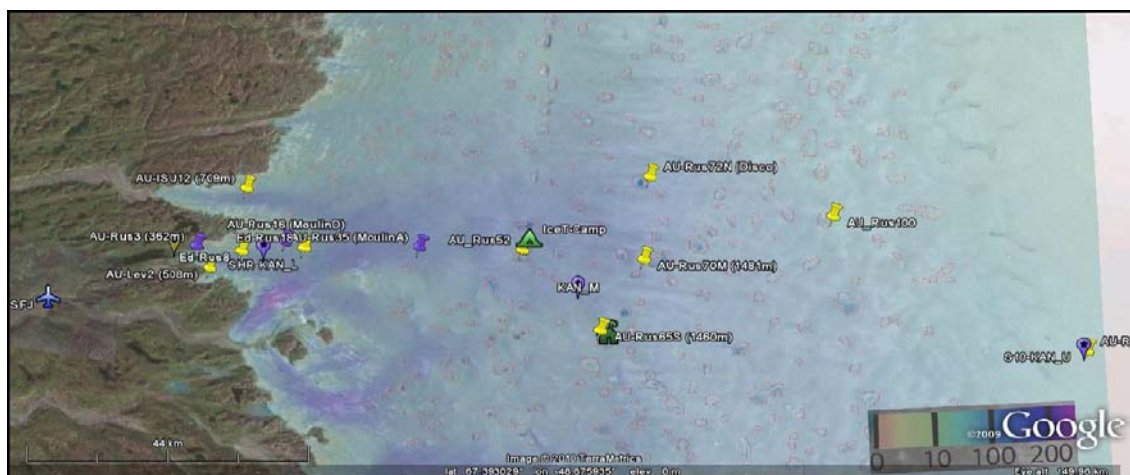


Figure 2-30. Permanent geodetic-GPS and AWS stations located across Russell Glacier Catchment shaded with mean (2002–2006) surface velocity overlain on a Landsat ETM image with outlines (red) of maximum supra-glacial lake extent.

Table 2-4. GPS sites occupied with Latitude, Longitude, Elevation and 4 letter codes.

Code	Name	Latitude (° N)	Longitude (° W)	Elevation (m)
base	Russell Base Station	67.08827	050.24749	228
kely	Kellyville Base Station	66.98742	050.94484	230
skb3	SKB3-MidS	67.00667	048.74166	391
disc	Lake Disco GPS	67.23994	048.60153	1,378
gf15	Seismo Camp	67.12649	049.00765	1,202
gf16	Ice-T West	67.12068	049.04981	1,225
gf21	Ice-T North	67.13412	049.03682	1,202
gf22	Ice-T East	67.11432	048.96621	1,246
skb1	SKB-1-MidM	67.11588	048.60423	1,381
hapy	Happy-L1	67.12080	049.03420	1,217
s10a	S10-AWS	66.99900	047.01500	1,885
lake	Lake1	67.12210	049.04480	1,510
skb4	SKB4 -Leverett	67.06450	050.13763	n.d.
s4aa	S4 (Sleepy)	67.09608	050.19279	351

Table 2-5. Data collected between 2007 and 2009. (Green: continuous record/Blue: – partial record.)

Site	2009											
	J	F	M	A	M	J	J	A	S	O	N	D
base			Green				Green	Green	Green	Green		
kely	Green	Green		Green								
Skb3		Blue										
Disc						Blue	Blue					
gf15							Blue	Blue				
gf21							Blue	Blue				
gf22							Blue	Blue				
isum	Blue											
Skb1	Blue	Blue	Blue	Blue	Blue	Blue						
hapy						Blue						
s10a				Blue								
Skb4					Blue							
lake						Blue						
Site	2008											
	J	F	M	A	M	J	J	A	S	O	N	D
base			Green									
kely	Green	Green		Green								
Skb3									Blue	Blue	Blue	
s4aa					Blue	Blue	Blue	Blue				
isum					Blue							
hapy	Blue	Blue	Blue	Blue								
lake				Blue			Blue	Blue	Blue	Blue	Blue	Blue
Site	2007											
	J	F	M	A	M	J	J	A	S	O	N	D
base												
kely	Green											
dope							Blue	Blue				
Disc							Blue	Blue				
hapy							Blue					
isum							Blue	Blue	Blue	Blue	Blue	Blue

Data acquisition issues

In 2009 there were two problems with the static base station installed on bedrock at the front of Russell Glacier in September, 2008. Prior to the service in May 2009, the antenna cable was chewed through by an Arctic Fox. In May 2009 the antenna cable was replaced and sheathed but the base station subsequently returned to default power-up mode and self-limited the quantity of files it could store thereby halting acquisition mid-July 2009. These problems have now been solved— the antenna cable is protected in hose; and the GPS is permanently configured to record all the data to one file. The receivers are powered by both internal batteries and two external 12 V 60–95 Ah lead-acid batteries. They are charged by a 38–78 W solar panels and 15 W Forgen vertical axis wind generators. They were initially regulated using standard Sunguard 4 Amp regulators. Despite this, battery failure has interrupted data acquisition especially during low-light/temperature periods in winter. Bench investigations of power-up and power-down voltages and conditions yields insight into conditions for optimal winter GPS acquisition and a more advanced regulator and an intelligent power management system has been developed and will be tested in spring/summer 2010.

2.3.2 Data processing

A long base-line kinematic GPS processing strategy is applied which assumes the antenna is moving and calculates a new coordinate triplet (x , y and z) for every measurement epoch /King 2004/. Processing is carried out using the TRACK script which is part of the GAMET/GLOBK suite of GPS processing software maintained by the Massachusetts Institute of Technology (MIT). TRACK runs under the Linux operating system and takes as input: at least one RINEX (Receiver INdependent EXchange) file from an off-ice static base station; at least one RINEX file from an on-ice receiver (said to be roving); a SP3 Precise Ephemeris file produced by the International Geodesy Society and a TRACK command file written by the user. The precise ephemeris file includes data on the precise orbits of the GPS satellites. The TRACK script applies a differential correction to the rover data against the off-ice base station. File recording problems with the base station sited at the front of Russell Glacier meant the base station record was incomplete. Where this data was missing, a differential correction was made against Kellyville base station, located ~ 16 km west of Kangerlussuaq. Unfortunately the Kellyville record is also partial, as the GPS receiver is turned off when the Kellyville radar is operating. This means there is a small amount of rover data (data from receivers on the ice) which cannot be differentially corrected using TRACK. Whilst an alternative base station is being sought, the Automated Precise Positioning Service (APPS) offers an alternative means of processing.

Processing Steps in TRACK

- (a.) Convert the raw receiver files into RINEX format using Trimble DAT conversion software, Trimble Convert to RINEX software or Leica Geomatics Office (LGO) and TEQC.
- (b.) Time bin the RINEX files into daily sections using TEQC.
- (c.) Acquire and concatenate precise ephemeris files into weekly sections with one day before and one day after to allow processing across the week boundary.
- (d.) Obtain a priori site coordinates using the Scripps COordinate Update Tool (SCOUT) provided online by the Scripps Orbit and Permanent Array Centre (SOPAC) or using APPS.
- (e.) Write TRACK command file and execute TRACK to process daily files.
- (f.) Examine summary file and check to see if ambiguities have been fixed. If not satisfactorily fixed re-run track with altered parameters.
- (g.) Plot the results using MATLAB.
- (h.) Concatenate daily NEU files and plot in MATLAB.

Processing using Automated Precise Positioning Service

NASA's Jet Propulsion Laboratory (JPL) updated their Auto-Gipsy web-based-GPS-processing service to allow kinematic GPS processing. The processing is fully automated and takes place on a computer at JPL. The stated accuracy is ± 3 cm. RINEX files are uploaded via a web browser and the results are sent by e-mail. Figure 2-31 was produced by averaging the position and time from daily APPS solutions and calculating the velocity. APPS does not require a base station reference and so allows processing of datasets when the base station record is incomplete. The advantage of using TRACK over APPS lies in TRACK's ability to solve kinematic positions at high sampling frequency (at least every second) and with good data the capacity to solve position at greater accuracy (mm-level) than APPS.

Ongoing improvements to processing techniques

APPS processing will be enhanced with potential secure FTP access to the APPS service allowing automated batch processing. Access to the GIPSY software, which is the software behind the APPS service, is also being sought. Track processing techniques are being improved, with recent development in understanding of the ambiguity fixing procedure. This will allow more robust solutions and greater accuracy and reliability. Batch processing using shell scripts is being developed to automate and speed-up data processing.

2.3.3 Results

Daily plots

With high quality and continuous data, TRACK processing enables accurate kinematic resolution of positions at every measurement epoch. Data measurement rates in use on the RGC vary between 1 and 15 seconds. Figure 2-33 illustrates changes in the displacement of the receiver in metres from the first measurement epoch on the 130th day of the year (DOY 130) for site S10. The x-axis is labelled the time. The data record for DOY 130 was not complete. Note the change in y-axis scale between graphs. Figure 2-33 shows negligible north/south and vertical motion and 6 cm of displacement to the west. This motion is expected for S10 which is situated ~ 90 km from the terminus of Russell Glacier.

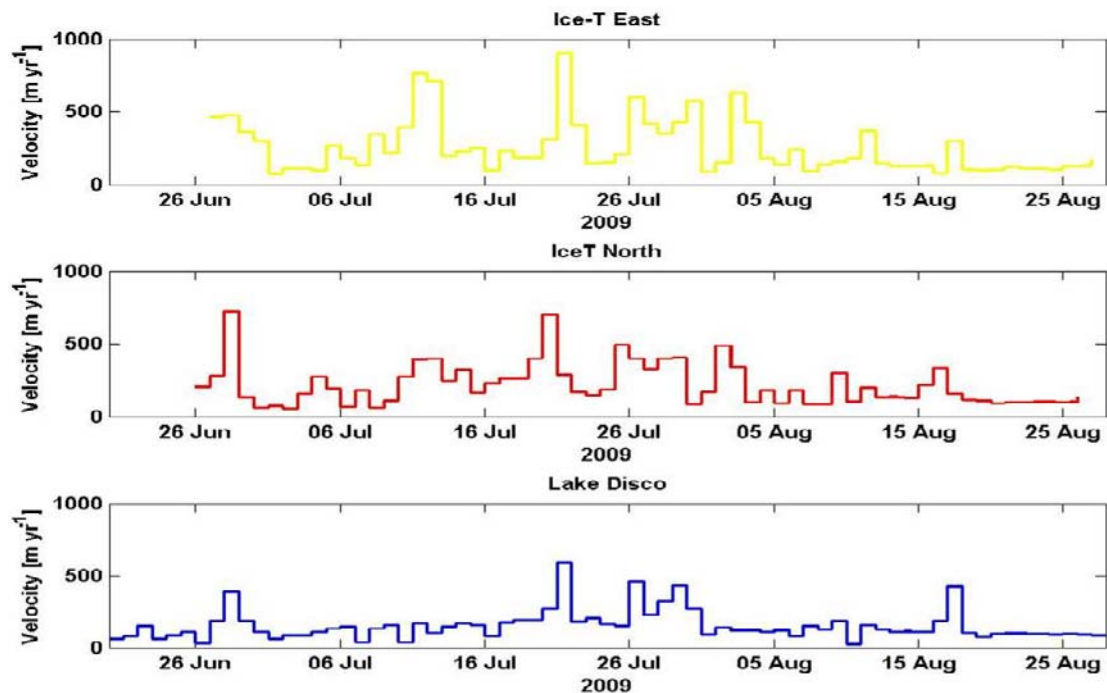


Figure 2-31. Time-series of daily ice velocities for sites Ice-T East, Ice-T North and Lake Disco in 2009.

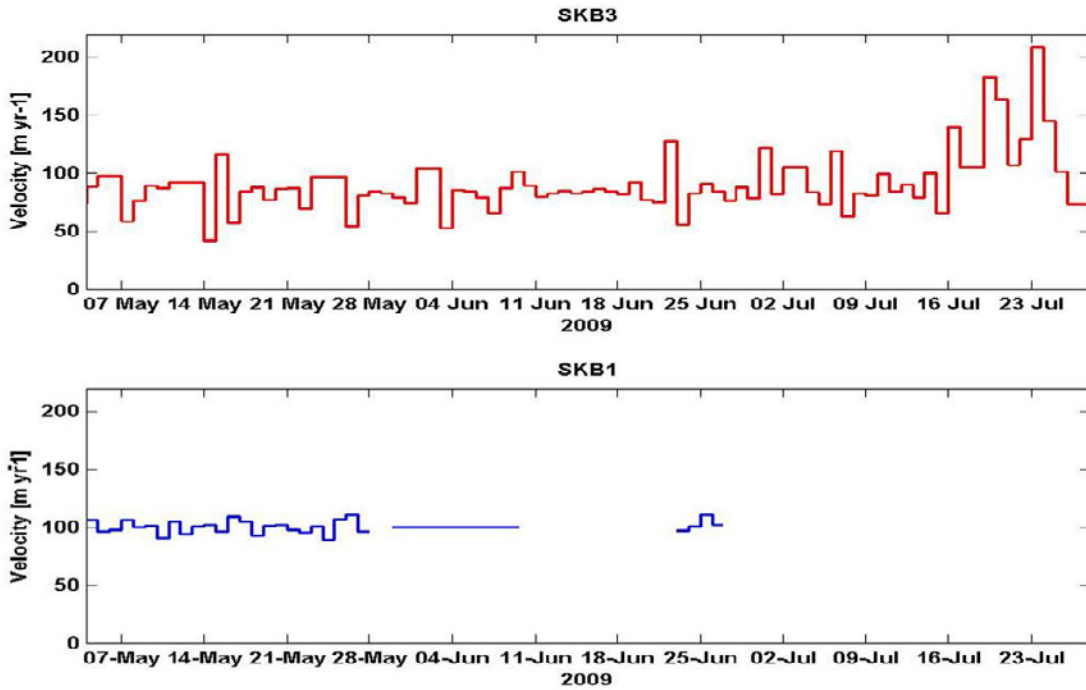


Figure 2-32. Daily ice velocities for Skb1 and Skb3. Plot of Skb3 (top) shows a seasonal variation in velocity from a mean winter time velocity of 50–100 m yr⁻¹ to a greater than doubling of velocity commencing on the 18th July coincidental with the timing of the peak melt. Skb1 shows less variability with a mean velocity of 100 m yr⁻¹. Skb1 not complete due to power up difficulties.

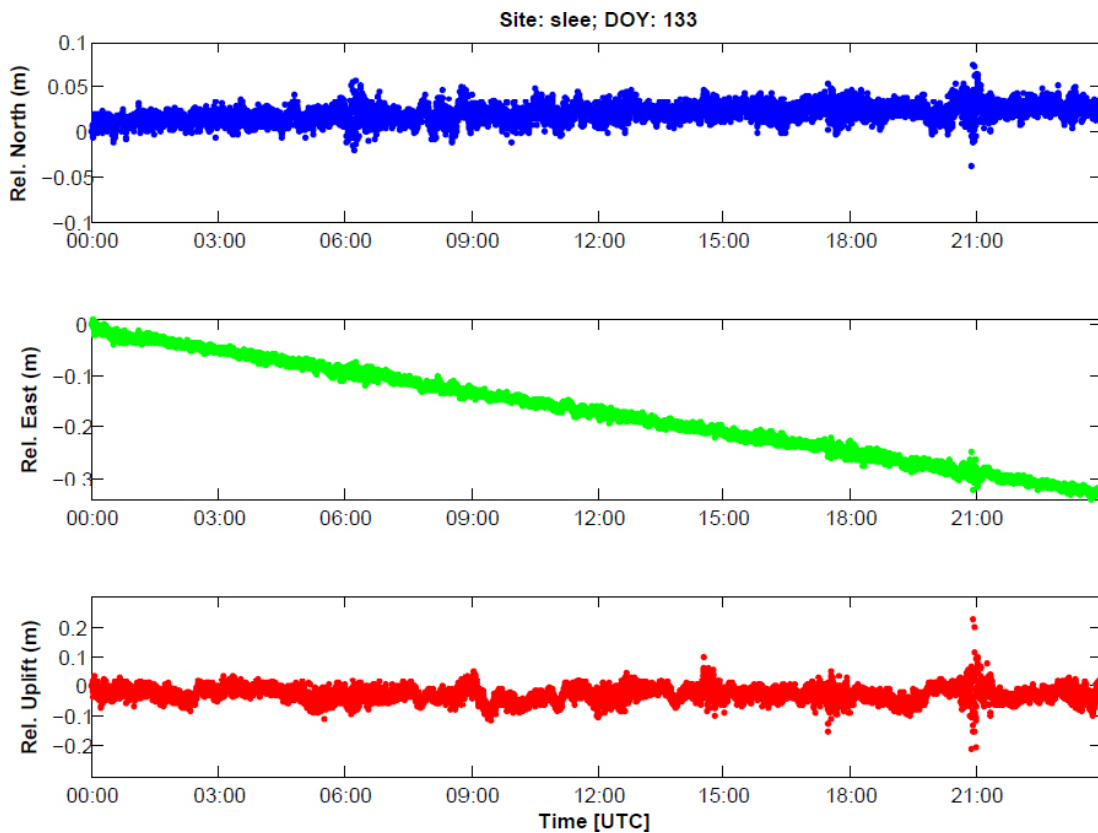


Figure 2-33. Relative North, East and Uplift for GPS Site SLEE on day of year (DOY) 133 showing displacement north (*n*), east (*e*) and up (*u*). Note the intentional change in axis scale between subplots.

Figure 2-34 illustrates hourly variations in velocity calculated from the average hourly position for site coded SLEE located at S4. For the same site, Figure 2-35 shows motion to the North plotted against motion to the East with 35 cm of movement to the West throughout the day.

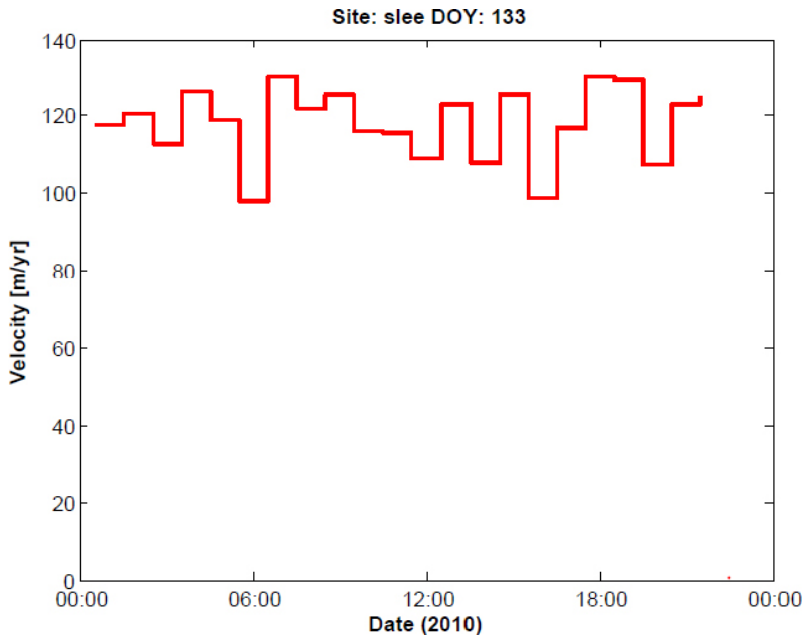


Figure 2-34. Hourly ice velocity for site SLEE located at S4 which varies $\sim 120 \text{ m a}^{-1}$.

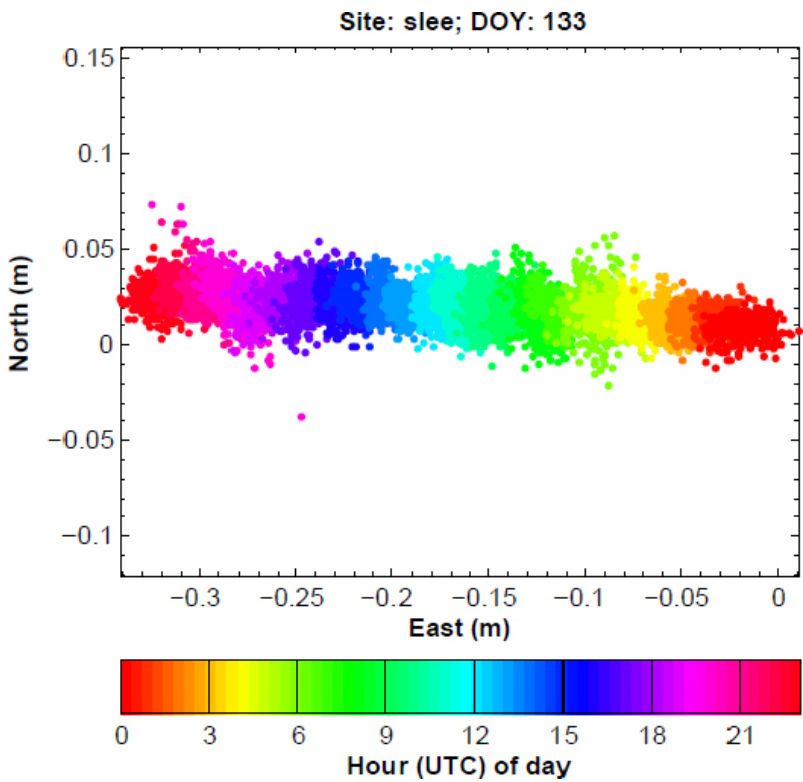


Figure 2-35. 24 hours of north vs east relative displacement at site SLEE, located at S4 indicating 35 cm of movement to the west. Time is indicated by the colour bar. Note on the x-axis easterly motion is taken as positive and westerly motion as negative. Likewise on the y-axis, northerly motion is positive and southerly motion is taken to be negative.

2.3.4 Future processing

Further work will involve processing all the data using TRACK and APPS software and plotting daily, daily range and weekly to seasonal trends in velocity. Mean winter time velocity will be subtracted from the peak daily velocity calculated hourly or 4-hourly allowing the trend in peak velocity to be plotted. In 2010 the RGC k-GPS network is to be substantially revamped (pre-2008 units are to be upgraded to SKB station standard – Forgen Wind-generator, 48 W solar panel, deep-cycle and larger battery capacity, intelligent regulation and power management) and boosted to ensure reliable acquisition and optimal coverage. In May 2010, four additional permanent GPS stations will be installed (two replacing defunct NetRS stations at Isunngata Sermia and S4 sites) and an additional 12 temporary stations will be installed from May/June until September 2010. These temporary stations will be configured in three strain diamond configurations centred on permanent stations located to support GAP SP-B and Ice2Sea (IMAU and AWI, <http://www.ice2sea.eu/>) who aim to hot water drill across Isunnguata Sermia and at SHR respectively to access and instrument the ice-bed interface.

2.4 Geophysics: radar sounding trials (Spring 2009)

A deep-look radio echo survey (RES) was carried out over 32 hours in early-May 2009 across RGC at $\sim 67^\circ$ N to assess and trial the deep look radar systems, mode of transport and safety. The purpose of the pre-survey was to acquire sufficient ice thickness data to provide insight into the mean geometry and variability in bed relief, to potentially identify englacial hydrological features and characterise basal hydrological conditions. In the following, the methodology employed in Spring 2009 is described, the results are presented and discussed, and finally the improvements for 2010 are presented.

2.4.1 Radar data acquisition

The RES was conducted along a number of tracks: i) 20 km to the west of SGL Ice-T towards a large moulin that is known to drain SGL Ice-T; ii) 50 km inland to the east of Ice-T Lake towards S10-AWS; and iii) 20 km to the north-east of Ice-T Lake towards Lake Disco (Figure 2-36).

Data were acquired using a 5 kV Kentech Instruments transmitter (Tx) with a pulse repetition frequency (PRF) of 1 kHz. The centre frequency of the antenna is determined by the antenna length with 20 m half-length dipole antennas producing a theoretical centre frequency of 5 MHz (3.5–4.0 MHz on analysis of data). The transmitter and receiver (Rx) were mounted on individual sledges separated by 60 m. The antennas, protected in hose, were attached fore and aft of the transmitter and receiver sledges. Both sledges were towed behind a skidoo at ~ 12 to 25 km h^{-1} . Each recorded trace is the average of a number of individual waveforms stacked approximately every 20 m. Profiles were recorded with different stacking and time window parameters to allow the optimum parameters to be selected (see Table 2-6). As there is a lack of data on ice thicknesses and bed elevation for the study area it was necessary to experiment with time windows ranging from 10,220 to 20,460 ns. Assuming a constant radio wave velocity in ice of 0.168 m ns^{-1} these time windows allow a depth penetration through ice ranging between 860 and 1,720 m respectively.

Table 2-6. Radar system specification and parameters.

Time Window	10,220–20,460 ns
Depth Penetration	860–1,720 m
No. of Stacks	64, 128, 256, 512
Sampling Interval	20 ns
Sampling Frequency	50 MHz
Pulse Repetition Frequency (PRF)	1 kHz
Transmitter Peak voltage	$\pm 2 \text{ kV}$

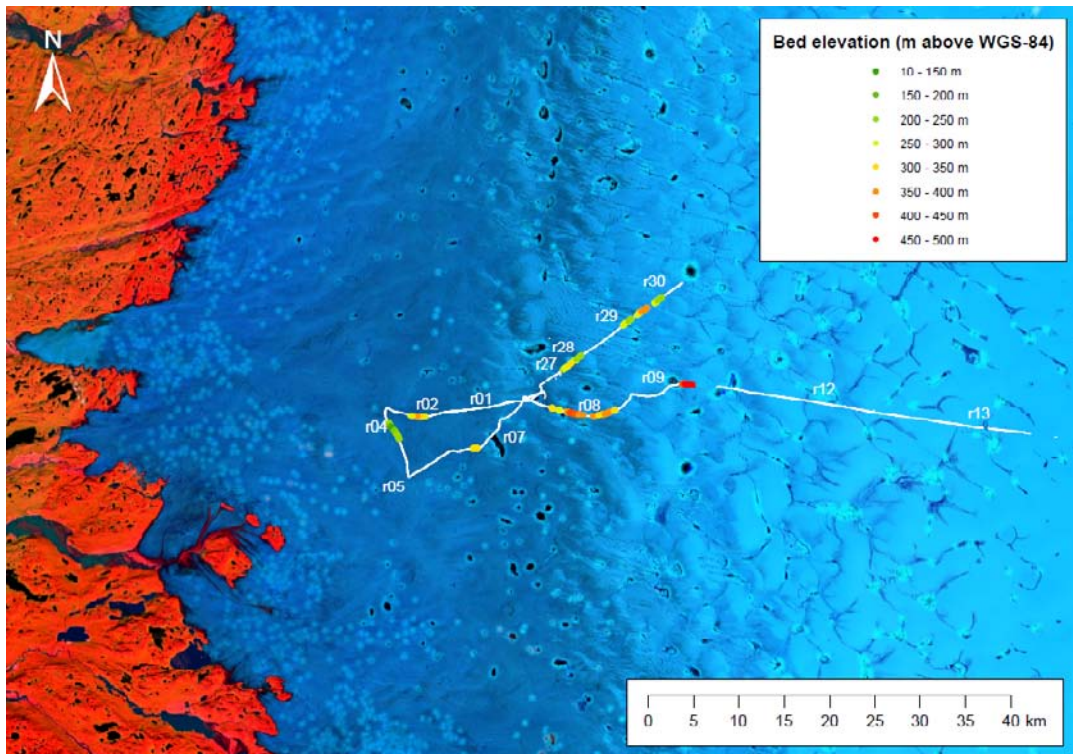


Figure 2-36. Location map of all radar profiles acquired in spring 2009 and picked (100% positive) bed elevation [m above WGS-84] data across RGC. Only selected lines are labelled for clarity. Permanent GPS and AWS sites are represented by green dots.

Position data acquisition

A Trimble Pathfinder XRH differential GPS recorded the latitude, longitude and altitude of each stacked waveform. The GPS simultaneously recorded kinematic GPS data which allows precise kinematic positions to be determined. During the survey anomalous times and positions were recorded by the GPS. It is possible that these are due to the obstruction of the antenna or loss of GPS signal. These anomalous positions were easily and effectively removed. MATLAB scripts were written to output CSV files for each profile that were converted to shapefiles and read into ArcMap. These profiles allow certain diffraction hyperbolae to be associated with surface features (e.g. crevasses and moulins) identified by observation in the field and from remote sensing. Bed elevation and ice thickness shapefiles were created using the same method (Figure 2-36).

2.4.2 Data processing

MATLAB scripts were written to remove the pre-trigger time and to improve the signal to noise ratio by applying a Butterworth bandpass filter with a passband of 1–4 MHz. Anomalous results from the GPS x, y, z data were removed and remaining data were linearly interpolated and the x-axis converted to distance and each trace assigned a UTM coordinate. The y-axis was converted from two-way travel time to depth assuming a radiowave velocity in ice of 0.168 m ns^{-1} .

Below is a step-by-step description of the optimum processing flow applied in ReflexW (software tool for seismic and GPR data processing and interpretation):

- Step 1: Move start time to remove pre-trigger period so the first break arrives after 200 ns.
- Step 2: Energy decay gain (Scaling value = 0.5).
- Step 3: Bandpass filter (LC = 1.5 MHz; UC = 6 MHz).
- Step 4: AGC gain (Scaling value = 107 ns, should be around 7% of time window).
- Step 5: Correct for 3D topography and depth axis using traceheader coordinates and a $V_{\text{ice}} = 0.168 \text{ m ns}^{-1}$.
- Step 6: Make equidistant traces to correct x-axis for horizontal distance.

The zero-amplitude of all bed reflectors identified from the final profiles were picked in ReflexW. The picks were exported as ASCII files and the two-way travel time (TWTT) was converted to ice-thickness using a radiowave velocity through ice of 0.168 mns^{-1} . From comparison with borehole measurements /Macharet et al. 1993/ suggests the accuracy of ice-thickness measurements determined in this way is in the region of $\pm 8\%$. Following this, the bed elevation was determined by subtracting the ice thickness from the ice surface elevation.

2.4.3 Results

Results were processed and plotted in MATLAB (e.g. Figure 2-37) and ReflexW (e.g. Figure 2-38). Simple diffraction hyperbolae were interpreted as bed reflectors (indicated by white arrows, in Figure 2-37, Figure 2-38 and Figure 2-40). More complex and often stacked diffraction hyperbolae are interpreted as moulins (e.g. left hand side of Figure 2-37), crevasses or supraglacial lake or stream features (e.g. right hand side of Figure 2-39).

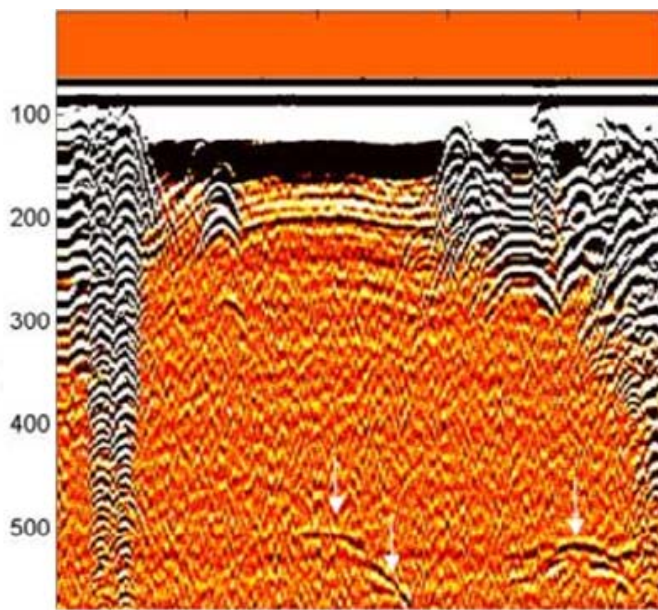


Figure 2-37. Profile r04 processed in MATLAB. Y-axis label denotes sample number not depth.

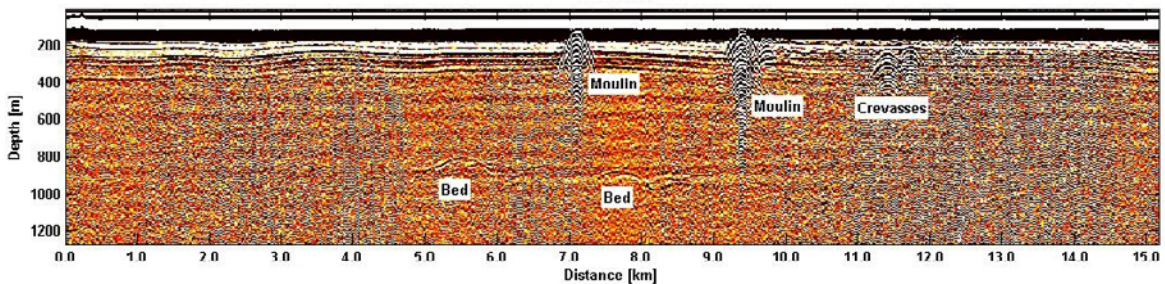


Figure 2-38. Profile r08. Processed and plotted in ReflexW.

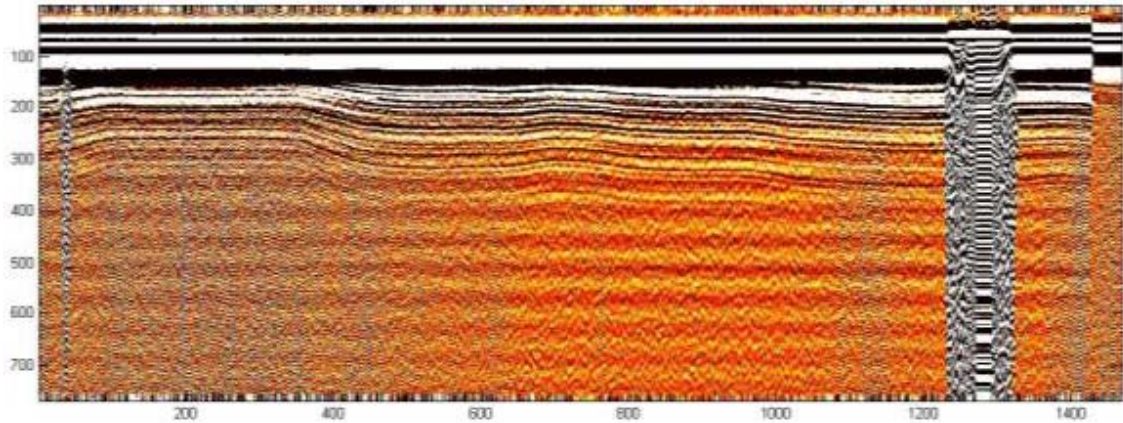


Figure 2-39. Profile for concatenated data for r12, 13 and 14. No bed returns likely due to too low a travel time. Ringing due to passing over a supraglacial lake can be seen on the right hand side of the profile.

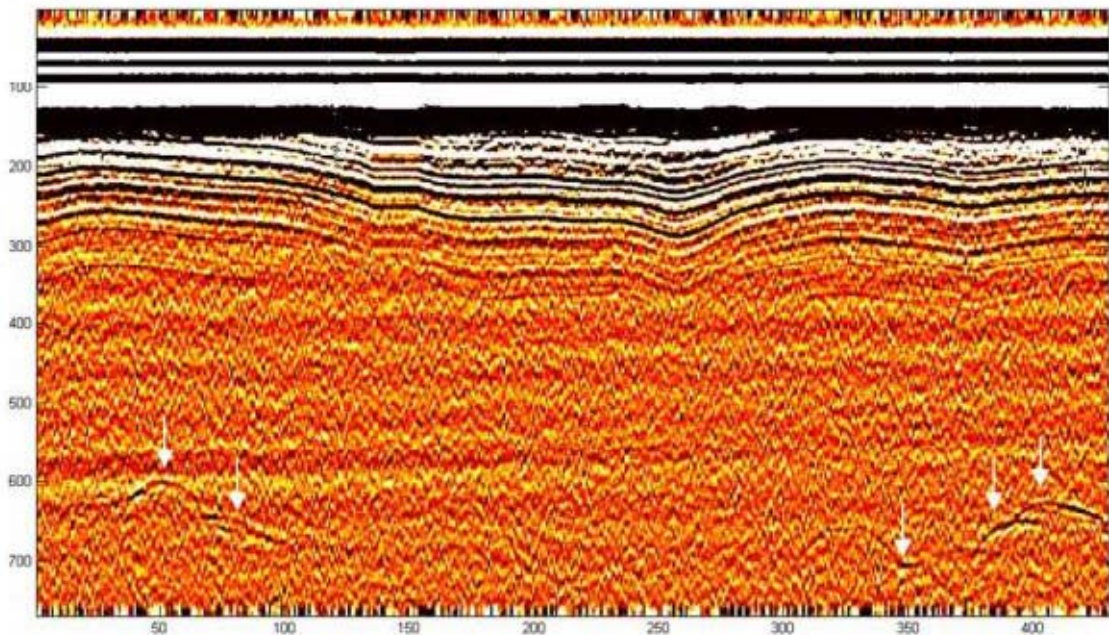


Figure 2-40. Profile for concatenated data for r28 and r29. White arrows show bed return at the start and end.

2.4.4 Data acquisition issues

The detrimental effect of excessive skidoo speed on data quality

Profile r09 (Figure 2-41, Figure 2-42 and Figure 2-43) demonstrates the effect skidoo velocity has on the quality of the radar data and the amount of bed returns.

The skidoo speed is plotted on Figure 2-42. During the first half of profile r09 the speed was $\sim 27 \text{ km h}^{-1}$. At around 80 traces the skidoo stopped and the radar was left running (standstill removed on Figure 2-41). After starting again the radar crossed over a supraglacial lake buried in snow (Figure 2-43) and then continued at a slower speed of $\sim 20 \text{ km h}^{-1}$.

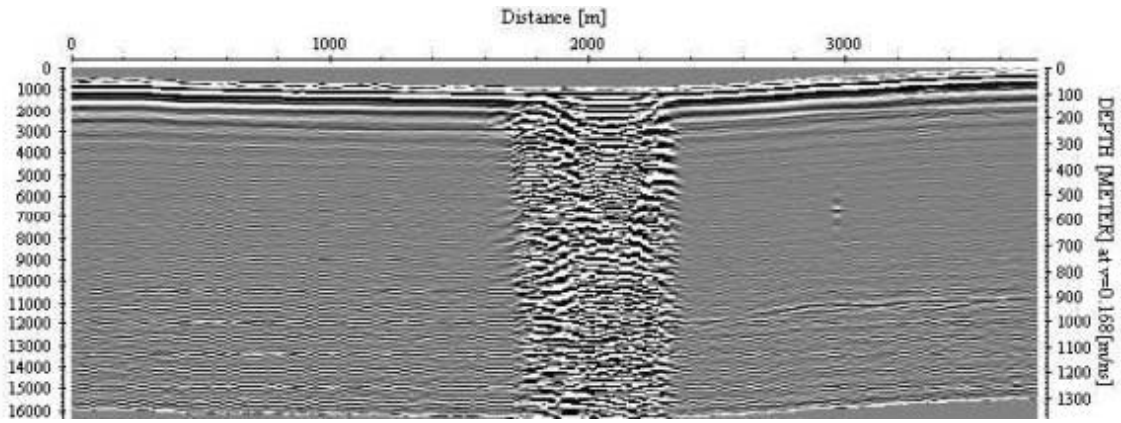


Figure 2-41. Radargram after processing in ReflexW of profile r09.

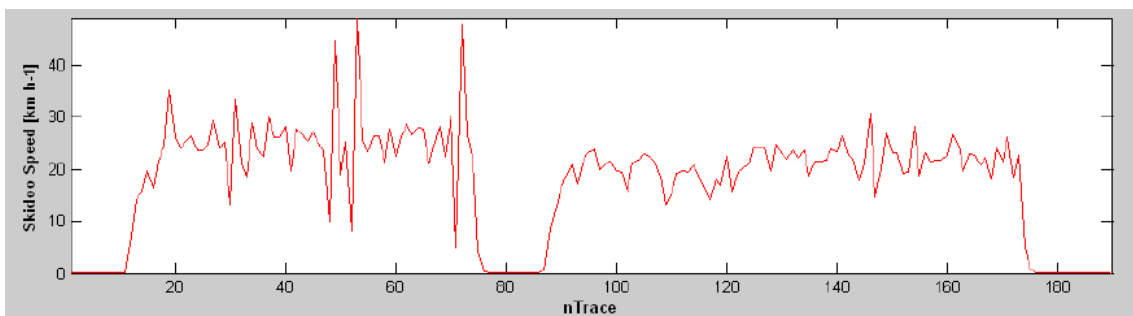


Figure 2-42. Plot of skidoo velocity against trace number for profile r09.

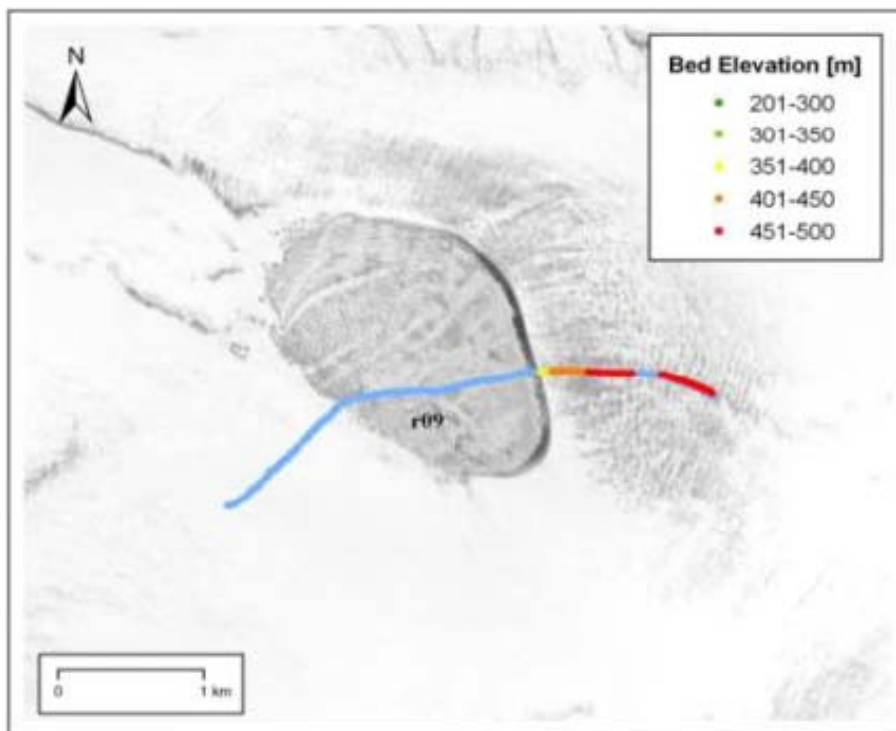


Figure 2-43. Map of bed returns from profile r09 overlaid on a 15 m resolution SPOT imagery of a supraglacial lake. The blue line is the skidoo track. The bed elevation colour scheme ranges from green (~ 100 m.a.s.l.) to red (~ 5–600 m.a.s.l.). Bed returns only obtained at slower travel velocity to the right of the lake.

After the lake, and whilst travelling at this slower speed, a continuous return from the bed was recorded. It should be noted that good data was collected whilst travelling at $\sim 25 \text{ km h}^{-1}$ on profile r08 (Figure 2-38). To improve data density and quality, the radar system should be towed behind a skidoo at $\sim 10\text{--}12 \text{ km h}^{-1}$. In addition to this, the number of stacks should be increased, possibly by increasing the PRF of the transmitter and the acquisition rate of the A/D converter used to log and store the return signal. However, there is a tradeoff with these parameters and Dr. Petterson has refined and optimised these parameters with new 16 bit A/D boards which are placed in rugged IP67 industrial 12 V computers rather than via a laptop.

Time Window Duration

The time window during profile r07 (Figure 2-44) was set to 10,220 ns allowing a depth penetration in ice of $\sim 860 \text{ m}$. One bed return can be seen at 4,600 m and $\sim 810 \text{ m}$ depth below the ice surface and this appears to be the top of a peak in bedrock elevation (Figure 2-44 – NB bed return is not that obvious in figure but can be seen as a small black reflector marked with white arrows). The pre-trigger period must be taken into account. This is the period before the first break of about 1,000 ns. The time window must therefore include an extra 1,000 ns (or whatever the pre-trigger period is set to) than is necessary for the required depth penetration. Profiles r12, r13 and r14 are orientated eastwards from Ice-T Lake towards S10-AWS (Figure 2-39). The time window was set to 14,060 ns. Taking into account the pre-trigger period this gives an effective time window of 13,060 ns and an effective depth penetration in ice of 1,100 m. Ice thickness from profile r09 (Figure 2-41) $\sim 2 \text{ km}$ down glacier of r12 and 50 m lower in elevation measured $\sim 920 \text{ m}$. It is therefore likely that the ice thickness exceeding the chosen time window is the main reason for no bed returns in profiles r12, r13 and r14 (i.e. due to too short a time window).

2.4.5 Ice thickness and bed elevation

Measured ice thicknesses range from ~ 690 to $\sim 1,140 \text{ m}$ with a mean ice thickness of 916 m (see Figure 2-36). Ice thickness increases with surface elevation as expected. The closest bed return to Ice-T Lake indicates an ice thickness of $\sim 870 \text{ m}$ and bed elevation of $\sim 340 \text{ m}$. The closest bed return to the moulin indicates a bed elevation is $\sim 300 \text{ m}$ and the ice thickness is $\sim 760 \text{ m}$. From this study, bed elevations in the area range between ~ 130 to $\sim 490 \text{ m}$ above WGS-84. More radio echo sounding profiles are required to map the bed in detail.

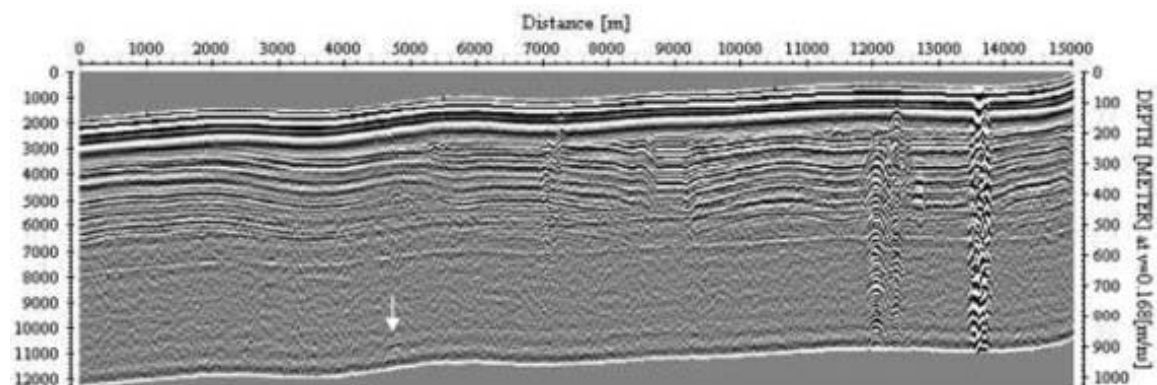


Figure 2-44. Radargram for profile r07. With close inspection one bed return can be seen marked by the white arrow. It is likely the time window was set too low for the ice thickness.

Improvements learnt from 2009:

- i. Frequent and systematic Centre Mid-Point surveys to characterise and refine acquisition parameters.
- ii. Securely mounting the GPS antenna 1 m above the sledge would prevent antenna obstruction.
- iii. Precise kinematic position data corrected against a static, local and on-ice base station would allow more accurate position measurement.

Each recorded trace is theoretically a time-domain record of reflections from subsurface features located directly below the centre-point between the transmitter and receiver antennae. The GPS used in this survey was mounted on the front of the receiver sledge. Recording the position of the receiver sledge is sufficient for processing long radar lines however greater position accuracy is desirable for accurately determining the position of reflectors. This can be achieved using kinematic GPS (kGPS) by at least three different methods:

- i. Computing the transmitter position at each trace by subtracting the measured antenna separation from the coordinates measured by the GPS mounted at the receiver in the opposite direction to the track azimuth.
- ii. Towing a kGPS on a separate sledge located at the centre point of the antenna separation and logging autopoints every second.
- iii. Mounting two kGPS: one at the receiver; and one at the transmitter, and recording autopoints every second.

2.4.6 Radar operations in 2010

Three different radar systems will be deployed in 2010. 1) A low-frequency impulse system will be used for catchment-scale mapping of properties and bed elevation (as above). 2) A novel continuously logging radio-echo sounding system will be used to study temporal evolution of basal hydrology, and, 3) a Frequency-Modulated Continuous-Wave (FMCW) radar system will be used for detailed high resolution studies around supraglacial lakes and moulins. Below is a summary of the work that has been done during 2009 on the different radar systems.

Impulse Radar System

During autumn 2009 an upgrading and improvements on an existing impulse radio-echo sounding system was started. This system will be finalized and complemented with a second identical system during winter/spring 2010. The experience gained by modifying the existing system will make it easier and faster to put together the second system during 2010.

The radar systems consist of receiver electronics and computer, an impulse transmitter of radio-echo sounding signals and resistively loaded dipole antennas built to have high tensile strength to avoid breaking while the system is dragged behind the snowmobile. The transmitter and receiver electronics will be battery powered and are mounted with shock absorbing suspension mounted in a plastic case. The cases will also have fittings to be easily mounted on snowmobile sleds. The new system will be tested on Svalbard in early March 2010.

Modification of the receiver electronics and computer has been completed and acquisition software for the new electronics has been developed. The following system upgrades are complete:

- New receiver and transmitter cases from *Hardigg Cases Inc.* has been ordered and delivered. The cases have been modified to fit transmitter and receiver electronics as well as mountings for securing the cases to snowmobile sleds.
- New shock absorbing suspension for the electronics mounted in the cases has been developed and manufactured.
- A new A/D converter has been ordered. The new board has 16-bit resolution and a sampling rate of 400 Ms/s and an analogue bandwidth of 165 MHz. The board is expected to be delivered in February 2010. A board for the second system will be ordered in January 2010.
- The existing acquisition-software has been adopted for the new A/D board, however, since the board has not yet been delivered any substantial bug testing and verification has not yet been done.
- A new ruggedized industrial grade computer has been delivered. The system is verified to down to -40°C and has high shock and vibration tolerance.

Continuously Logging Radio-Echo Sounding System

The start of development of a complete new autonomous continuously recording radio-echo system was initiated during 2009. The system is intended as a stationary unit that will switch on and measure and store radar waveforms at even time intervals over a full year.

The radar system is intended to be built from relatively cheap components to minimize losses if the system cannot be recovered and it needs also to have low power consumption to be able to run as long as possible. The system is intended to include an A/D converter with logging capacity to a solid-state data card and a low power transmitter.

A prototype of the receiver electronics has been developed. The system has 8-bit resolution and an analogue bandwidth of 65 MHz and sampling rate of 100 Ms/s. It is based on Field-Programmable Gated-Array (FPGA) technology with an A/D converter. However, the system still needs development of data storage capacity and a cheap powerful transmitter needs to be designed before a fully functional system exists.

FMCW radar

An existing helicopter mounted FMCW radar system intended to be used for detailed high resolution studies in late 2010 on the Greenland Ice Sheet requires upgrading to work optimally for measurements through thick and broken ice characteristic of RGC. The system needs to be modified i.e. increase transmitted power and range gating (device for switching transmitter part off while receiver is recording to eliminate the risk of saturating the receiver). The design of amplifier and range-gating components started in 2009.

During 2009 the concept of a range-gating device has been developed but not built or tested. The range-gate device consists of a series of RF-switches controlled by a logical circuitry. The range-gate device is called “free floating”, which means that the switching is done without triggering and with an even time interval. This concept has been proven to work on continuous systems in earlier studies. Suitable amplifier stages have been investigated and identified.

2.5 Geophysics: passive seismic trials

Swansea University have committed to conducting a range of passive (labelled A) and active (labelled B) seismic experiments in 2010, contributing to the following specific aims and objectives:

- i. What are the hydrological, mechanical and rheological controls on surface to bed melt water routing?
- ii. How do the basal hydrological system and thermal regime respond to variable inputs of melt water on diurnal to seasonal and supraglacial lake-tapping scales?
- iii. How does the basal hydrological system evolve and interact with overlying ice to determine temporal and spatial distributions of basal stick/slip traction which, in turn, governs basal decoupling?
- iv. Isolate the principal mode of basal motion of the ice-sheet region of the Russell Glacier Catchment.
- v. Identify and characterize the modification of that mode as forced by catastrophic ingress of surface-derived meltwaters.

We are confident that, together, the passive and active seismic experiments in summer 2010 will enable characterisation of melt water flow through moulins or crevasses from the ice sheet surface to the base, and the fate of that melt water upon ingress to the subglacial environment together with any ice-sheet mechanical response. A further aim is the characterisation of the geological setting underneath the ice sheet, including any potential fault-related processes that generate seismic energy and have similar characteristics to those recorded for earthquakes. The data will support a range of numerical models of ice sheet hydrology and rheological (flow) response to the hydrological forcing.

2.5.1 2009 field trial program, equipment and installation

The principal aim of the preliminary field season in 2009 was to identify the most promising strategy to install seismometers on a rapidly melting and water-logged surface, so that appropriate preparations could be undertaken prior to the main 2010 field season. A total of 8 days (22–29 June 2009) was spent on site at the ICE-T lake testing the passive seismic stations. A decision was then made to install the stations as reliably as possible, and leave them logging automatically until September 2009, taking advantage of the opportunity that arose for Dr. Hubbard to uplift the stations in September.

Kulesa and Hubbard were able to secure a loan of a total of 12 high-frequency passive seismic stations through the NERC's SeisUK geophysical equipment facility, for use in the 2010 summer field season. SeisUK also kindly lent us four seismic stations for testing in June 2009. This type of passive seismic station was previously used successfully by Kulesa in the Antarctic and on a glacier in the European Alps, which leaves us confident that they will also be highly suited to our work on the RGC. Each passive seismic station consists of a three-component geophone (Figure 2-45 left) connected by cable to a custom-built preamplifier and a bespoke seismograph and data logger (Figure 2-45 right). The SAQS and preamplifier have separate battery power supplies that are charged by solar panels. Apart from the geophone and the solar panel all station components are conveniently housed within a single Zarges box.

Installation of the geophones presents a particular challenge since our aim is to use these sensitive 'microphones' to receive very small ground vibrations caused by glacial or subglacial hydrological or mechanical processes. It is therefore mandatory that the geophones are firmly coupled to the ground. It is also mandatory that they are aligned to the North so that full advantage can be taken of their three-component capability. The latter allows seismic signals to be received from vertically-down and horizontally along North-South and East-West axes. Installation of the geophones on a rapidly melting and water-logged surface is a non-trivial task and requires careful in situ testing. Thus, in June 2009 we tested a host of different installation strategies, ranging from [a] mounting on custom-built brackets at the top of aluminium poles drilled into the ice; [b] deployment in shallow holes together with blanketing by snow and ice chips from drilling; possibly together with [c] mounting on concrete slabs; and [d] weighting down by batteries or other suitable items outside or within a Zarges box. We found that concepts [a] and [d] were so highly susceptible to wind noise as to be entirely unsuitable. Strategy [b] yielded good results as long as the geophones were indeed in a horizontal position, aligned to the north and covered by snow and ice. The best results were obtained using strategy [c], which will therefore form the basis of our installation strategy for the 2010 summer field season. We thus intend to mount the geophones on slabs or plugs of concrete that are firmly inserted into holes drilled into the ice surface. These slabs or plugs will additionally be guided downwards with the melting ice surface by concrete cylinders, to ensure that the geophones are protected from wind noise and are not able to either tilt or rotate away from the north.



Figure 2-45. Passive seismic equipment including (Left): three-component geophones to be installed at the ice surface, connected to (Right): SAQS passive seismic data loggers.

2.5.2 Preliminary data analysis

Following in situ equipment testing in June 2009, the passive seismic stations were permanently installed and left logging until September 2009, yielding an extensive data set (> 100 GByte) that is yet to be analysed in detail by the postdoctoral research assistant (PDRA) employed on one of the NERC grants. The PDRA will start in April 2010, and we expect exciting and pioneering results within the following few months (see next section). More specifically, we expect exciting results because preliminary data analysis is encouraging. Although most stations stopped recording useful data after a few weeks (after toppling over due to surface melt and wind), the first few weeks of data recorded by each station are consistent and useable. For example, we regularly recorded a larger number of seismic events during the afternoon and early evening, as compared with the night and early morning (compare Figure 2-46 top and bottom graph). The events shown in Figure 2-46 are attributed to glacial processes occurring within or beneath the ice. The fact that the number of events commonly increases noticeably during the afternoon is consistent with a hydrological forcing mechanism. This is strongly encouraging and is the first exciting evidence that the passive seismic data will indeed reflect the coupled hydrological-mechanical mechanisms that are the target of our study, although the exact glacial processes generating the observed seismic events remain yet to be ascertained.

Indeed, we already see consistent evidence for typical passive seismic events expected to occur at dynamic ice masses, as illustrated in Figure 2-47 based on data reported by /Stuart et al. 2005/ for the surge-type glacier Bakaninbreen, Svalbard. For instance, preliminary interpretation of upper panel of Figure 2-48 reveals the presence of a ‘Type B style’ tectonic quake followed imminently by a ‘Type A style’ ice quake. The latter is likely to reflect surface crevassing several hundred metres away, and therefore possibly originating in a crevasse field observed at that approximate distance downstream of our survey site. We are particularly excited to have noted also seismic events such as those shown in bottom panel of Figure 2-48, which are likely related to resonance to englacial water channels below the Ice-T lake. The preliminary seismic data do therefore not only appear to confirm the presence of seismic events beneath and within the ice body at the Russell Glacier Catchment, but also that the glacial processes generating them are temporally variable.

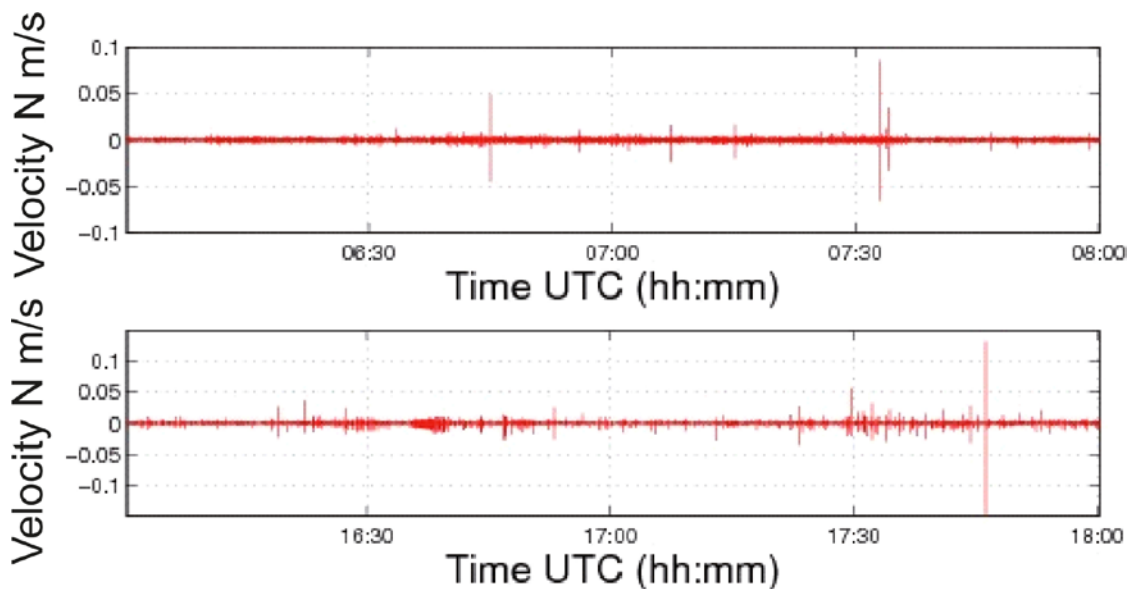


Figure 2-46. Example North component passive seismic data recorded on (top) July 10th, 2009 between 0600 and 0800 UTC; (bottom) and between 1,600 and 1,800 hrs UTC.

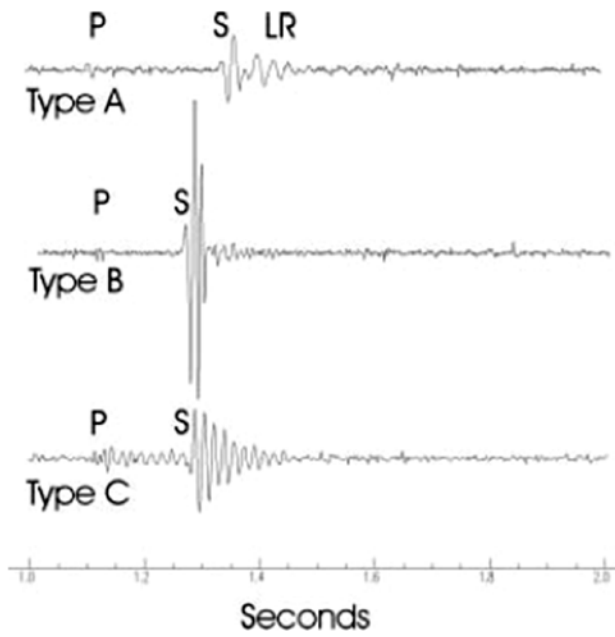


Figure 2-47. Typical passive seismic events expected at our field site(s), following /Stuart et al. 2005/. Type A: ice quakes, Type B: Tectonic-style quakes at the glacier bed and Type C: Resonance in englacial water bodies.

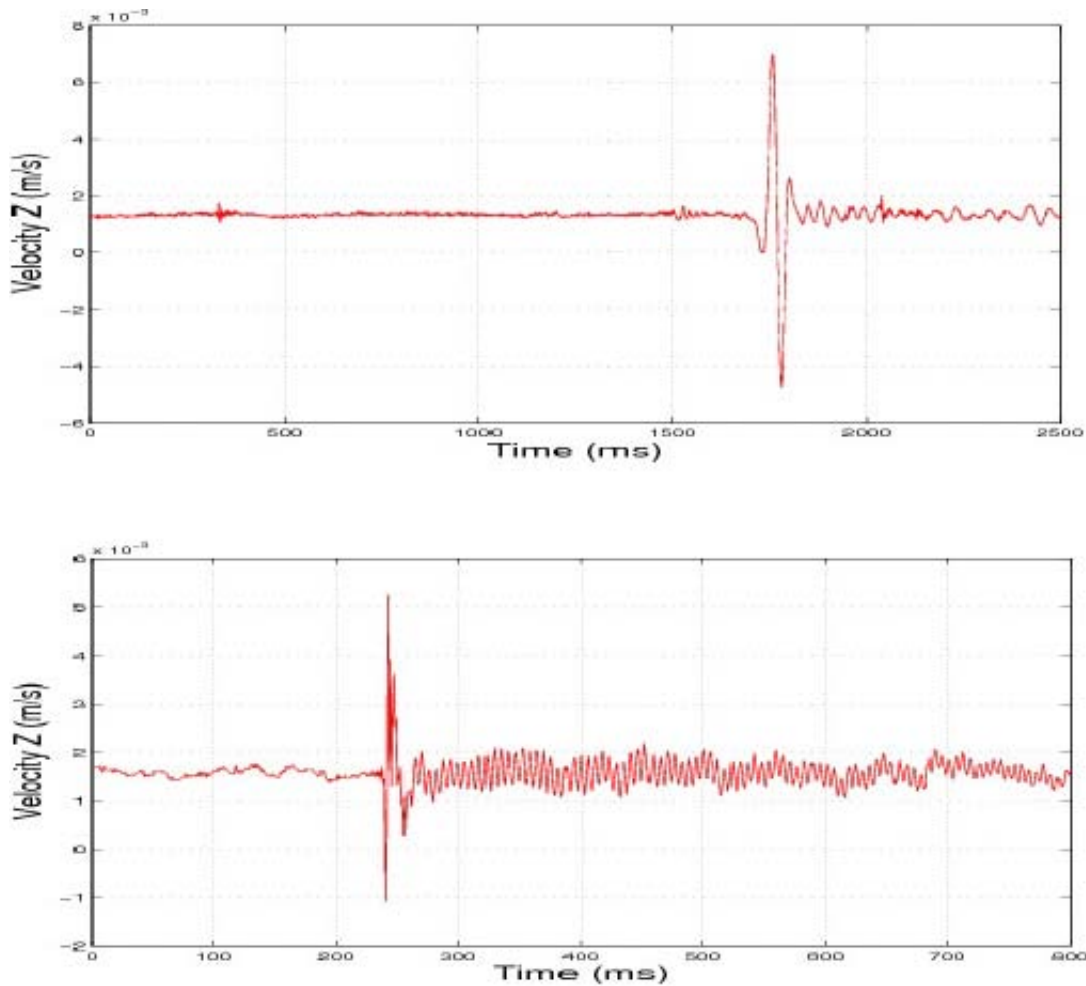


Figure 2-48. Top: example vertical component passive seismic data recorded on July 10th, 2009 that are characterized by a 'Type B style' tectonic quake followed imminently by a 'Type A style' ice quake. Bottom: example vertical component on the same day that likely reflect resonance in glacial water channels.

2.5.3 Future work

Once the PDRA has started in April 2010, we will commence an intensive 2-month period of analysis of the 2009 passive seismic data. The results will complement those to be obtained in the summer of 2010. We expect to be able to identify and characterise [a] englacial hydraulic processes as surface melt waters propagate downwards by hydro-fracture or reactivation of existing conduits; [b] subglacial hydraulic transients e.g. as such waters reach the glacier bed or as the subglacial drainage system evolves over time; [c] basal motion triggered by the ingress of surface melt waters to the glacier bed; and [d] deeper seismic activity related to tectonic processes in the crust underlying the study area. We expect, specifically, that the subglacially generated seismicity will reveal and distinguish whether inflowing water encounter: a) a warm and well lubricated bed and follows a discrete pathway incised into the ice, b) a warm and well lubricated bed but follows distributed pathways, or c) a cold bed that induces further fracturing ‘events’. Constraints on local ice thicknesses (from the radar studies) and the englacial seismic velocity structure (from seismic reflection experiments as funded by one of NERC grants) will assist identification of event foci and their temporal variability.

2.6 Tracer experiments

2.6.1 SF₆ and dye tracing

We employed sulphur hexafluoride (SF₆) via a series of tracer experiments from moulins located along a flow line at the land-terminating Russell Glacier (Figure 2-49 and Figure 2-50), about 12 km from the “K-Transect” /Wal et al. 2008/, with the aim of providing direct information on englacial and sub glacial drainage mechanisms during the height of the melt-season on Greenland /Wadham et al. in review/. SF₆ is a volatile gas and has been used across a wide range of marine and terrestrial environments to trace the flow of water where dilution is high /Watson et al. 1988, Wanninkhof et al. 1991, Gamlin et al. 2001/, but never in glacial systems. Simultaneous injections of SF₆ and Rhodamine dye (Figure 2-51) were conducted at moulins located at 2 km (Site 1; 380 m.a.s.l.; ice thickness = 180 m), 8 km (Site 2; 580 m.a.s.l. ice thickness = 370 m) and 35 km (Site 3; 1,020 m.a.s.l. ice thickness = 820 m) from the margin of the southern lobe of Russell Glacier (Figure 2-49), with concentrations monitored in the single proglacial channel. The injection sites are located within the main zone of summer ice acceleration within the Russell catchment (Figure 2-49).

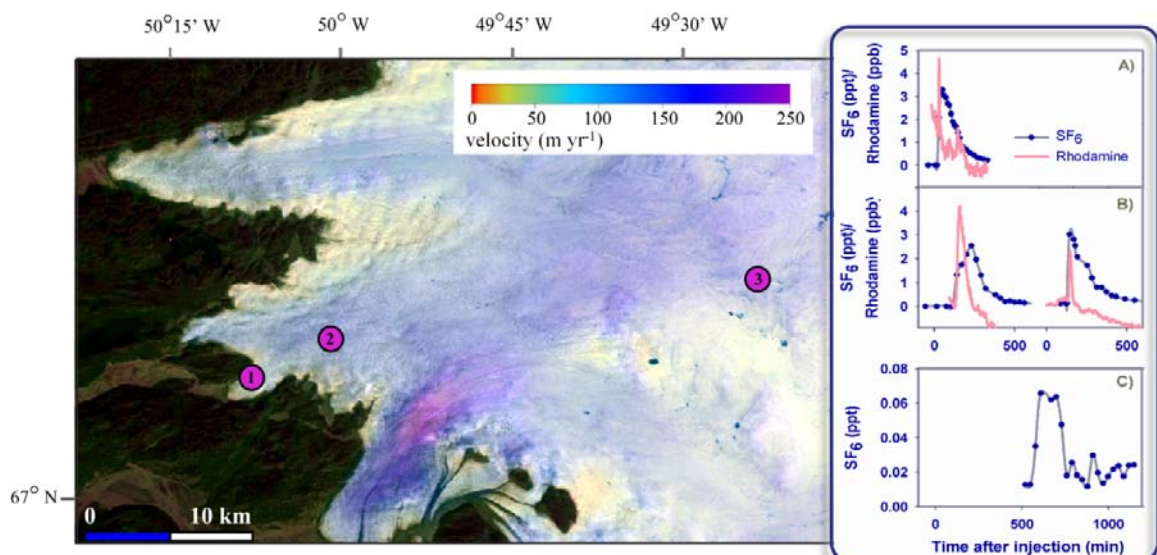


Figure 2-49. Landsat ETM+ image (7th July, 2009) of the Russell Glacier Catchment showing mean horizontal ice velocities (2004–2007) based on speckle and feature tracking of RADARSAT and SPOT images respectively, with the tracer Sites 1–3 indicated as pink circles within the southern lobe. Inset – Representative Rhodamine dye and SF₆ breakthrough curves for A) Site 1 (2 km), B) Site 2 (8 km) and C) Site 3 (35 km) (where dye concentrations have been normalized to 1 kg).



Figure 2-50. Photo showing employment of sulphur hexafluoride (SF_6). Photo by Jemma Wadham.



Figure 2-51. Photo showing Rhodamine dye injected into a moulin. Photo by Jemma Wadham.

SF_6 and Rhodamine displayed coherent behaviour in the initial phases of all breakthrough curves (Figure 2-49 A–C), enabling determination of minimum transit times and therefore, maximum melt water velocities from SF_6 breakthrough curves. SF_6 and dye traces provide direct evidence for rapid melt water transport within the ice sheet over all distances traced, where mean maximum water velocities were $1\text{--}1.3\text{ m s}^{-1}$ for dye and $0.9\text{--}1.5\text{ m s}^{-1}$ for SF_6 across all three injection sites, including high velocities (1 m s^{-1}) for meltwaters traced 35 km from the margin using SF_6 . Dispersion coefficients (D , $\text{m}^2\text{ s}^{-1}$) and dispersivity (d , m) values calculated /Seaberg et al. 1988/ for dye breakthrough curves at Sites 1 and 2 and for SF_6 at Site 3 display low values (generally < 10 for both D and d) indicating that there is little dispersion of dye/ SF_6 during transit through the drainage system. These velocity and dispersion characteristics are typical of those reported on valley glaciers in the main melt period for efficient, channelized routing of meltwaters /Nienow et al. 2005/. They provide unprecedented direct evidence that surface meltwaters are routed rapidly to the bed of the Greenland

Ice Sheet during the peak melt season through up to ~ 1 km of cold ice (Site 3), and transported efficiently to the margin from 2–35 km inland. They support previous inferences drawn from summer ice velocities on Greenland that melt water is transported during the height of the melt-season via a network of discrete channels beneath the lower ablation zone of the ice sheet /Das et al. 2008, Wal et al. 2008, Shepherd et al. 2009/, where diurnal variations in velocities reflect variations in channel and extra-channel pressurization /Shepherd et al. 2009/.

2.6.2 Electronic tracers

A significant hurdle to the understanding of ice sheet basal hydrology and its coupling with ice motion is the difficulty in making in situ measurements along a flow path. While dye and SF₆ tracing techniques may be used to determine transit times of surface melt water through the sub-glacial system, they provide no information on in situ conditions (e.g. pressure). The use of tethered sensor packages is complicated by the long lengths (~ 100's m) and torturous path of the moulins and conduits within ice sheets. Recent attempts to pass solid objects (rubber ducks) and other sensor packages through glacial moulins have confirmed the difficulty in deploying sensors into the sub glacial environment. In 2009, we trialed the use of electronic tracers on Leverett Glacier (via pilot funding from the University of Bristol) (Figure 2-52). We can report the first successful deployment and recovery of compact, electronic units to moulins up to 7 km from the margin of a large land-terminating Greenland outlet. The technique uses RF (Radio Frequency) location to create an electronic tracer (an 'e-tracer') enabling a data-logging sensor package to be located in the pro-glacial flood plain once it has passed through the ice sheet. A number of individual packages are used in each deployment mitigating for the risk that some may become stuck within the moulin or lodge in an inaccessible part of the floodplain. In preliminary tests on the Leverett glacier in West Greenland during August 2009 we have demonstrated that this technique can be used to locate and retrieve dummy sensor packages: 50% and 20% of the dummy sensor packages introduced to moulins at 1 and 7 km from the ice sheet terminus respectively, emerged in the sub-glacial stream. It was possible to effectively detect the e-tracer units over a horizontal range of up to 5 km across the pro-glacial floodplain and locate them to a high accuracy, allowing visual recognition and manual recovery. These performance statistics give this technique strong potential for investigating in situ conditions along a flow path at ice sheet scale.



Figure 2-52. Photo of the electronic tracer. Photo by Jemma Wadham.

3 Sub-project B activities 2009

This chapter details activity carried out during the period April–December 2009. As part of the GAP project’s goal to elucidate how ice sheets influence deep groundwater flow, Sub-project B is focused on two primary research activities; 1) to make in situ measurement of sub glacial hydrological conditions of the Greenland Ice Sheet, and 2) to conduct a suite of numerical modelling experiments focused on ice sheet and basal conditions.

Sub-project B is directed by Dr. Joel Harper at University of Montana and Dr. Neil Humphrey at University of Wyoming. Dr. Jesse Johnson at the University of Montana is providing ice sheet modelling expertise to the project. Toby Meierbachtol (Ph.D. candidate) at the University of Montana is working on both modelling and field activities, thus providing a strong link between the two initiatives. Clair Landowski and Chris Cox are M.Sc. candidate students at the University of Wyoming and are not supported by GAP funds, but their work efforts are contributing to the project. Douglas Brinkerhoff is a M.Sc. Candidate at University of Montana, also unsupported by GAP but conducting GAP-related modelling activities.

Research activities during the early stages of this project were centred in seven main areas. The work efforts in these areas and associated results are described individually in the following sections.

The following field data were collected in Sub-project B during 2009:

1. Point measurements of ice thickness at seven locations near the margin.
2. Time-lapse radar measurements at one location near the margin.

3.1 Field reconnaissance of drilling sites

In Mid-May of 2009 Dr. Harper, Dr. Humphrey and graduate student Dan West were in Kangerlussuaq conducting the final field season of a separate research project. Two layover days were spent conducting field reconnaissance of potential ice drilling sites for the GAP project. The field team rented a vehicle and drove to Point 660 to investigate the ice in the region of the proposed deep bedrock hole, planned to be drilled during 2011 by Sub-project C (Figure 3-1).

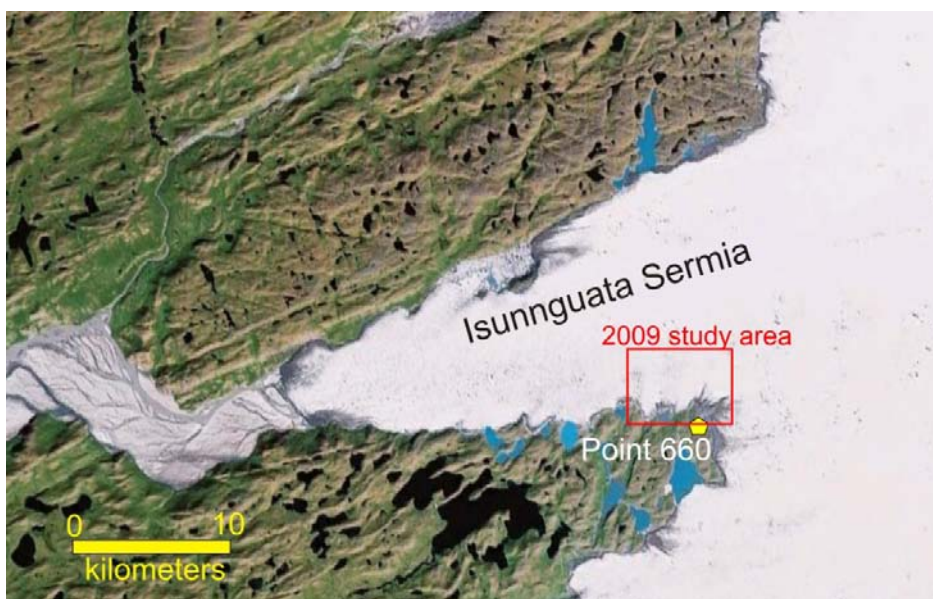


Figure 3-1. Satellite image showing area visited during May of 2009. Reconnaissance measurements were conducted in the red box on the glacier named “Isunnguata Sermia”.

3.1.1 Ice penetrating radar

We conducted a limited radar survey focused on determining ice thickness at potential drilling sites. This radar work differs from that collected by Sub-project A in that measurements targeted specific locations where drilling was expected to occur during the 2010 drilling season. Our radar measurements were collected near the ice sheet margin where the topography is very rough and Sub-project A generally avoided with their radar measurements.

To measure the glacier thickness we used a Narod Geophysics type georadar transmitter and oscilloscope receiver. Both 5 MHz and 10 MHz antennas were used to collect individual radar traces (Figure 3-2). Our data were collected on 5 m intervals and georeferenced using a hand-held GPS receiver (accurate to 1–3 m). In total we collected 2–8 radar traces at six different sites. We identified the two-way travel time (TWT) of the first reflection of the bed for each trace and converted the TWT to depth assuming a constant radar velocity of 0.168 m/ns. Based on this propagation velocity, the $\frac{1}{4}$ wavelength resolution of the radar is 4.2 m. We assume that all reflections come from directly below the acquisition point.

Measured ice depths ranged from 100 to 190 m (Figure 3-3). As expected, ice depth generally increases with distance inward from the margin. However, the progression is not monotonic, indicating that basal topography has amplitude variations of tens of m over distances of approximately 100 m.

Our GPS and radar measurements were used to construct 2-dimensional profiles of the ice surface and bed surface within the region of the proposed bedrock drilling site (Figure 3-4). The elevation of the glacier bed decreases away from the margin, similar to basal topography of a trough within a valley glacier. An off-vertical bedrock borehole will therefore penetrate several hundred meters inward from the margin, but because the glacier bed is lower elevation than the drilling site, the depth of the hole relative to the glacier bed will be less than the depth of the hole relative to the drilling site. In other words, the bottom of the bedrock hole could be drilled to 800 m below the ice surface, but this would only be 650 m below the glacier bed. An ice borehole will need to be drilled within a few 100 m of the margin in order to intersect the bed above a potential bedrock hole. However, this may prove challenging due to the steep ice surface near the margin.

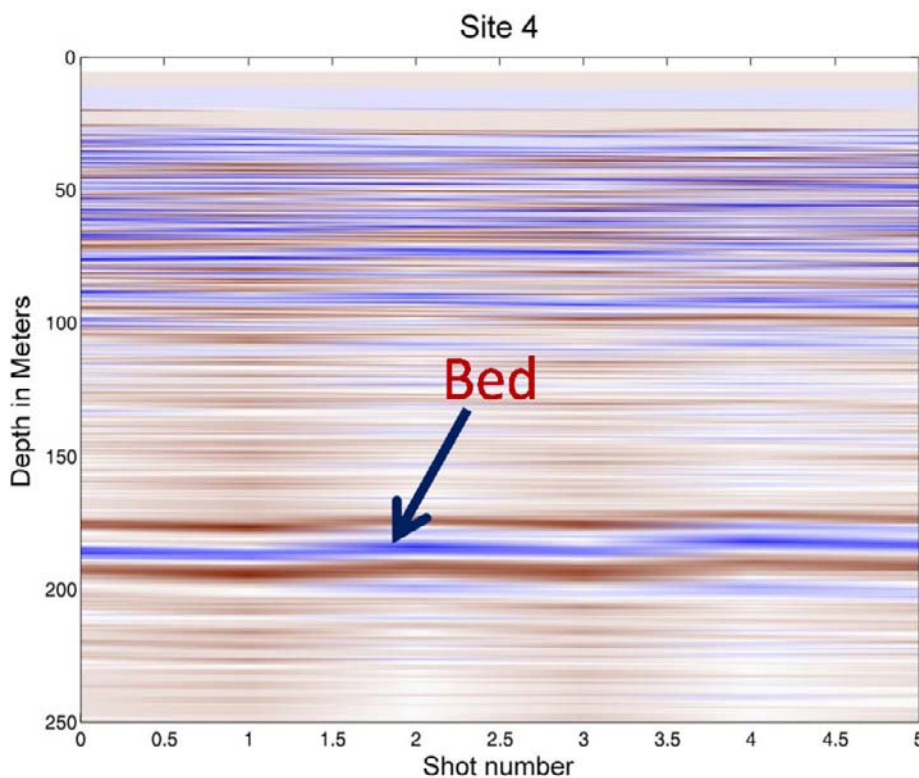


Figure 3-2. Example radargram from Site 4 where the base of the ice provides a strong reflector 180 m below the ice surface.



Figure 3-3. Map showing location of six radar measurement sites (red dots) and proposed deep bedrock hole (yellow square). Ice depths in m are labelled at each of the sites.

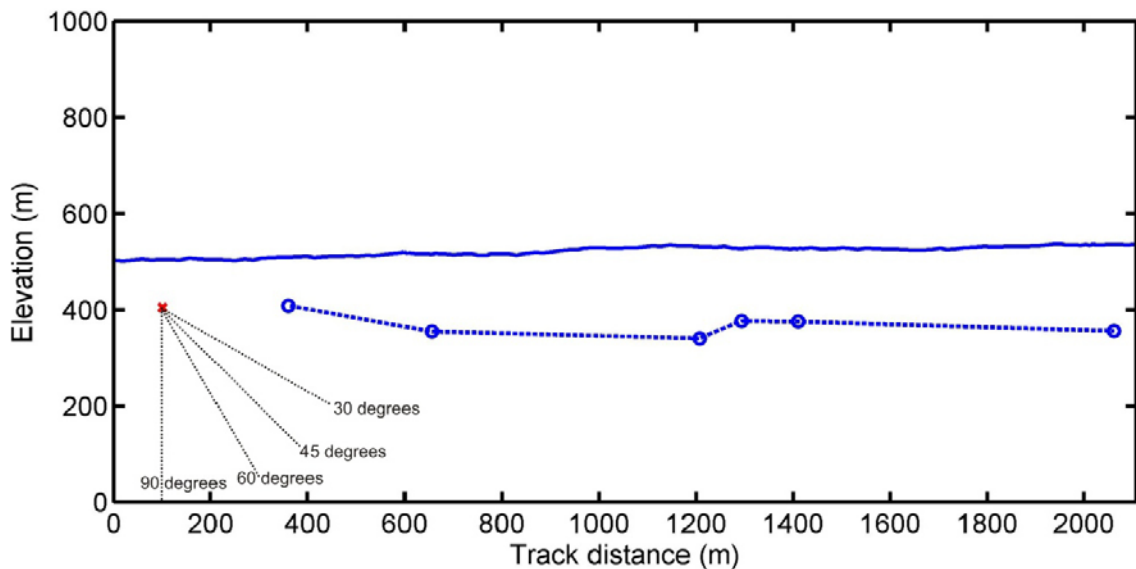


Figure 3-4. Sketch showing ice surface (blue line), bed measured by georadar (blue dots), interpolated bed (blue dashed line) and location of nearby bedrock (red x). Dotted black lines show the orientation of potential 400 m long boreholes angled at 90, 60, 45, and 30 degrees. View is looking West. We note that these data are sparse and projected 100s of meters onto this 2D profile. The interpretation of these limited data may be questionable, and more should be collected in this region in order to fully elucidate the relationship between the bedrock hole and the ice sheet bed.

We installed time-lapse radar at site 4 (Figure 3-3, 160 m ice depth). Each recorded measurement represents 32 stacked traces and one measurement is recorded to the data logger every 3 minutes. The system was installed on 19 May and we recovered data one day later on 20 May. The radar system remains in place and data will be downloaded during the 2010 field research season. Time lapse radar measurements spanning the 24 hr period between 19 May and 20 May 2009 reveal that the radar gram changes over a time period of hours (Figure 3-5). The data have a strong return from the glacier bed at 160 m depth. Later in time, there is a change in the character of the noise occurring between afternoon and evening hours. The later noise is likely from out-of-plane englacial reflectors, not from directly below the position of the transmitter-receiver. This englacial noise gradually decays during the night. We therefore believe the most likely cause of these reflectors is englacial water which drains during cool night when the surface experienced freezing conditions.

3.1.2 Surface drilling conditions

The ice surface consists of variable amplitude hummocks that reach 5–10 m (Figure 3-6). The bumpy terrain makes travel slow, and will pose a challenge to the ice drilling operation. Drilling equipment will need to be placed in the troughs between hummocks and occasional flat spots. A chainsaw may be necessary for flattening out portions of the ice, and ice anchors will be needed to hold equipment in place. This area receives approximately 4.5 m of ablation per year, and this also poses a challenge to keeping drilling equipment secure and in place. We believe these challenges are surmountable, but the drilling operation will be much slower than otherwise. The topography does have one advantage: the bumps result in numerous small ponds of water which can be used for drilling water.

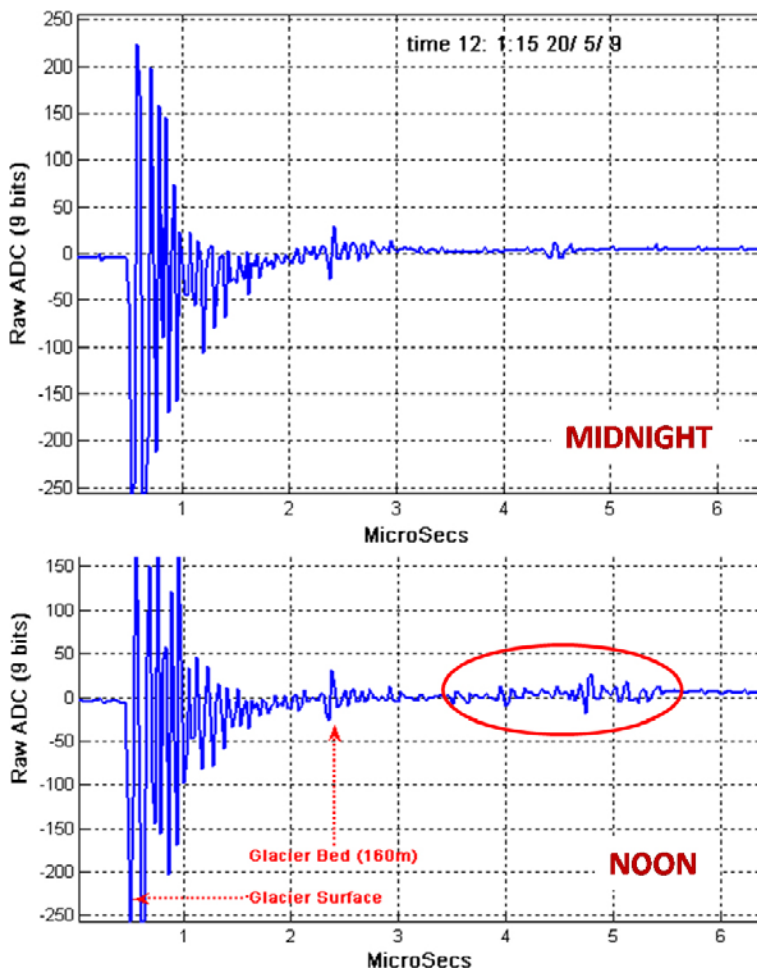


Figure 3-5. Raw trace data from the deployed 10 MHz monitoring radar shown without any filtering or amplification. Bottom panel shows stacked trace collected at noon; top panel shows trace collected 12 hrs later at midnight. Note the change in reflector noise between noon and midnight at 3.5 to 5.5 microseconds.



Figure 3-6. Photograph showing ice surface topography near the margin of Isunnguata Sermia. Photograph taken May 19, 2009. Photo by Joel Harper.

3.2 Radar reconnaissance of drilling sites

We have acquired all available radar data collected by CReSIS (Center for Remote Sensing of Ice Sheets, Univ. of Kansas) airborne radars (Figure 3-7). Unfortunately, data are limited in the vicinity of Isunnguata Sermia. The two flight lines that pass up-ice sheet from our proposed drill sites in 2010 suggest that a very deep trough runs east-west and potentially intersects the region of our centreline boreholes (Figure 3-7).

We acquired data from the NASA 2009 IceBridge flights which also has airborne radar. Unfortunately, these data were not useful since the radar sensor was not operating properly when flights were conducted over our area of interest. We have requested that IceBridge flights be conducted over our area of interest in 2010, and that both radar and surface laser (ATM) measurements be collected. We are also attempting to acquire NASA radar data collected by JPL flights during 2008.

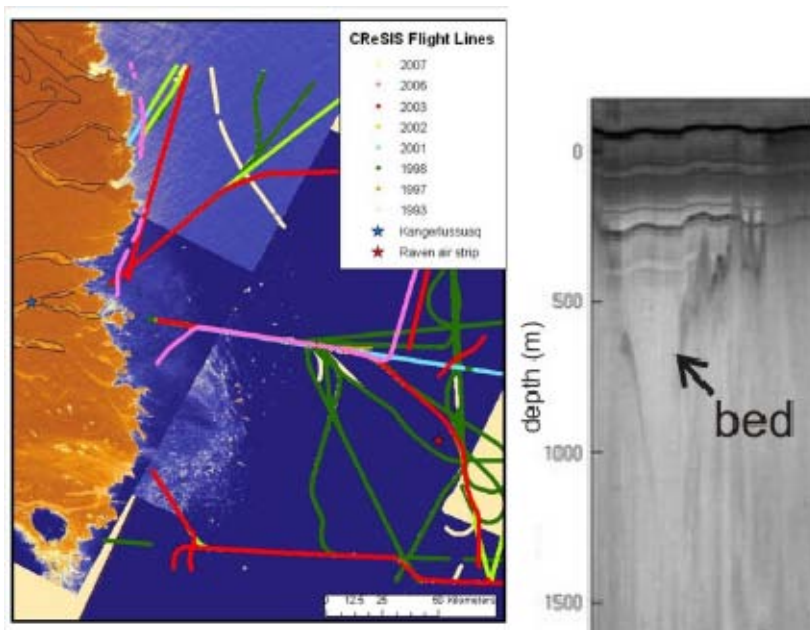


Figure 3-7. Map showing CReSIS radar data available for study area (Left). Radargram from flight path crossing Isunnguata Sermia (Right). Note apparent deep topographic trough. Also, the topography of this trough has a considerable vertical exaggeration, which makes it look much steeper than in reality.

3.3 Transport of Alaskan drill

In June of 2009 Dr. Humphrey travelled to Alaska with an assistant to move our Alaskan drill and all of its associated parts and equipment from Alaska to a storage facility at the University of Wyoming. Our Alaskan drill needs major modification to make it suitable for drilling in Greenland. The Alaskan drill is built to drill through ~ 250 m of temperate ice (0°C). In Greenland, we expect to drill up to 1,000 m and the ice could be as cold as -20°C. Hence, drilling in Greenland will require delivering up to 40% more heat to the advancing drill tip. Also, when the drill hole is completed, up to 1,000 m of drill hose will need to be pulled from the hole very rapidly in order to avoid freeze-in. Parts from the Alaskan drill will be salvaged and incorporated into the new drill. Further, the drill and its extensive array of parts and supplementary equipment are being used as a template for designing the Greenland drill. Hence, having the drill available in Wyoming is essential for preparing the Greenland drill.

3.4 Deep-Ice hot water drill design and fabrication

Dr. Humphrey has made a substantial time investment in design work for the new Greenland Drill. The design work included calculating specifications for the power plant, the pumping system, and the drilling hose. The drill hose required custom manufacturing of 150 m lengths because high pressure hose is normally only produced in short sections. A suitable manufacturer had to be identified and Dr. Humphrey has worked closely with the company during the manufacturing process.

Additional work hours were invested in researching specifications and prices for various components of the drilling system, such as heaters and generators. Choices have been made and this equipment has all been purchased.

The drill tower has been designed and the manufacturing specifications have been delivered to the University of Wyoming machine shop. The main design challenge was to engineer a capstan drive wheel that would not damage couplings, and would provide controlled lowering into the hole, and rapid withdrawal from the hole (Figure 3-8). The University of Wyoming machine shop began fabricating the Greenland Drill in fall 2009 and will have the project completed in March 2010. Table 3-1 lists the other mechanical devices apart from the Greenland Drill that were under construction for use in the field during 2010.

Table 3-1. Other mechanical devices under construction.

Mechanical samplers	Details
Basal water sampler	Designed, weight of sampler hitting bottom of hole closes sampler.
Sediment corer	2 different designs of commercial core samplers are being modified for borehole operation.
Penetrometer	A device to drive into the bed to determine if it is soft (till) or hard (bedrock)
Dye Injector for water dye tracing	Designed, and in stock.

Note: All of the mechanical samplers use the same high strength mechanical line and winch system, based on commercial deep sea fishing gear.



Figure 3-8. The main drive wheel of the modified drill, under construction in the University of Montana machine shop. The drive wheel is 4 ft in diameter, and is being milled from an original 4 ft square plate of 1.5 in thick aluminium. Photo by Neil Humphrey.

3.5 Sensor design and testing

Because no off-the-shelf pressure transducers readily meet our specifications (i.e. high pressure, small diameter, and ultra low power), we made the decision to build our own pressure transducer installations. Our home-built pressure transducers will cost an order of magnitude less money, but will take considerable time to manufacture. We have considerable experience with this process as we have built on the order of 100 pressure transducers over the last 10 years.

After searching through numerous product lines of various manufacturers of electronic components, we have located appropriate components for the Greenland pressure transducers. Data loggers for the pressure transducers have been designed and a prototype data logger has been tested.

We have developed proto-types of all the major down hole sensors (Table 3-2), and are now moving into the production phase. A major criterion is that all the electrically based sensors operate on cheap cat5 cable, and use a common winch system. A prototype thermister string has been manufactured and tested. After researching commercially available tilt metres, we decided that building our own sensors would be required in order to install an adequate number of sensors at a reasonable cost. Electronic components for this purpose have been located and a prototype tilt sensor string has been manufactured (Figure 3-9). In addition to the down hole sensors, all the devices require a surface control and readout (and in some cases data logging) devices. These devices are currently being tested.

Table 3-2. Sensor development for 2010 field season.

Primary Sensors	Down-hole	Surface control and readout
Basal water pressure*	6 units using Omega PX309 series transducers	Either Bench project or Omineca Loggers (in-house, in stock)
Ice Temperature*	3 sensor strings, each with 40 units of SE95 temperature sensors at nominal 10 m spacing	Omineca loggers modified for I2C communication, with software for SE95 sensors
Borehole Ice deformation*	2 sensor strings, each with 40 Honeywell HMC series compass/tilt modules, and down hole multiplexers	Omineca loggers modified for I2C communication, with software for HMC modules
Secondary Sensors		
Down hole disposable still camera*	3 unit 4D Systems JPEG 680×460 resolution camera	Video camcorder, used as view screen. 5 V power source.
Flourimeter	Commercial, Tanner Designs	Either Bench project or Omineca Loggers (in-house, in stock), or Campbell sci. loggers
#1 Sliding metre, basal velocity metre*	Magnetic field strength metre based on HMC5843 chip and sacrificial disk magnet	Omineca loggers modified for I2C communication, with software for HMC modules
#2 Sliding metre*	Weight and string method, with 'soft pot' environmentally sealed potentiometer	Either Bench project or Omineca Loggers (in-house, in stock)
Till deformation sensor, or Ploughmeter*	Weak Aluminum tube, with 10 embedded tilt sensors	Omineca loggers modified for I2C communication, with software for HMC modules
Borehole Caliper	Will only have 200 m of cable, used in initial drill testing to assess the quality of the ice holes	

* Sensors that will be permanently installed in boreholes.



Figure 3-9. Compass and tilt (inclinometer) module under laboratory testing (the module is the 2 cm red square). This module forms the core of the ice deformation string, which will consist of 40 individual inclinometer modules. The module is being tested on a specially made micrometer tilt plate. The surrounding electronics are prototypes of the control, power and data-logging electronics, which are also developed in-house. Photo by Joel Harper.

3.6 Modelling

We have completed ice sheet scale models of the Greenland Ice Sheet, simulating the 3-dimensional geometry and flow field. Using the Community Ice Sheet Model /Rutt et al. 2009/, known as CISM, we have spun-up model runs over a full interglacial time scale using palaeo-climate data as forcing. The model solutions serve as a large-scale reference frame for more detailed modelling and field research in the GAP study region. For example, the ice-sheet scale model runs provide boundary conditions to our study area for the internal ice deformation and thermal fields. Hence, we will be able to nest future detailed modelling work focused on our study area within this larger framework. In addition, we have collected and organized numerous data sets that serve as boundary conditions to the ice sheet, such as measured surface elevation change, surface mass balance, and surface ice velocity (Figure 3-10).

Little is known about melt conditions at the bed of the Greenland Ice Sheet. Some modelling studies show the centre of the ice sheet to be frozen and the margin areas thawed /e.g. Huybrechts 1996/. Other modelling studies suggest the bed of the entire ice sheet is at the pressure melting point /e.g. Greve 2005/. Since the GISP and GRIP ice core holes showed frozen bed conditions /Huybrechts 1996/ at least some regions of frozen bed exist. The nature of the transition between frozen and thawed bed conditions is unclear and various scenarios are possible. For example, the boundary could be 1) very abrupt, essentially represented by a line with frozen on one side and thawed on the other, 2) transitional, represented by large (10s of km-scale) interleaving patches of frozen and thawed regions, 3) transitional, represented by small (1 km-scale) interleaving patches of frozen and thawed bed. Several other potential scenarios exist too. Further, the entire thawed region may contain frozen patches at any scale, perhaps dictated by topography and ice depth.

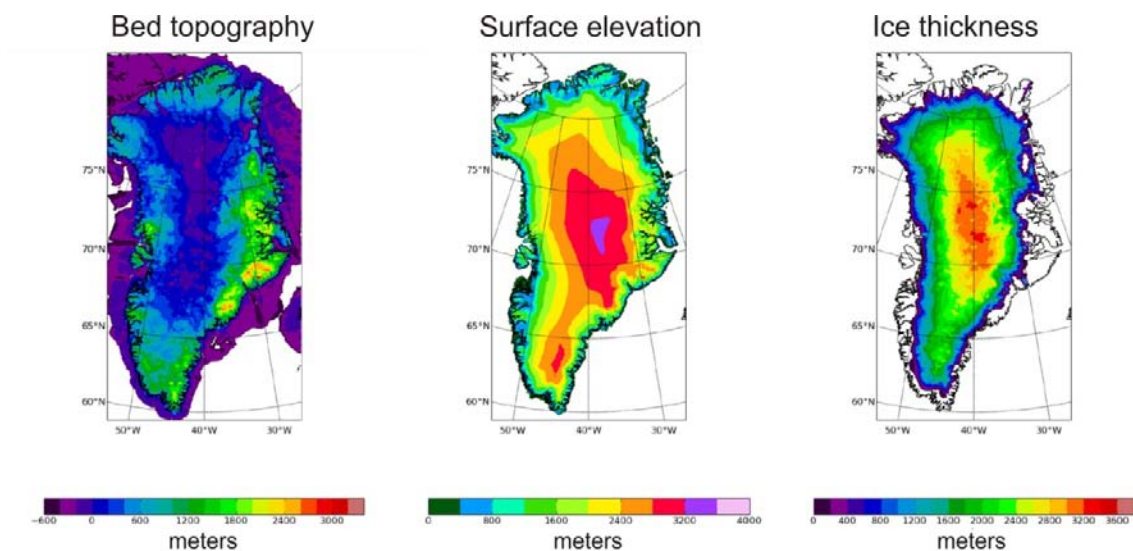


Figure 3-10. Examples of boundary condition data sets collected and available for modelling work. Left shows bed topography, centre shows surface elevation, and right shows ice thickness.

Understanding the spatial distribution of frozen and thawed bed beneath the GAP study area is an important part of elucidating general processes dictating sub glacial hydrology and groundwater recharge beneath the ice sheet. Consequently, we have initiated a modelling project to further understand detailed processes within the GAP study site. We are employing a finite element approach for a full Stokes solution of ice flow. The slip potential of the bed, representing a frozen or thawed state, is incorporated into the model solution through a parameter β . Our ongoing modelling work is investigating the length-scale variations in β that have an impact on the surface velocity field. The model framework has been constructed (Figure 3-11) and we have completed model runs for simplified conditions: periodic boundary conditions, simplified basal topography, and simple variations in β . Continuing work will add levels of complexity to this modelling initiative.

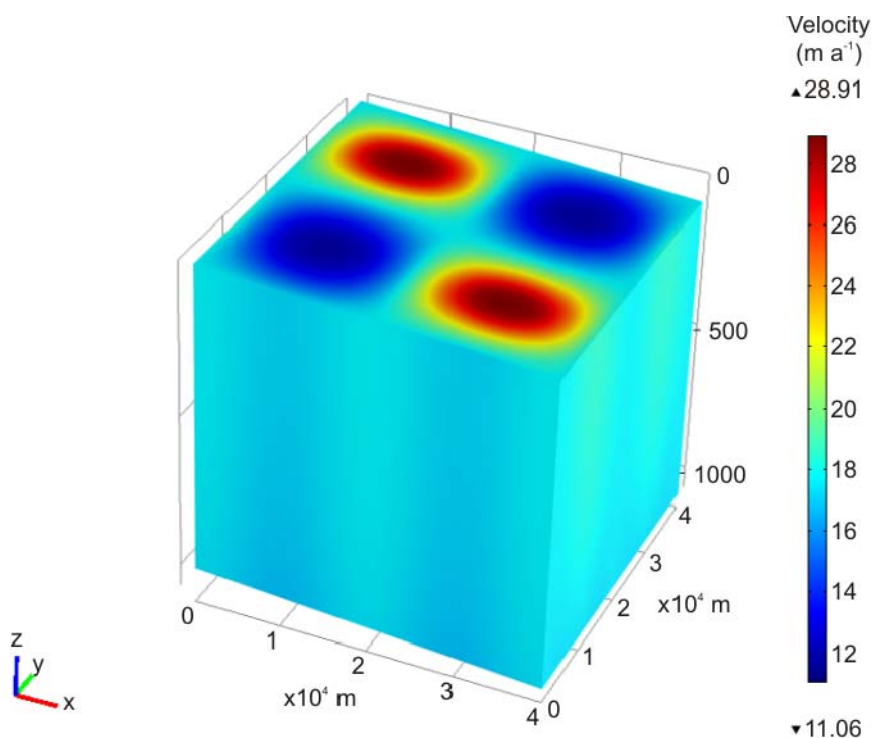


Figure 3-11. Model output from a finite element solution to the full Stokes problem for ice flow. The parameter β , a proxy for frozen or thawed bed, has been varied between highly frozen and highly thawed.

3.7 Logistics planning

Logistics planning for the 2010 field season began in August 2009. We had numerous meetings with the NSF logistics officer regarding shipping of equipment on Air National Guard flights. Plans were made to drive the majority of the heavy drilling equipment to New York so that the equipment could be flown to Kangerlussuaq on a C-5 scheduled for April 5, 2010. Arrangements were made for a small amount of equipment to travel by C-130 on May 21st, 2010. We also made arrangements to fly 8 persons, personal gear, and 5 weeks of food supply on a June 2, 2010 C-130 flight. Unfortunately, no returning Air Guard flights are scheduled within 3 weeks of our intended return date. Our return from the field will therefore require commercial flight via Copenhagen.

Other arrangements with NSF logistics include, delivery of all 2010 drilling fuel, to be contained in special-ordered 20 gallon barrels. Arrangements were made to bring in a storage container from Copenhagen for storing our drilling equipment during the winter. The storage container will be located near the NSF equipment warehouse in Kangerlussuaq.

We worked closely with NSF logistics personnel on helicopter availability during the 2010 field season. NSF arranged with AirGL (Air Greenland) a plan to ferry a helicopter south from Ilulissat three times for one day of flying: one put-in day, one move day, and one take-out day. The limited helicopter availability reduces our drilling capabilities (namely, the ability to move the drill from place-to-place within the hummocky topography). However, our arrangements assure our ability to install boreholes at near-margin and interior sites.

4 Sub-project C activities 2009

The objective of the field investigations conducted in 2009 was to collect supporting information for the planning of deep drillings and groundwater studies, which are the main sub-project C (SPC) responsibilities in GAP. Field trips in 2008 and literature reviews gave a good picture of the present understanding of the geological and periglacial conditions at the site, but also revealed some critical gaps in the knowledge. Poor understanding of permafrost conditions, the lack of fracture information in 3-dimensions and entirely missing reference data for groundwater chemistry and prevailing hydrogeological conditions were identified as such data gaps.

Growth and extent of permafrost is essentially related to the climatic conditions. The main source for the temperature records in the area is the Denmark Meteorologiske Instituts (DMI) weather station at the Kangerlussuaq airport. The long-term records indicate -5.7°C as mean annual air temperature (MAAT). So far we have been able to locate some temperature profiles from shallow boreholes (max. 14 m) showing that the mean annual ground temperature (MAGT) close to the airport is around -2°C . Based on this data, the permafrost is modelled to be 100–160 m thick /van Tantenhove and Olesen 1994/. It is argued that the infrastructure (i.e. the airport runway asphalt) may somewhat increase the temperatures, but the main uncertainty is due to the difference in altitude. The weather station at the airport is located 50 m.a.s.l. while the potential drilling sites close to the ice margin are situated considerably higher up, around 300–500 m.a.s.l. This will certainly affect both the MAAT and MAGT. Hypothetically, the temperature lapse rate in the atmosphere is around $0.6^{\circ}\text{C}/100\text{ m}$, which means that both MAAT and MAGT at the ice margin would be around 1.8°C lower than at the airport (i.e. $-7.5/-3.8^{\circ}\text{C}$). Additionally, the temperatures in the upper part of bedrock (deeper than 50 m), reflects the past climate. The past oscillation of the ice sheet margin may further complicate the situation in the present foreground and nothing is known about the extension of frozen ground beneath the ice sheet.

Our understanding of the bedrock fracture network is based on the surface mapping carried out in 2008 /Aaltonen et al. 2010/. Under the harsh climatic conditions at the ice margin it is possible that freezing-thawing cycles have influenced the fracture patterns at the surface. There are no drill cores available and, therefore, no information on how the fracturing behaves as a function of depth.

During the 2008 reconnaissance field trip a feature adjacent to the ice sheet referred to as “pingo” in previous literature /Scholz and Baumann 1997/ was investigated. The pingo turned out to be a flowing spring (ca. 20 l/min). Water chemistry was similar to that reported in the literature 10 years before /Aaltonen et al. 2010/. Isotopic analyses revealed the fluids to be distinctive from sub glacial discharge and surface water bodies in the region. For further information see Section 4.7 in this report. To our knowledge the pingo spring water gives the only indications of the chemical composition of deeper groundwater in west Greenland, at least, in the Kangerlussuaq region.

To fill the described data gaps it is necessary to conduct investigations, which require diamond drilling to obtain drill core or to facilitate down-hole monitoring. Therefore, it was decided to drill two or three boreholes to serve this purpose during the 2009 field investigations. Originally, it was only planned to carry out temperature profiling in these holes and to investigate fracturing in the cores. However, after the planning meeting for the GAP in Helsinki in November 2008, the research targets were expanded to include groundwater sampling and hydraulic monitoring. It was argued that the project should try to get the maximum benefit from the expensive drilling and that groundwater sample collection and monitoring techniques should be undertaken where possible. Further, one of the boreholes was dedicated to study the existence and nature of a talik. The design and construction of the required down-hole instrumentation for water sampling and physico-chemical measurements were ordered from the Lawrence Berkeley National Laboratory (LBNL), US. To our knowledge LBNL was the only manufacturer who had the background to provide the required equipment at short notice. The functionality of the technique under frozen ground conditions has been tested in High Lake, Canada by the Permafrost Project /Freifeld et al. 2008/.

The drilling campaign and the instrumentation of the boreholes were conducted within a four week period in June/July 2009. The first sampling and monitoring round was done immediately after the drilling was completed and a second one in September when the disturbance due to drilling was assumed to decrease. The drill cores were shipped to Finland where they now are stored at Posiva's premises in Olkiluoto. The 'pingo' spring was instrumented with drive-point piezometers in June 2009 to measure the hydraulic head in the system and to facilitate the undisturbed sampling of the water. The heads were measured and re-sampling was conducted in September. Some lakes located in a fault valley were sampled also during the field trips.

The main activities conducted and the current status of investigations is described in the following sections. The field teams and their main responsibilities are given in Table 4-1. The different data types produced during 2009 are presented in Table 4-2. Figure 4-1 shows the area where sub-project C carried out their fieldwork investigations and denotes the locations of the pingo spring and the boreholes drilled.

Table 4-1. Field personnel during the 2009 field trips.

Field trip	Name	Organization	Activity	
June 16–July 9 2009	Claesson Liljedahl, Lillemor	SKB	Project coordination, geology, borehole instrumentation and monitoring	
	Engström, Jon	GTK	Geology, DTS-measurements, drilling supervision	
	Frape, Shaun	Univ. Waterloo	Hydrogeochemistry	
	Freifeld, Barry	Lawrence Berkley National Laboratory, USA	Borehole instrumentation	
	Henkemans, Emily	Univ. Waterloo	Hydrogeochemistry	
	KATI Drilling crew	KATI, Finland	Bedrock drilling	
	Klint, Julia	GEUS	Camp maintenance	
	Klint, Knud Erik	GEUS	Contacts with authorities, logistics	
	Lehtinen, Anne	Posiva	Project coordination, hydrogeochemistry, borehole instrumentation and monitoring	
	Liimatainen, Jyrki	Posiva	Bedrock geology	
	Makahnouk, Mike	Univ. Waterloo	Mineralogy	
	Ruskeeniemi, Timo	GTK	SPC coordination, drilling supervision	
	September 1–8 2009	Bense, Victor	University of East Anglia, UK	DTS-measurements
		Claesson Liljedahl, Lillemor	SKB	See above
Engström, Jon		GTK	See above	
Henkemans, Emily		Univ. Waterloo	See above	
Laakso, Tomi		TVO, Finland	Borehole instrumentation	
Lehtinen, Anne		Posiva	See above	
Stackhouse, Brandon		Univ. Princeton, USA	Microbe studies	

Table 4-2. Data types produced during 2009.

Activity	Data type	Status
Geology		
– Drill core	Drill core logs, lithology, fractures, fracture infillings	
	– DH-GAP01	reported
	– DH-GAP02	not logged
– DH- GAP03	reported	
– Bedrock mapping	Lithologies, tectonic measurements	reported
Physical monitoring		
– DH-GAP01	DTS temperature profile	Data exists from June/July and September, 2009. More data will be collected in 2010
	AquaTroll: pressure, temperature, electrical conductivity	Data exists from June, 2009. Additional data will be collected in 2010
Hydrogeochemistry (chemistry, isotopes)		
– DH-GAP01	Hydrogeochemical analyses, 2 sampling rounds	Analyzed
– Surface waters (Pingo Spring, lakes)	Hydrogeochemical analyses, 2 sampling rounds, Pingo gas composition	Analyzed
Meteorological data		
	Pressure and temperature from the sites of DH-GAP01 and DH-GAP03. Record since September 2009	Data to be collected in 2010

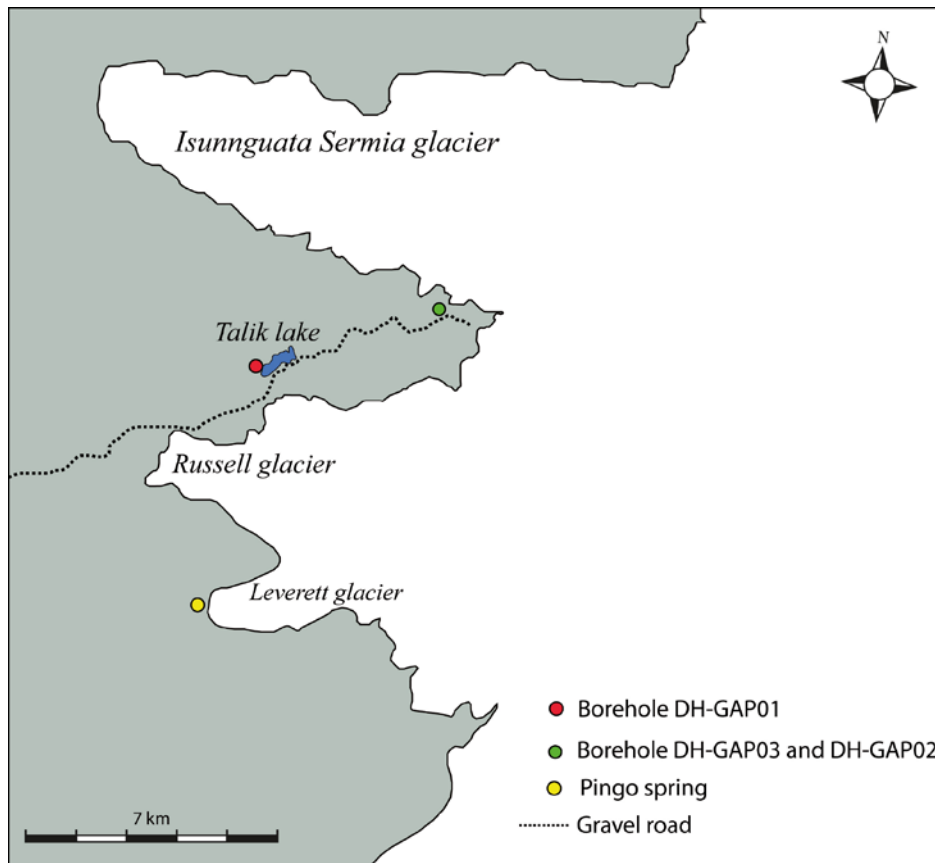


Figure 4-1. Location map of boreholes, the Talik lake and the Pingo spring across the sub-project C fieldwork investigation area.

4.1 Objectives of diamond drilling and drilling site selection

The general targets of the diamond drilling campaign were: 1) to obtain bedrock temperature profiles in order to define the (maximum) depth of permafrost at the ice sheet margin; 2) to demonstrate the presence of talik structures beneath lakes; 3) to collect core material for geological and structural studies; and 4) to provide groundwater sampling and hydraulic testing opportunities. For budgetary reasons the total drilling metres were limited to about 600 m. It was concluded that two holes would be drilled with an option for a third to improve the opportunities for water sampling. Thus, the first borehole would be drilled for talik investigations and the second one to observe the maximum thickness of the permafrost. Tentatively, it was estimated that these holes should be 200 m and 400 m long. Following this reasoning the down hole instrumentations were ordered from LBNL. They were to include one inflatable packer mechanism to collect pristine gas and water samples, sensors to monitor physico-chemical parameters and heating cables to keep the system operational under freezing conditions.

Selection of the lake for *talik investigations* was based on the general knowledge of the formation of taliks, the experience gained in the Canadian Arctic by the Permafrost Project /e.g. Stotler et al. 2009/ and the field investigations carried out in 2008. The main criteria were that the water body should be large and deep enough not to freeze down to bottom during winter and that it should be located in a lineament or fault. The first criterion is the physical precondition for the existence of an unfrozen zone and the second aims to increase the probability of a higher hydraulic conductivity connection with the geosphere. The selected lake, referred to as the “Talik Lake”, is 1,200 m long, 300–400 m wide and the greatest depth is approximately 40 m (see Figure 4-1 and Figure 4-4). The SPC team measured the talik lake to be 33 m deep. The NE-SW trending elongated lake basin is located in a lineament, but the exact nature of the structure is unknown. The distance to the northern flank of the Russell’s Glacier is about 500 m to the SE and the distance to Isunnguata Sermia is 3 km to the north.

The borehole for *permafrost studies* was drilled close to the margin of Isunnguata Sermia, about 6 km NE from the ‘Talik lake’ (see Figure 4-1 and Figure 4-4). The aim was to determine the maximum depth of the permafrost and it was assumed that the mean average air temperature would be lowest near the ice margin and at a high elevation where the snow cover, vegetation or other potentially insulating factors would be minimized. Additional considerations for siting the permafrost borehole included the presence of sparsely fracture bedrock which would best represent the preferred conditions for a repository, but balanced with a proximity to zones of increased fracturing if possible. A nearby source of sufficient amounts of drilling water (other than silty melt water) and reasonably thin overburden were other technical criteria.

Aside from the scientific requirements for the drilling sites, it was for logistical reasons desired that the drilling sites should be located relatively close to the road without any difficult crossings of water courses. Easy access was considered necessary not only for the drilling, but also for all the future activities at the boreholes. This was a practical and also a cost related decision. It was planned to use a mobile drill rig, which could operate independently to reasonable distance from the road. Additional reasons to stay close to the road include the variable topography and the need to limit the damage induced in the terrain. Safety issues related to personnel and material were carefully analyzed. Natural risks like animals, flooding, calving of the ice front and accidental or intentional human actions were taken into consideration. Selection of higher elevation sites within a safe distance from the ice margin were preferred so as to limit risks from natural incidents. The risk for human interaction was limited by the fact that the upper part of the road is closed by a gate and the access is allowed only for research teams and for organized tourist groups. The boreholes are clearly marked and sheltered by a plywood cabin, which prevents animals from getting tangled with the cables and tubing. An attached poster explains the purpose of the research and gives the contact information to the manager of the Kangerlussuaq International Science Support Centre (KISS), a contact person at GEUS and the project manager.

Prior to the drilling, geological mapping was conducted around the selected drilling sites. Foliation and the main fracture sets were observed in order to optimize the drilling orientation and the drilling angle. Mapping data from the 2008 field campaign was also utilized.

4.2 Diamond drilling

The drilling contractor was KATI Oy from Finland. The drilling crew included five men. About 15 t of drilling material was shipped to Kangerlussuaq in two sea containers. The sea containers were unloaded at the village and the drilling material was transported up road using a local semi-truck. The material was mobilized to the drilling site using a mini-dumper (Figure 4-2). When possible the transportation of material took place along outcrop ridges and wind erosion spots to minimize the tracks in the terrain.

4.2.1 Drilling technique

The drilling was done using double tube WL-56 equipment providing 56.8 mm hole and 39 mm core. The Onram 1000 rig was disassembled to about 1,000 kg units to facilitate easy moving of the equipment. The maximum drill depth capacity of the rig is about 400 m. A three metre core barrel was used for drilling. In order to obtain *in situ* orientation of the drill core a steel spear method was applied after every third run. In case of failure, a second attempt was made after the next run. In total 54 markings were made for the drilled cores. After completing the drilling a deviation measurement was done using a DeviFlex instrument.

Drilling was conducted in 12-hour shifts, seven days a week. Two men were working in each shift and the fifth was at rest. During moves the whole crew was working. The accommodation was arranged to a field camp, except for the spare shift that stayed at the Kangerlussuaq International Science Support (KISS) facility.

4.2.2 Flushing water

Local lake water was applied as a source for flushing water for all drillings. Originally it was estimated that the total water consumption could be as high as 300 to 400 m³. Therefore, it was important to have a sufficient source, where the quality would remain as constant as possible. The suitability of the water was ensured by field measurements. Furthermore, water samples were taken for chemical and isotope geochemical characterization.

Due to drilling in frozen ground the drilling water was warmed up to 30 to 60°C using oil-burning waterline heaters (Figure 4-3). The aim was to facilitate drilling without adding any antifreeze chemicals and to provide enough time for the instrumentation of the boreholes before they refroze.

The hot water was led to 1,000 l plastic tanks and was labelled using sodium fluorescein prior to use. The target concentration was 250 µg/l. The labelling was done by adding 10 ml of sodium fluorescein solution to 1,000 l of water. The sodium fluorescein solution was produced in the TVO (Teollisuuden Voima Oyj) laboratory, Finland. A member of the drilling crew collected a control sample from the first batch of each drilling shift. Altogether 12 control samples were measured at the laboratory of TVO to measure the sodium fluorescein levels and the average was 221 µg/l for the talik borehole (DH-GAP01) and 194 µg/l for the permafrost borehole (DH-GAP03) (Table 4-3).



Figure 4-2. Onram 1000 rig and a mini-dumper for moving material. Photo by Timo Ruskeenieni.



Figure 4-3. Flushing water heater. Photo by KATI OY.

Table 4-3. Sodium fluorescein concentrations ($\mu\text{g/l}$) in the flushing water. The drilling length indicates the position (in metres) when the exploitation of the batch begun.

Borehole	Date	Drilling length (m)	$\mu\text{g/l}$
DH-GAP01	26.6.2009	4.40	220
	26.6.2009	47.60	230
	27.6.2009	122.60	195
	27.6.2009	179.60	230
	28.6.2009	221.40	230
DH-GAP02	29.6.2009	8.70	172
	29.6.2009	71.70	185
DH-GAP03	30.6.2009	5.80	182
	30.6.2009	50.80	205
	1.7.2009	125.80	215
	1.7.2009	182.70	177
	2.7.2009	308.20	191

4.2.3 Supervision and monitoring measurements

Except for short periods of time, one of the GAP geologists was constantly supervising the drilling. The tasks were to carry out preliminary core logging, accept the orientation of the core, carry out the monitoring measurements of flushing water (temperature) and the return water (temperature, pH, electrical conductivity). The temperature was monitored in order to estimate the time available before the boreholes would start freezing. In order to monitor for signs of inflowing groundwater in the borehole, which would aid the decision of where to locate the sampling section, return water samples were collected by the driller from the overflowing water coming out from the borehole casing. In optimal circumstances the sample was collected just before ending each run.

4.2.4 Orientation of the boreholes based on geological mapping

The first SPC team arrived to Kangerlussuaq on the 16th of June – a week before the drilling crew. During this period, field reconnaissance was done to: 1) locate the exact drilling sites from the selected areas; 2) find sufficient sources for flushing water; and 3) find a suitable place for the base camp serving both drilling sites. Geological mapping was focused around the Talik Lake, because the chances to obtain water samples were considered better from a talik than beneath permafrost of unknown depth. Thus it was important to learn how to intersect the main fracture sets and how to reach the fault possibly located somewhere beneath the lake basin. Less effort was put on the mapping around the permafrost borehole site, where the geological setting was simpler and there was more freedom to orientate the borehole.

The orientation and the drilling angle of the boreholes were mainly defined by the prevailing foliation (Figure 4-4). The location for the DH-GAP01 (talik borehole) was set to the SW side of the lake, because it was beneficial to drill against the NW dipping foliation (Figure 4-5). This meant a longer, but still reasonable transport distance from the road. Considering the geometry of the lake basin, the location of the deepest water, and also the orientation of geological structures, it would have been better to go further north along the western shore. However, the terrain was too steep to move the rig any further and the situation was the same should the rig be transported from the north side (Figure 4-4 and Figure 4-6). Depth soundings showed that the maximum water depth along the trace of the planned borehole was close to 20 m, which is considered to be more than enough to support a talik beneath. Taliks are found beneath water bodies, which do not freeze down to bottom during winter /Mackay 1992, Burn 2002/. Under the prevailing winter temperatures at Kangerlussuaq, 2–3 m of water is enough to satisfy this requirement. The optimal intersection of the essential geological structures was achieved with the drilling orientation of 035° (Figure 4-5), *i.e.* the dominant foliation was cut with a sufficiently high angle to promote the intersection of rock units instead of the tendency to drift parallel to the foliation plane. Further, most of the repeated fracture sets were cut with this orientation. The dip of the borehole was chosen to 60°, which is steep enough considering the installation of down hole instrumentation and still provides reasonable horizontal advance to reach the central depression of the lake and sufficient vertical depth.

The foliation was also a defining factor when the location for the permafrost borehole (DH-GAP02 and DH-GAP03) was determined. At this site the foliation has a rather uniform NNW-SSE trend with a sub-vertical dip towards ENE (Figure 4-4). The orientation of the hole was set to 288°. The drill site was located in a NW facing hill slope, about 50 m higher than the nearby stream valley, close to the road. The distance to the ice margin is about 600 m. As the target was to penetrate the permafrost, a steeper dip was applied here than at the Talik Lake. However, due to the foliation it was not possible to exceed 70°, which was selected for the drilling angle. Drilling of DH-GAP02 had to be terminated due to technical reasons and the substitute hole DH-GAP03 was drilled one metre away.

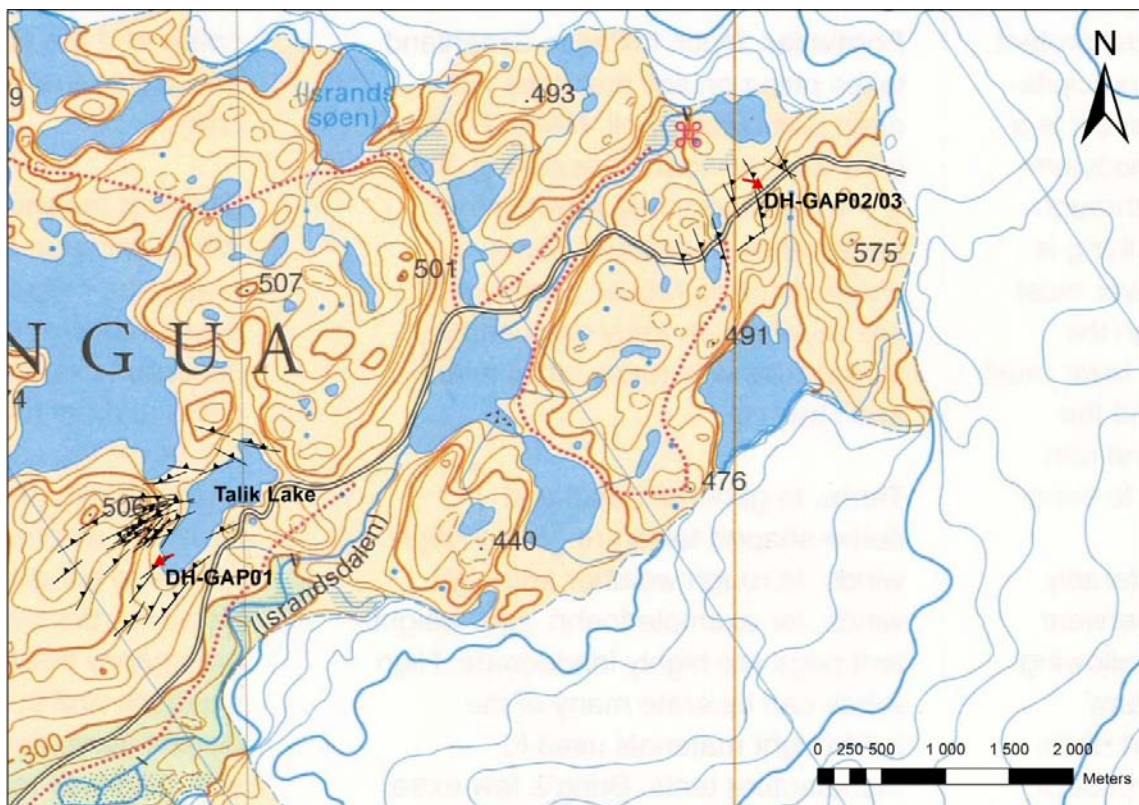
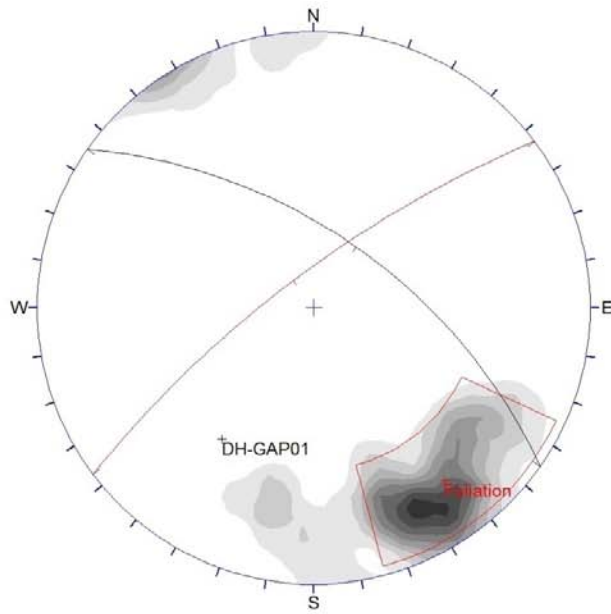
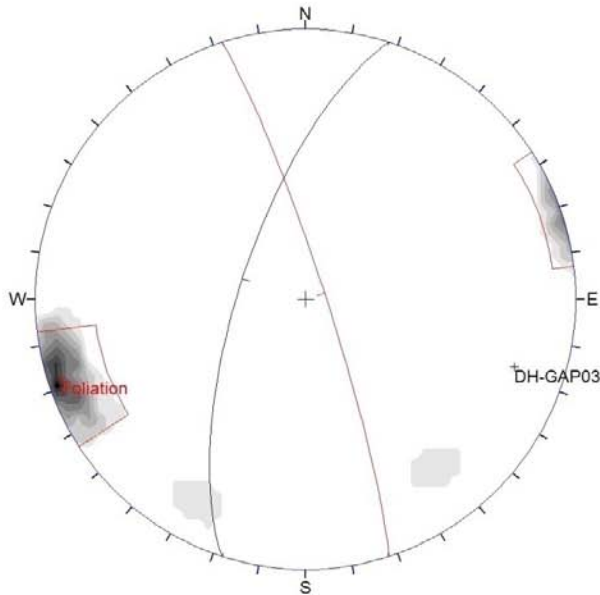


Figure 4-4. Foliation map showing the outcrops for the geological mapping done during fieldwork 2009, around the two drilling sites (red arrows).



Orientations		
ID	Dip / Direction	
1	60 / 035	DH-GAP01
1 m	76 / 323	Foliation

Equal Angle
Lower Hemisphere
48 Poles
48 Entries



Orientations		
ID	Dip / Direction	
1	70 / 288	DH-GAP03
1 m	84 / 072	Foliation

Equal Area
Lower Hemisphere
12 Poles
12 Entries

Figure 4-5. Cutting relationship between the dominating foliation (red line) and the trace of borehole (grey line) for upper figure: borehole DH-GAP01 and for lower figure: borehole DH-GAP03 (Equal area, lower hemisphere projection).



Figure 4-6. View to NNE along the shore of the Talik Lake. The steep topography restricts the mowing of vehicles, especially when trying to protect the terrain from damage. Photo by Timo Ruskeeniemi.

4.2.5 Drilling schedule

The diamond drilling was commenced in the morning of the 26th June 2009 by the drilling of the 'talik borehole, coded as DH-GAP01. The drilling of the 221 m long (191 m of vertical depth) borehole took only about 45 hours. There were no technical problems and the recovery of the core was excellent. After ending the hole in the morning of the 28th June it was flushed for an hour and the deviation measurement was conducted. The hole had turned 5.86 m to the right and 2.84 m up. The drilling schedule and the technical details of the hole are given in Table 4-4 and Table 4-5.

In total 40 m³ of flushing water was used. The temperature of the inflow ranged from 30°C to 41°C and the temperature of return water was most of the time 30 to 35°C. After about 20 metres drilling, the amount of return water decreased considerably. Flushing water came up basically only when the core barrel was retrieved. There was no means to measure the amount of return water to know how much water was forced into the fracture network, but judging from the relatively quick cleaning of the sampling section, the volume at the deeper levels was not great. At around 204 m the driller observed a significant drop in flushing water pressure (60 bar → 35 bars). This was taken as an evidence of greater hydraulic conductivity, especially because it was possible to link the drop in flushing water pressure to a fracture in the core. Electrical conductivity and pH monitoring of the return water failed to observe anomalous inflow at 204 m (Figure 4-7).

On June 28th the drill rig and other material were moved about 6 km up road and the drilling of the 'permafrost borehole' DH-GAP02 began on the 29th June. The flushing water disappeared into fractures after only 3 metres drilling. Therefore, it was decided to run a casing down to 5 m depth. After that the flushing water circulation recovered. However, during the next night the drilling was terminated at 128 m due to technical problems. The drilling string was jammed and 30 m of rods were lost into the hole. The rig was moved a metre backwards and the drilling started again. The new hole was coded as DH-GAP03 and it had the same orientation and dip as DH-GAP02. The first 5 m were cased again, because it was likely that the same fractures would complicate drilling again.

The drilling advanced on average about 50 to 70 m per shift down to 330 m. Then a highly fractured and altered zone was hit and the runs were shortened to few tens of centimetres and core was lost (Figure 4-8). Drilling was slowly continued to 341.20 m until the fault started to cave and there was a risk to lose the borehole. Although the target length of 400 metres was not reached, drilling had to be terminated. The drilling of DH-GAP03 took 65 h. The borehole extended down to 320 m of vertical depth. The hole turned 4.94 m left and only 0.88 m up.

Total flushing water consumption was 65 m³. For the first 130 m the flushing water temperature was 45 to 50°C and the return water temperature was stabilized close to 40°C. But when one of the oil heaters broke down, the temperature of the flushing water dropped ca. ten degrees (Figure 4-9). The temperature of return water reacted correspondingly and settled to about 28°C.

Table 4-4. The drilling schedule for the 2009 campaign.

Action		Start date	time	Completed date	time	Note
DH-GAP01						
	Arrangement and geological mappings	16.6	10:00	25.6		– The cargo ship from Copenhagen arrived on the 18th June and the sea containers were delivered on the 20th of June – Arrangements related to field work and camp – Selection of the drilling sites and geological mapping
	Drilling	26.6	7:40	28.6	3:40	035°, incl. 60°; soil 2.70 m; EOH 221.60 m; casing (74/67 mm): 63 cm a.g.s.l, 1.3 m in bedrock
	Deviation measurement	28.6				5.88 m right, 2.84 m up
	Hot water circulation			28.6	4:30	Heating 45 h in total
	Installation of DBA	28.6		28.6	10:40	Lower end of the packer 150 m, Aqua TROLL 162 m (140 m vert.)
DH-GAP02						
	Drilling	29.6	10:00	30.6	2:00	288°, incl. 75°; Soil 1.4 m; EOH 128.30 m; Casing (74/67 mm): 25 cm a.g.s.l, 5.0 m in bedrock. Drilling terminated due to the jam of drilling string
DH-GAP03						
	Drilling	30.6	10:50	3.7	3:30	288°, incl. 75°; Soil 1.4 m; EOH 341.20 m; Casing (74/67 mm): 45 cm a.g.s.l, 5.0 m in bedrock
	Deviation measurement	3.7				4.94 m left, 0.88 m up
	Hot water circulation			3.7	6:00	Heating 67 h in total
	Installation of DBA	3.7	9:00		3:00	220 m of insulation from the lower end was removed to ease the installation. The DBA did not go deeper than about 120 m. Had to be taken out. A heating cable was lowered down to 150 m (stopped here because cable too short).
	Borehole frozen	4.7	7:00			The heating cable was frozen at 152 m, groundwater table at 34 m.
	Heating of the borehole	4.7	?		23:00	After few hours warming the cable was released and was moving 1.5 m and a few hours later it moved ca. 20 m, before the weight was plugged by ice. The total time of warming was ca. 12 hours. After negotiations with the drillers the whole cable was pulled out leaving the weight into the borehole (about 23:00).
Moving of	rig back to DH-GAP03	5.7	7:30	5.7	14:00	
	Ice drilling	5.7	19:00	6.7	13:10	Soft ice 40–163, hard ice 163–280 m, 280–309 m soft intervals, breakthrough 309 m, rods up
	Instrumentation of borehole	6.7	14:30	6.7	17:40	DTS, Aqua TROLL 329 m, heating cable 1: 329 m, heating cable 2: 329 m; Testing of equipment.
	Moving the rig back to Kangerlussuaq	6.7	19:00	6.7	21:00	

Table 4-5. Technical details of boreholes DH-GAP01, 02 and 03. The data is stored in Posiva's borehole database, as well as in the GAP database.

Hole ID	DH-GAP01	DH-GAP02	DH-GAP03
Northing	7445607	7448566	7448565
Easting	535489	540176	540177
Elevation	347	450	450
Length	221.6	128.3	341.2
Hole Path	Linear	Linear	Linear
Azimuth	35	288	288
Dip	60	70	70
DH survey dip	-59.96		-70.5
Project	Greenland Analogue Project	Greenland Analogue Project	Greenland Analogue Project
Location	Kangerlussuaq/Greenland	Kangerlussuaq/Greenland	Kangerlussuaq/Greenland
Date drilled	27.6.2009	29.6.2009	2.7.2009
Remark		Hole terminated, drill string got stuck	Drilling terminated due to a severe deformation zone
Name hole	GAP	GAP	GAP
Name number	1	2	3
Survey type	GPS	Estimated	GPS
Grid ID	UTM zone 22, WGS84	UTM zone 22, WGS84	UTM zone 22, WGS84
Survey note	Garmin GPSmap 60CSx	Garmin GPSmap 60CSx	Garmin GPSmap 60CSx
Overburden (m)	2.70	1.40	1.50
z of casing	c. 347 m	c. 450 m	c. 450 m
Casing above ground level (m)	0.63	0.25	0.45
Storage	Oikiluoto	Oikiluoto	Oikiluoto
No of core boxes	42	23	63
Casing	74/57 steel	74/57 steel	74/57 steel
Hole diameter	56.8	56.8	56.8
Sample diameter	39	39	39
Equipment	WL-56	WL-56	WL-56
Deviation survey			
– Hole ID	GAP1	GAP2	GAP3
– Method	DeviFlex		DeviFlex
– Surveyor	Oy Kati Ab		Oy Kati Ab
– Survey date	27.6.2009		3.7.2009

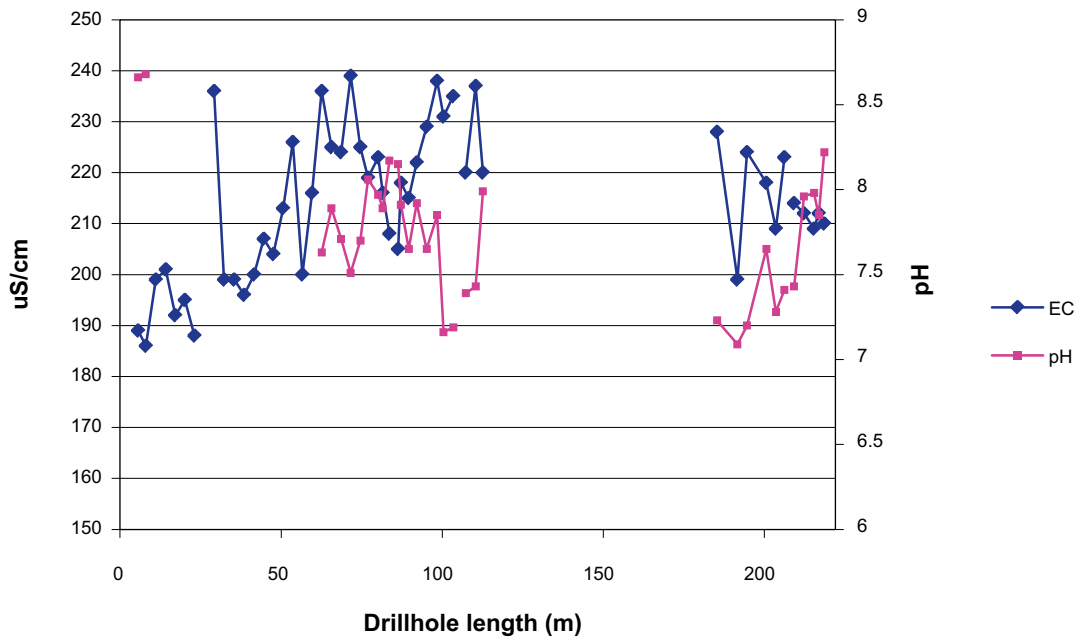


Figure 4-7. Electrical conductivity (blue) and pH (pink) measured from the return water during the drilling of DH-GAP01.



Figure 4-8. Highly fractured zone at 331.70–340.50 m, which terminated the drilling of DH-GAP03. Photo by Timo Ruskeeniemi.

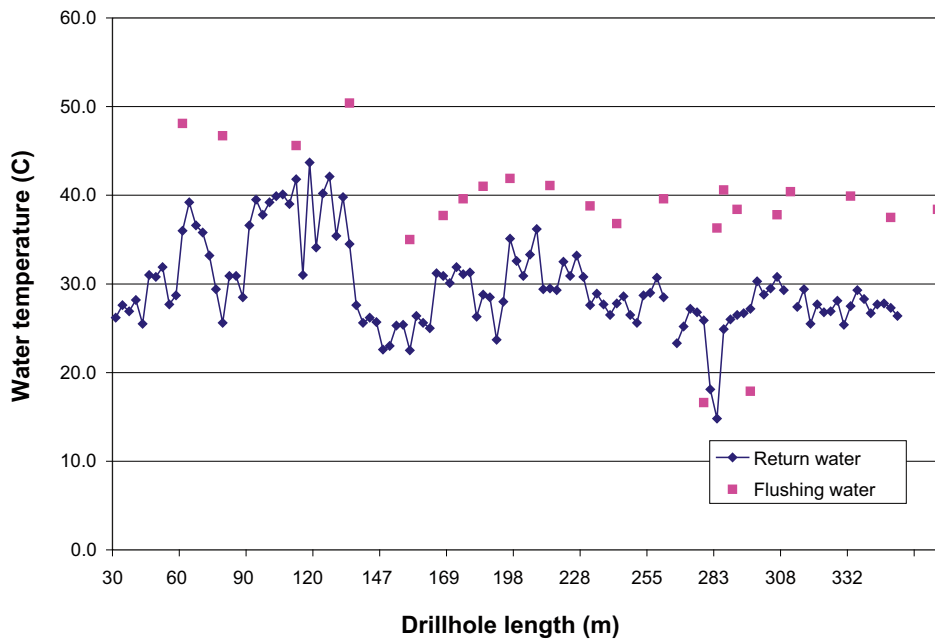


Figure 4-9. Temperatures of the flushing water (pink) and the return water (blue) during the drilling of DH-GAP03.

Prior to the drilling, some geothermal calculations for different drilling scenarios were carried out to estimate how long the boreholes would remain open after drilling for allowing instrumentation. The calculations were based on the assumptions that the temperature of the flushing water would be 60°C and the lowest bedrock temperature would be -3°C. The talik borehole was not considered to be particularly risky, since drilling distance in frozen ground was relatively short before entering the unfrozen zone. The situation was different with the permafrost borehole, which would mainly be under subzero conditions. The calculations indicated that after 60 hours of hot water circulation the borehole would stay open at least 24 hours, which would be more than enough for the lowering of the installation-ready instrumentation (see Figure 4-10).

During the installation of DH-GAP01 it was noticed that there was quite a lot of friction between the insulation hose and the wall of the borehole. The outer diameter of the jacketed string was about 29 mm, in principle allowing a sufficient tolerance in a 56 mm borehole. However, bending of the 6 mm steel tubing applied for sampling and pressure lines during transportation consumed the tolerance. The 36 kg weight of the U-tube sampler and monitoring unit was not enough to straighten the string (see Section 4.5 for instrumentation details). Therefore, it was decided to remove the insulation from the lower part of the DH-GAP03 instrument to ease the lowering. This operation delayed the instrumentation for a few hours and despite this precaution the friction became too high already at 120 m and the installation had to be terminated after 18 hours. Instead of the borehole instrumentation, a 150 m heating cable with an attached weight was lowered into the hole. In the morning of the 4th of July, after about 24 hours after completing the drilling, the hole had started to freeze. This was somewhat earlier than expected and was probably due to the malfunction of the flushing water heaters resulting in 20°C lower flushing water temperatures than originally planned (see Figure 4-9). The borehole was warmed up with the heating cable for 12 hours, but there was not enough capacity to stop the freezing. Therefore, a decision was made to pull out the heating cable and open the hole by drilling. The idea for the full-scale instrumentation was abandoned and it was instead decided to lower a slim set of sensors, which would allow temperature, pressure and electrical conductivity monitoring (see section 4.5).

The hole was filled with ice from 40 m depth down to 309 m. It took 14 hours to drill and remove the ice after which the modified instrumentation was successfully installed into the borehole.

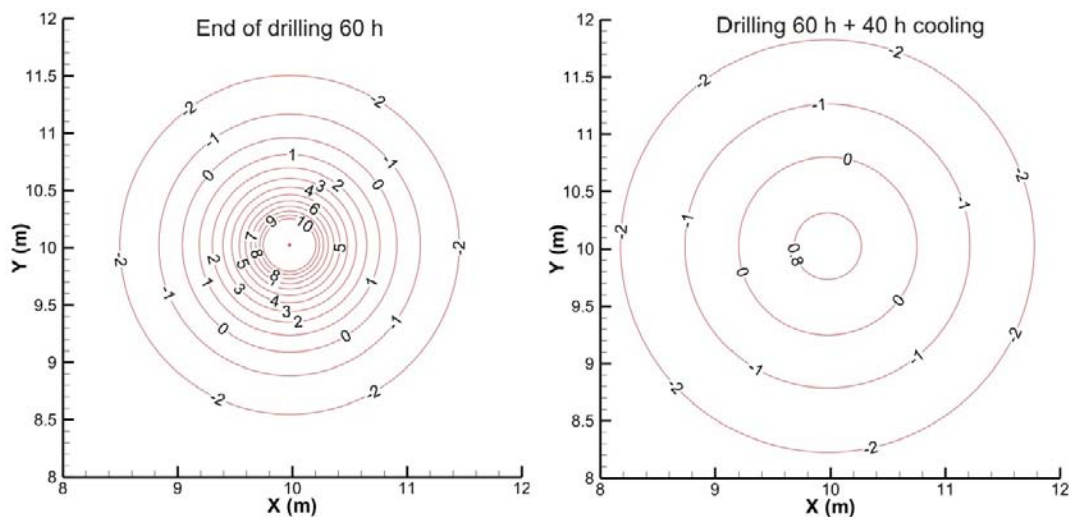


Figure 4-10. Theoretical cooling of a borehole after drilling 60 h with hot water (60°C). The temperature of the bedrock is assumed to be -3°C and the typical geothermal properties of felsic gneiss were applied. A) Immediately after completion of the drilling the hole temperature is 60°C and the 0°C isotherm is in the distance of 90 cm from the borehole. B) After 40 h the hole temperature is still about +1°C and 0°C isotherm would be 75 cm away from the hole.

4.3 Preliminary core loggings

The preliminary logging of the drill cores was made at the drilling site to assess the general geological features (rock type, fracture frequency, fracture infillings), with special emphasis on fracture zones. This was especially important when deciding the depth for the packers. All the drill cores were subsequently photographed and logged in detail by Posiva's personnel. The following description is a combination of the two loggings.

Drill core DH-GAP01 consists mainly of feldspar-rich felsic gneisses interlayered with shorter sections of mafic, amphibole-rich gneisses (Figure 4-11). Gneisses with intermediate composition also occur. The rock is generally foliated throughout the whole core. The intensity and type of foliation vary along the core, but felsic gneisses generally exhibit a gneissic foliation. Both banded and gneissic foliation types occur in mafic gneisses. The gneisses are frequently crosscut by younger undeformed and unmetamorphosed veins of K-feldspar -rich granitic material.

Close to the surface the rock is more fractured and many of the fractures are filled with drill cuttings. These fractures are likely responsible for the loss of flushing water. Natural fracture fillings are relatively rare and thin. A few distinct fractured and faulted zones (fracture frequency 10 or more) were mapped from the core (Figure 4-11). These zones are slightly altered and the fault zones contain cohesive breccia and intensive alteration on the fracture surfaces with chlorite, calcite and clays. There are also zones where fracturing is virtually missing. The groundwater sampling packer was placed in such a zone at 150 m of borehole length. The total number of fractures in DH-GAP01 is 496, giving a fracture frequency of 2.24 fractures/m.

The drill core DH-GAP03 consists mainly of feldspar-rich felsic gneisses interlayered with sections of intermediate gneisses (Figure 4-13). The intermediate gneiss has a more heterogenic character than the felsic gneiss and it occasionally contains garnets. The rock is generally foliated throughout the whole core. The intensity and type of foliation vary, but felsic rocks generally exhibit a gneissic foliation with minor banding. The grain size in the felsic gneiss varies from a fine to medium. The core contains a few shorter sections of mafic gneiss and pegmatites.

A redox front is observed in the first 40 m of the DH-GAP03 core. It is demonstrated by abundant rusty fracture surfaces. The oxidized zone seems to be related to an intermediate rock type, because it disappears when the rock type changes to more felsic. This feature was not observed at all in the 'talik borehole' DH-GAP01.

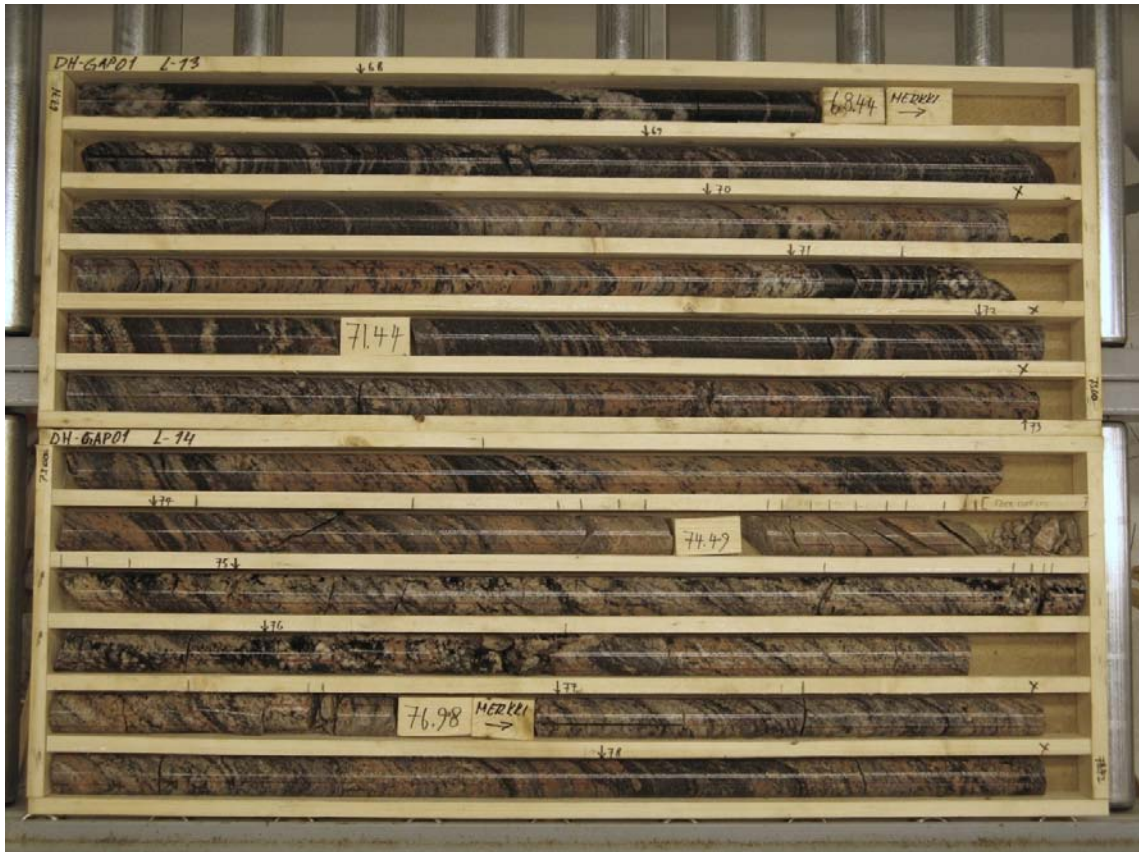


Figure 4-11. Typical feldspar-rich felsic gneiss interlayered with narrow sections of mafic and/or amphibole-rich gneisses. The continuous red line is drawn based on the core orientation marks and indicates the footwall (lower side) of the borehole. DH-GAP01, 67.71–78.42 m. Photo by Tuomas Pere.

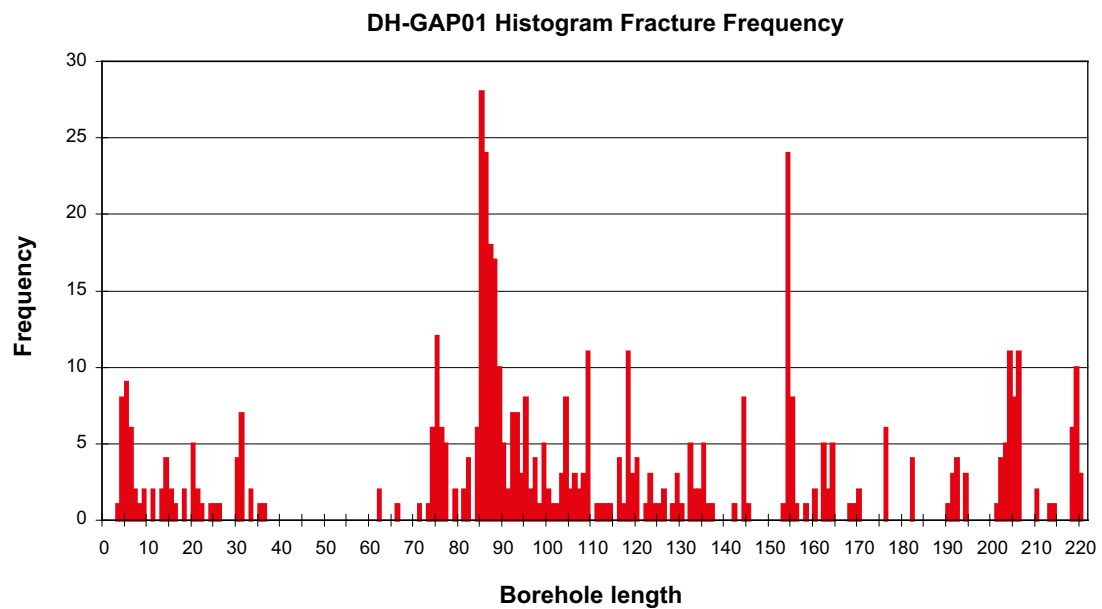


Figure 4-12. Chart showing the fracture frequency in DH-GAP01.



Figure 4-13. Transition from mafic and/or amphibole-rich gneisses to felsic gneisses in DH-GAP03, 34.10–44.91 m. Photo by Tuomas Pere.

The fracture infillings in DH-GAP03 differ significantly from DH-GAP01. While the fracture fillings in DH-GAP01 are rather scarce and mainly concentrated to fracture zones, most of the fractures in DH-GAP03 have at least some kind of infillings. Glassy, greenish slickensides are a characteristic feature (Figure 4-14). The total amount of fractures in DH-GAP03 is 1,080, and the fracture frequency is thus 3.17 fractures/m (Figure 4-15).



Figure 4-14. A typical “greenish” fracture surface in DH-GAP03, located at 269 m of borehole length. Photo by Jon Engström.

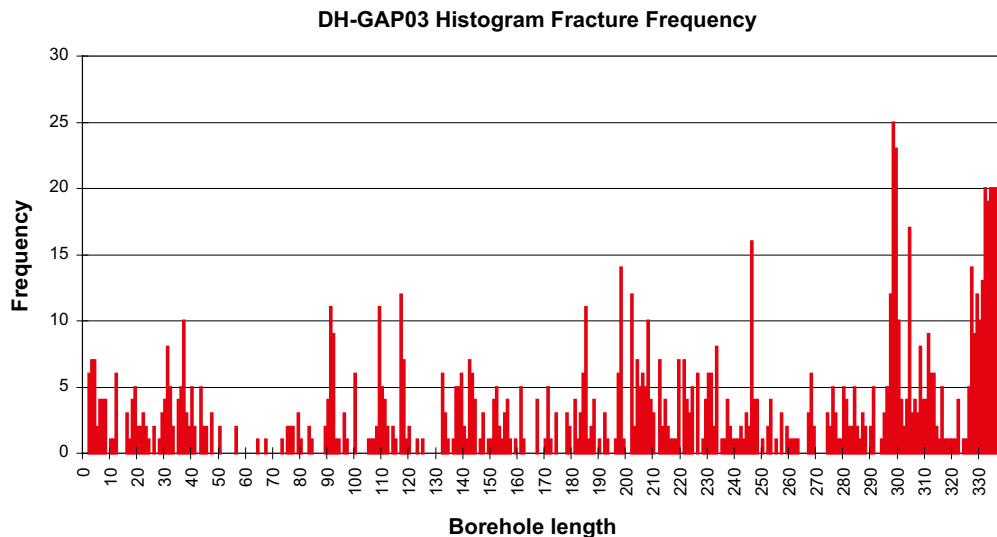


Figure 4-15. Chart showing the fracture frequency in DH-GAP03.

4.4 Fracture mineral investigations

In total 13 representative fracture infilling samples were collected in the field from DH-GAP03 in order to get a view of the main infilling minerals and their feasibility for detailed investigations, such as fluid inclusions studies. Care was taken that samples were picked only from fractures with abundant material so that forthcoming investigations are not disturbed.

Powder diffraction patterns of the fracture minerals in the DH-GAP03 core were collected on a Bruker D8 diffractometer (40 kV and 30 mA) at the University of Waterloo, Canada. Diffraction patterns were characterized with the Inorganic Crystal Structure Database (ICSD-2009 version) using the EVA software package.

Powders were characterized from depths of 28.54 m, 41.10 m, 77.53 m, 90.95 m, 275.77 m, 328.84 m and 329.68 m in the DH-GAP03 borehole. All fracture minerals were ground up and mixed in an agate mortar and pestle to ensure sample homogeneity. There are four distinct crystalline calcite types in the core. Three of these calcite groupings correspond to increasing depth throughout the core: those associated with iron rich and uranium rich minerals, clays (two different types), and a high temperature calcite. These calcites were identified with powder diffraction along with an unidentifiable grayish-blue mineral that was found in fracture DH-GAP03/329.68 m. A reflection angle (2θ) at $\sim 28^\circ$ was the major peak for this unidentified mineral and it was also observed in fractures 28.54 and 90.95 m. IR spectra of powders from fractures 28.54 m and 329.68 m had matching peaks in the spectra, which suggest that this unknown phase is present throughout the permafrost hole. An interesting finding was that fracture 90.95 m contained a fourth calcite type: a low temperature, rhombohedral calcite. This was supported by evidence in the diffraction pattern, where this calcite had broad peak width and low intensity when compared to high temperature fractures (Figure 4-16). The XRD method used a silicon wafer, which allowed for low weight analysis /Makahnouk 2004/ and thus preserved a majority of the core for SEM and fluid inclusion studies. Microscopy work will help identify the clays and grayish-blue mineral using crystal habit in images and elemental data from EDX analyses.

Isotope analyses of ^{13}C and ^{18}O of calcite were completed by the Environmental Isotope Laboratory at the University of Waterloo using small aliquots of calcite powder. Mass analysis was performed by reacting calcite with 100% orthophosphoric acid (H_3PO_4) at 90°C to generate CO_2 gas /Al-Assam et al. 1990/. All measurements were conducted using an Isoprime Multiflow (now manufactured by Elementar) instrument and results for ^{13}C and ^{18}O were reported in the δ notation, expressed in parts per thousand (per mil ‰) with respect to PeeDee Belemnite (PDB). Isotopic analyses have been submitted for multiple rhombohedra sampled from fracture 90.95 m, but instrumental problems have delayed the results. Isotopic data from DH-GAP-03 are displayed in $\delta^{13}\text{C}$ and $\delta^{18}\text{O}$ plots (Figure 4-17) and compared to sites associated with granitic gneiss and mafic rich crystalline environments across Canada and Fennoscandia.

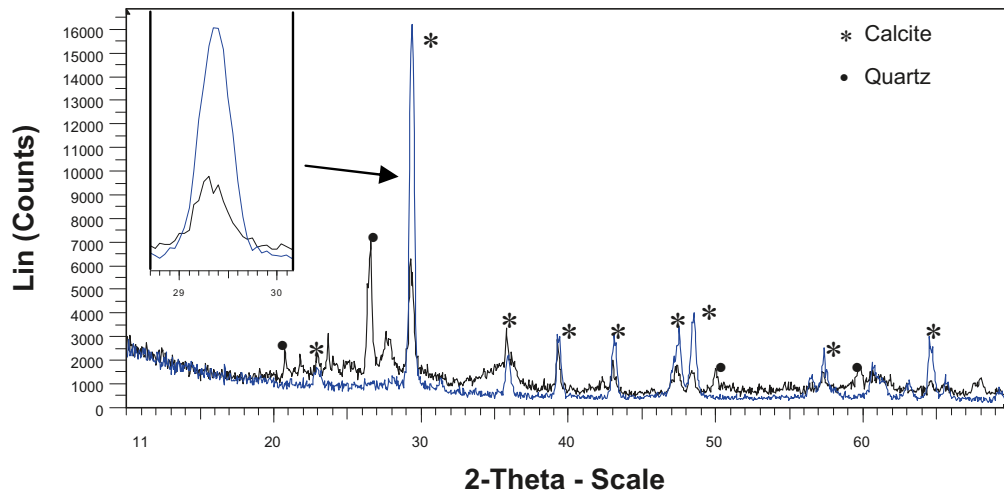


Figure 4-16. Comparison of diffraction patterns for fractures 90.95 m (black) and 328.84 m (blue). The high temperature phase, which has a greater degree of crystallinity, has a higher intensity for the major peak (blue) compared to the lower temperature phase (black) (shown in inset).

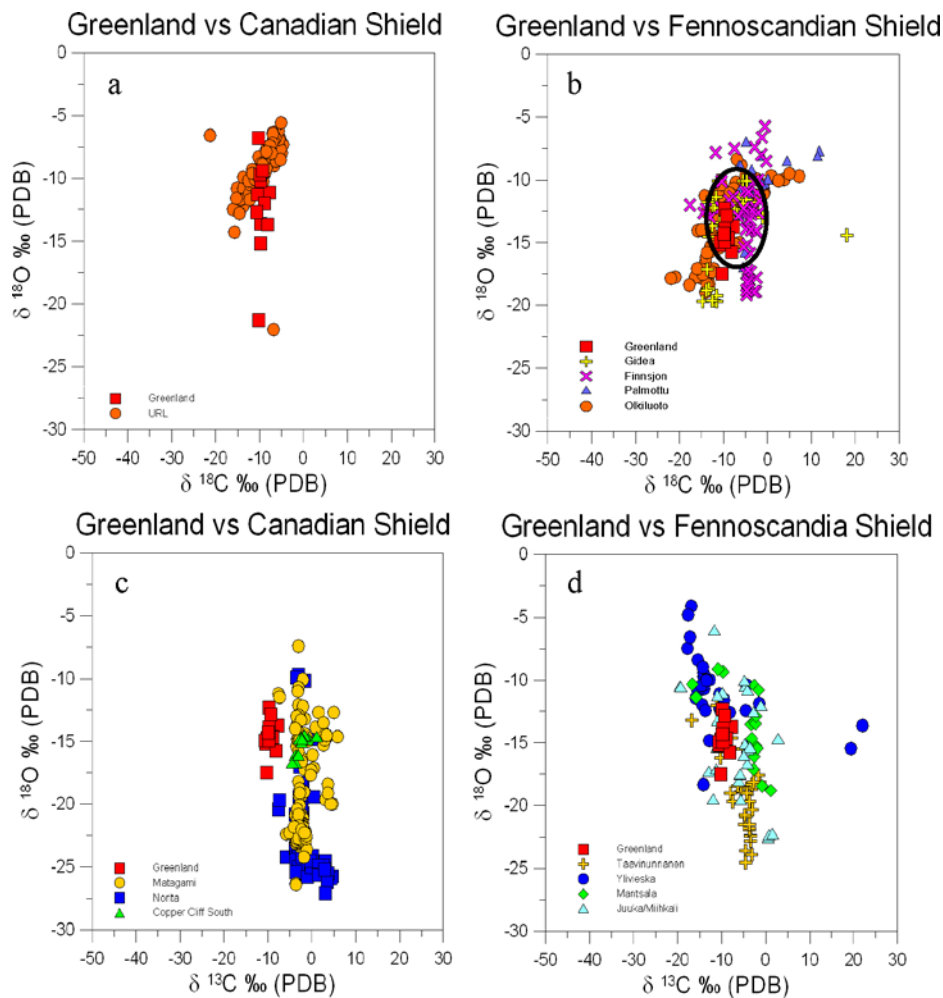


Figure 4-17. A comparison of $\delta^{13}\text{C}$ – $\delta^{18}\text{O}$ data between Greenland, Canadian Shield, and Fennoscandian Shield sites. Plots are divided into granitic gneiss (a and b) and mafic (c and d) sites. The oval depicts the region of plot (b) where Olkiluoto data is masked by Finnsjön data. After Blyth et al. 2009/.

Fluid inclusion studies will be conducted at the University of Waterloo using a Linkam heating/freezing stage manufactured by Fluid Inc. The technique used is described by /Roedder 1984 Ch. 7/ and this technique will also be used on calcite samples collected at Palmottu, Finland /Blyth et al. 2004/ in a study complementary to GAP. SEM work will continue mineral characterization within the fractures of all core collected from the GAP 2009 field season.

4.5 Instrumentation of DH-GAP01 and DH-GAP03

In order to allow for down hole fluid sampling and to obtain *in situ* pressure/temperature and conductivity information from the boreholes, two borehole observatories (BO) were designed and manufactured by the Lawrence Berkeley National Laboratory, University of California, USA. The system consists of a pneumatic packer, a U-tube sampling system with a sample fluid reservoir and pressure/temperature/conductivity sensors. Schematics of a one packer borehole observatory are shown in Figure 4-18, Figure 4-19 and Figure 4-20. Figure 4-21 is a photo of the BO designed and constructed for the GAP. The fluid, electrical and fiber-optic lines running between the BO and the surface are referred to as the deployment string (Figure 4-22).

The overall length of the borehole observatory unit is 12 m. It is composed of (from top to bottom) a fluid reservoir for packer inflation, a pneumatic packer (Baski Model MD18, Denver, CO, USA), a sample fluid collection reservoir, a pressure-temperature-conductivity sensor (In situ Aqua TROLL 200, Fort Collins, CO, USA) and a U-tube inlet composed of a 40 μm sintered stainless steel filter connected to a check-valve (see Figure 4-21 and Figure 4-23). The filter prevents the check-valve from plugging. Table 4-6 lists the specifications for the individual BO equipment items.

The U-tube sampler consists of a looped tube, forming a “U” that is open to the formation via a check valve. To collect a sample, the U is filled by venting the sample and drive legs to the atmosphere, thus allowing fluid to rise to the formation hydrostatic level. The sample is recovered by supplying compressed N₂ gas to the drive leg, which closes the check-valve and forces fluid out of the sample leg. Oxygen can enter the system as it is occasionally opened up to atmosphere (e.g. when connecting the N₂-gas cylinders). By repeating sample collection cycles, the borehole fluid can be flushed and fresh fluid pulled in from the formation. The volume of the sample depends on the formation pressure as well as the diameter and wall thickness of the tubing used. The U-tube systems constructed for instrumentation of the boreholes utilizes 3/16” stainless steel supply lines (6.4 mm diameter tube), which allow for a sample volume of 11.8 liter. The reservoir for packer inflation fluid is required only above the uppermost packer. Prior to deployment of the BO, the fluid reservoir is filled with propylene glycol. Propylene glycol is chosen because of its low freezing point and its inability to permeate through the rubber packer gland. To inflate the packer, a N₂ head is applied to the reservoir forcing the fluid into the packer and inflating the packer gland. The central mandrel of the packer serves as a conduit for transport of sampled fluid and electrical signals between the surface and the BO. The U-tube system and sensors are connected to the surface by the deployment string, which consists of stainless steel tubes to inflate the packer, drive line to force the fluid in the reservoir to move, and a collection line to collect water from the reservoir at the surface. Since permafrost is a dominating feature in the bedrock, the instrumentation used insulating jackets around the sampling and heater lines (16 AWG Teflon insulated, OMNI) in order to prevent freezing while sampling and promote heating if required. The outer diameter of the insulation tube was 29 mm.

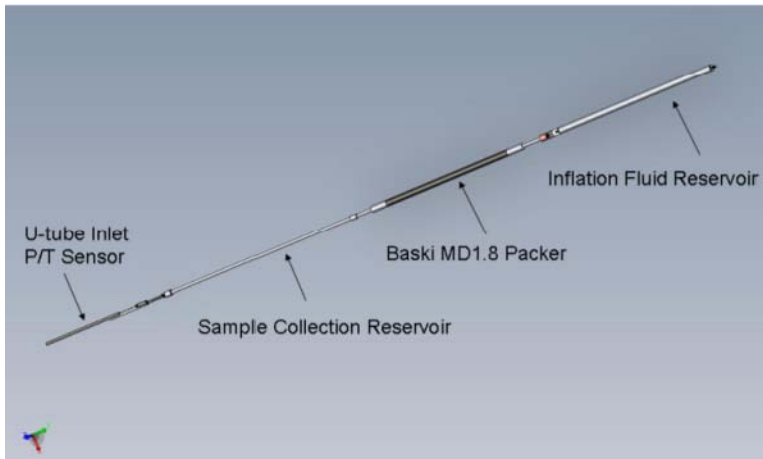


Figure 4-18. Schematic layout of the U-tube sampling system as deployed at DH-GAP01. The U-tube sampler after Freifeld et al. 2005, 2008. The fluid, electrical, and fiber-optic lines running to the surface are not shown. Only one inflation fluid reservoir is required above the uppermost packer.

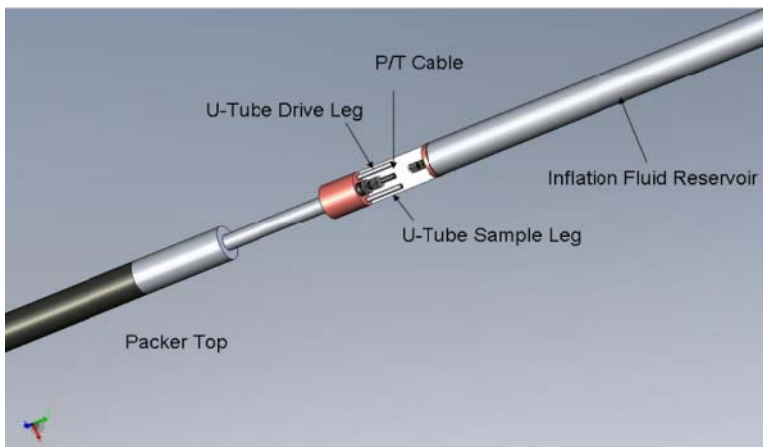


Figure 4-19. The upper connector above the packer /Freifeld et al. 2005, 2008/.

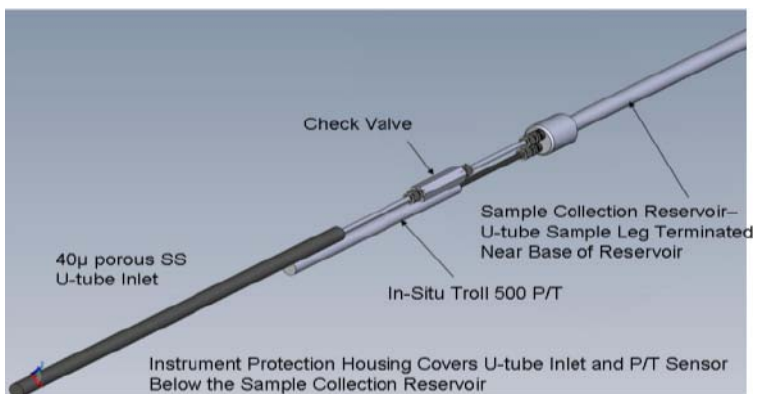


Figure 4-20. The assembly below the packer /Freifeld et al. 2005, 2008/. Note: In DH-GAP01 an in situ Troll 200 with P/T/EC sensors was used rather than the in situ Troll 500 shown in the figure.



Figure 4-21. Photo of the borehole observatory showing the packer, the fluid sampling stainless steel tubes and the cable for the P/T/EC (Aqua TROLL200) sensor. The BO is connected to the deployment string, i.e. sampling and heating lines before lowered into the borehole. Total length of the BO is 12 metres. Photo by Anne Lehtinen.



Figure 4-22. Photo of the deployment string, i.e. tubing and cables attached to the top of the borehole observatory. DTS cable (blue), sampling tubing (stainless steel), heater cable (black), P/T/EC sensor cable (black with blue tape). The black insulating jacket is also shown. Photo by Lillemor Claesson Liljedahl.



Figure 4-23. Photo showing the bull nose equipment (i.e. the Aqua TROLL 200 with P/T/EC sensors at the check valve, below which the sintered stainless steel 40 μm filter is connected). The conductivity sensor in the Aqua TROLL 200 is calibrated during manufacturing, and the specific conductivity reading was checked without remarks before the BO was assembled. Photo by Barry Freifeld.

Table 4-6. Equipment specifications for the borehole observatories.

Equipment/item	Specifications
Pressure/temperature/conductivity sensor	In situ ©Aqua TROLL200, non-vented: S/N DH-GAP01: 138643; S/N DH-GAP03: 138684
Packer	Hank Baski MD1.8
Insulating jacket	OD ~ 29 mm
U-tube lines and packer inflation line	¼" SS tubing \times 0.028"
Heater lines	16 AWG Teflon insulated, OMNI cable type A11602F 16G/2C N/S VNTC, resistance 0.0132 Ω /m. Recommended maximum current through wire is 25 A to prevent overheating.
Pressure seals	Conax Buffalo PG2-262-A-V
Check valve	Autoclave Engineers, SWB4400
Bullnose filter	40 μm

The instrumentation for permafrost investigations was supplemented by the installation of pressure and temperature stations (Solinst Junior Leveloggers, model 3001) next to the boreholes (Figure 4-24). The loggers were installed in September 2009 to record air temperature and atmospheric pressure every 15 minutes. Specifications of the loggers are outlined in Table 4-7. The aim is to compare the weather records from the Kangerlussuaq airport and from the ice margin to assess the influence of the ice sheet and higher elevation to the climatic forcing. This has influence on the formation of the active layer. Finally, due to permafrost conditions, any equipment installed in the boreholes are considered permanent.

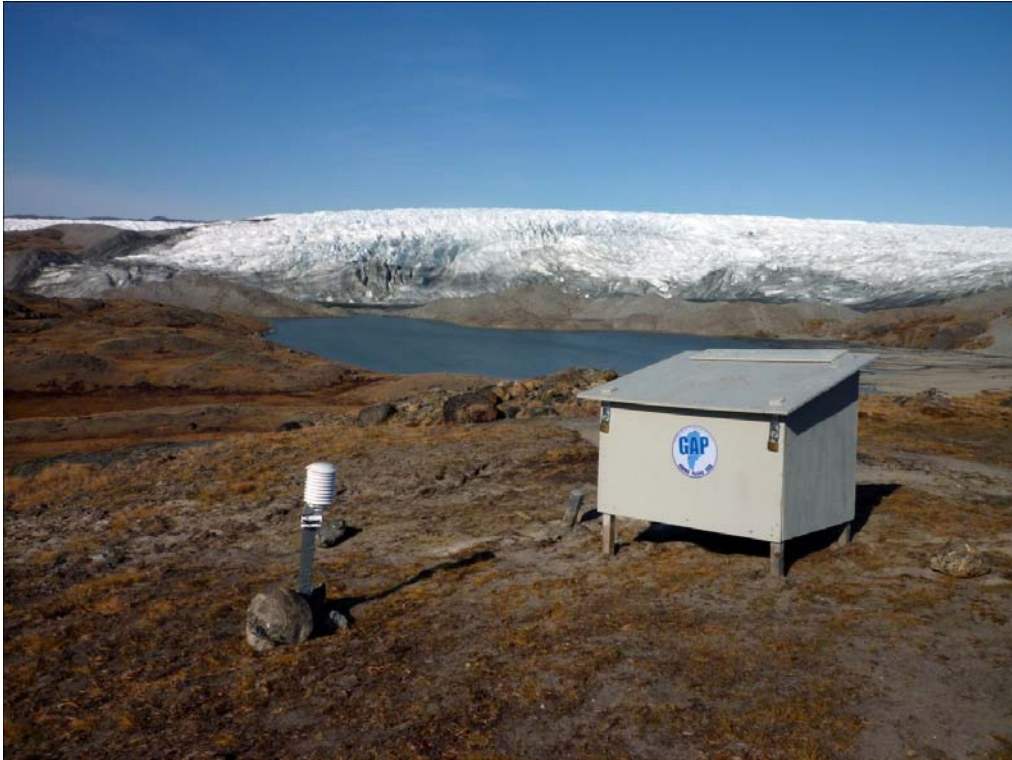


Figure 4-24. Pressure and temperature logging station beside the DH-GAP03 borehole.
Photo by Lillemor Claesson Liljedahl.

Table 4-7. Technical specifications of the Solinst Junior levelloggers 3001.

Level Sensor:	Piezoresistive Silicon in 316L SS
Ranges:	F15/M5, F30/M10
Accuracy (typical):	0.1% FS
Resolution:	M5/F15 – 0.028%, F30/M10 – 0.021%
Normalization:	Automatic Temp Compensation
Temperature Sensor:	Platinum RTD
Accuracy:	±0.1°C
Resolution:	0.1°C
Temp Compensation Range:	–10°C to 40°C
Battery life:	5 Years
Clock Accuracy:	±1 minute/year
Operating Temperature:	–20°C to 80°C
Memory:	Non-volatile EEPROM, FRAM back-up
Maximum # Readings:	32,000 sets of readings
Communication:	Optical Infra-Red to USB or RS232
Size:	7/8" × 5.5" (22 mm × 140 mm)
Weight:	154 g (5.4 oz)
Wetted Materials:	316 L Stainless Steel, Delrin®, Viton®, Buna-N
Sampling Mode:	Linear, SDI-12, Real Time View (from 0.5 sec to 99 hrs)
Barometric Compensation:	Software Wizard and Barologger Gold
Controlling software:	Solinst Levellogger version 3.0

4.5.1 DH-GAP01 P/T/EC sensors

The BO designed to be used in the borehole drilled into an assumed talik measured in total 221 metres, including the BO and insulated deployment string (sampling and heater lines). Testing of the Aqua TROLL was carried out before deployment of the BO. After completed drilling of DH-GAP01 the BO was lowered by hand to a vertical depth of 130 m using the stainless steel U-tube and the deployment string as the strength member. The inflatable packer is located at 130 metres and the P/T/EC sensors (Aqua TROLL 200) at 140 metres.

Table 4-8 outlines a detailed description of the specifications of the Aqua TROLL 200 unit. Table 4-9 outlines the specifications of the sensors and operating range. The Aqua TROLL is connected to the surface via a non-vented cable. A non-vented (absolute) pressure sensor measures all pressure forces exerted on the strain gauge, including atmospheric pressure (PSIA units measured with respect to zero pressure), which implies that corrections for barometric pressure variations are necessary in order to obtain the real pressure at depth.

Once the BO was in place the Aqua TROLL was connected to a PC and the Win Situ software, and a reading was taken and the instrument's depth was checked. The pressure beneath the packer measured 14.08 Bar, equivalent to a vertical depth of 143.6 metres. Table 4-10 shows the results from the three initial readings taken directly after deployment. Since numerous cubic metres of spiked, warm drill water were pumped down into the bedrock during drilling, the stabilization time is expected to be extensive.

The first water sampling test from the U-tube was carried out approximately one hour after the first P/T/EC reading. The following day the Aqua TROLL was set to log every 30 seconds while purging the hole (Figure 4-25 and Figure 4-26).

From 28 June to 1 July a total of 28 pumping cycles were carried out. During this time several different logging intervals were applied. Given the large volume of drill water pumped down into the system, it was obvious that the stabilization of the system would take a long time. At 2 July 2009 the logging frequency was set to 15 minutes. In September 2009, a two months log (15 minutes frequency) was recovered (Figure 4-27 and Figure 4-28). From Figure 4-27 it can be noted that the temperature is steadily decreasing towards a level of ~ 1.3°C. From the pressure data it can be noted that the subsurface system is recovering well following sampling and purging.

As the logged pressure data originates from a non-vented Aqua TROLL, the effects of changes in barometric pressure are detected. Post-corrections of absolute (non-vented) level sensor data should therefore be carried out in order to eliminate barometric pressure from the measurements. In order to post-correct it is important to have access to the barometric pressure for the general time period covered by the log that should be corrected. To monitor the variations in air temperature and barometric pressure a pressure/temperature logging station was installed next to the DH-GAP01 station during the fieldwork in September. However, post-correction to account for barometric pressure variations from July to September was not possible since the P/T logging station was installed in September. Data collected from September 2009 and onwards will be corrected accordingly.

Table 4-8. Aqua TROLL 200 specifications. Campbell 2007.

Equipment/item	Specifications
Cable for power and communication signals.	Non-vented RuggedCable TM, TPU-jacketed. Rugged Twist-Lock cable with all-Titanium connectors.
Communication cable	TROLL Com RS232
Internal power	3.6 VDC (completely sealed non-replaceable AA lithium battery). Battery life time is guaranteed for 5 years or 200,000 readings, whichever occurs first.
Control software	Win-Situ 5

Table 4-9. Detailed specifications of the Aqua TROLL 200 /Campbell 2007/. 1 reading = time plus all available parameters read from device or logged; 1 data point = time plus one parameter in a data log; FS = full scale. Accuracy with 4-20 mA output option $\pm 0.25\%$ FS typical.

Specifications	Range/information
Operating temperature	-20° to + 65°C
Storage temperature	-40° to + 65°C
Dimensions	18.3 mm (O.D.) 31.5 cm (length) 0.45 kg (weight)
Material	Housing (Titanium) Nose cone (Black Delrin)
Power	Internal battery (3.6 V lithium) Battery life (5 yrs or 200,000 readings) External power (8-36 VDC) External battery (14.4 V lithium)
Real-time clock	Accurate to 1 second per day
Real-time reading rate	1 per second
Memory	4 MB, 380,000 data points
Sensor type (Conductivity)	Balanced 4-electrode cell
Material	PVC, titanium
Range	5 μ S/cm to 100,000 μ S/cm
Accuracy	Below 80,000 μ S/cm $\pm 0.5\%$ of reading + 1 μ S/cm Above 80,000 μ S/cm $\pm 1.0\%$ of reading
Resolution	0.1 μ S/cm
Supported parameters	Actual conductivity (μ S/cm, mS/cm) Specific conductivity (μ S/cm, mS/cm) Salinity (PSU) TDS (ppt, ppm) Resistivity (ohms-cm) Water density, based on salinity (g/cm ³)
Sensor type (Pressure/Level)	Silicon strain gauge
Material	Titanium
Range, non-vented	30, 100, 300, 500 PSIA
Units of measure (non-vented)	PSI, KPa, mm, cm, m, in, ft, Bar, mBar, mm Hg
Accuracy	At 15°C $\pm 0.05\%$ Full Scale (FS) 0° to +50°C $\pm 0.1\%$ FS -20° to -1 and 51 to 80°C $\pm 0.25\%$ FS typical
Resolution	$\pm 0.005\%$ FS or better
Max. pressure	2 \times range
Burst pressure	3 \times range
Range non-vented Aqua TROLL 200	0-341.3 metres useable depth (500 PSIA)
Sensor type (Temperature)	
Material	Titanium
Range	-20° to +65°C
Units of measure	Celsius, Fahrenheit
Accuracy	$\pm 0.1^\circ$ C
Resolution	0.01°C

Table 4-10. First three readings from Aqua TROLL (S/N 138643) installed in DH-GAP01. Note that time is given in local Greenlandic time (i.e. GMT-3).

Date and time	28 June 2009, 13:58	28 June 2009, 14:58	28 June 2009, 15:58
Pressure (Bar)	14.08	14.13	14.06
Temperature (°C)	3.31	3.12	3.01
Actual conductivity (μ S/cm)	155.65	162.192	206.515
Specific conductivity (μ S/cm)	265.741	278.646	356.128
TDS (ppt)	172.731	181.12	231.483

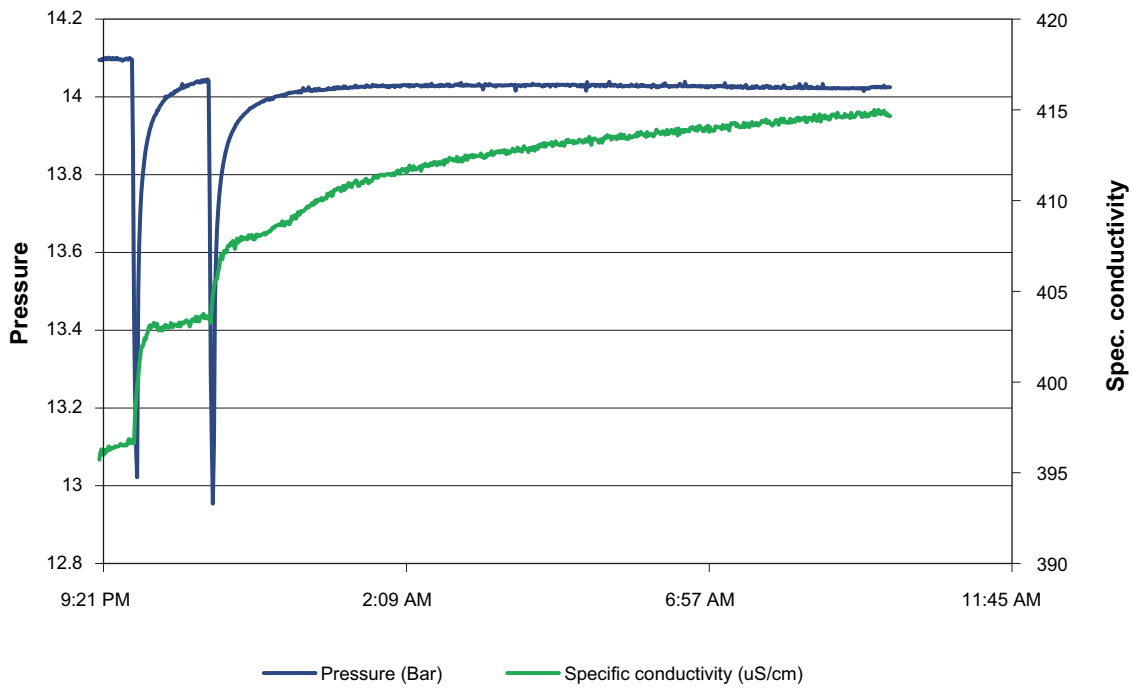


Figure 4-25. DH-GAP01 pressure and specific conductivity changes over time while performing purging (x2). The purging can be seen clearly in the chart as significant pressure drops and specific conductivity increases. Data is from 28 to 29 of June, 2009. The logging interval was 30 seconds. Note that time is given in local Greenlandic time (i.e. GMT-3).

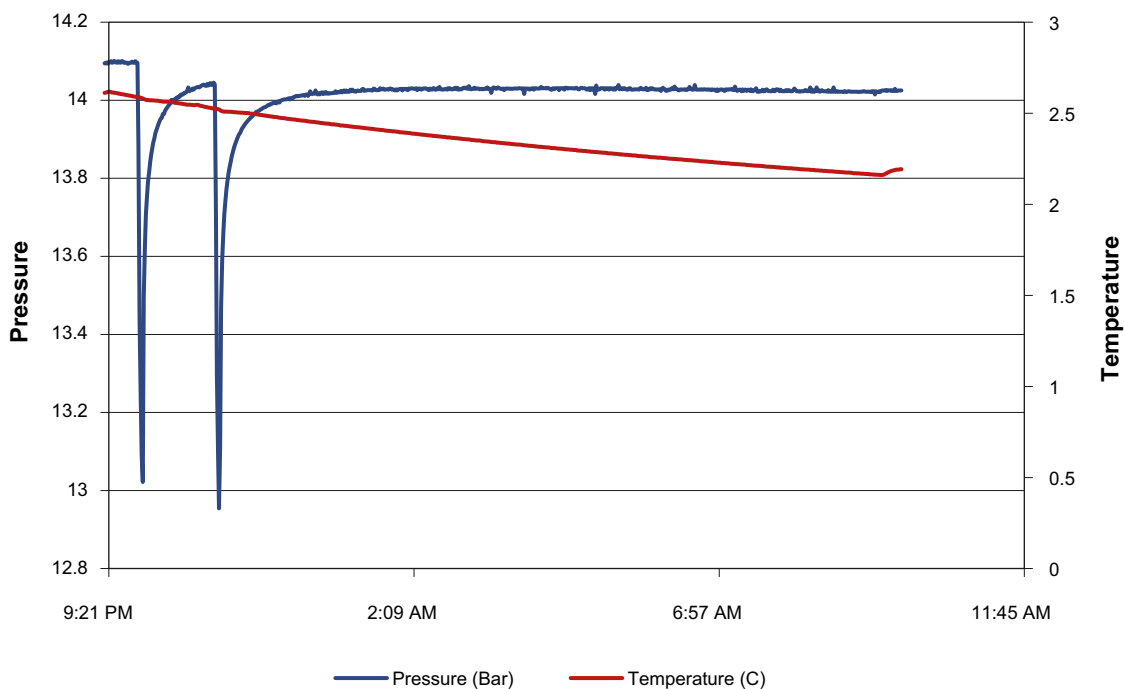


Figure 4-26. DH-GAP01 pressure and temperature changes over time while performing purging (x2). The purging can be seen clearly in the chart as significant pressure drops while the temperature is decreasing continuously. Data is from 28 to 29 of June, 2009. The logging interval was 30 seconds. Note that time is given in local Greenlandic time (i.e. GMT-3).

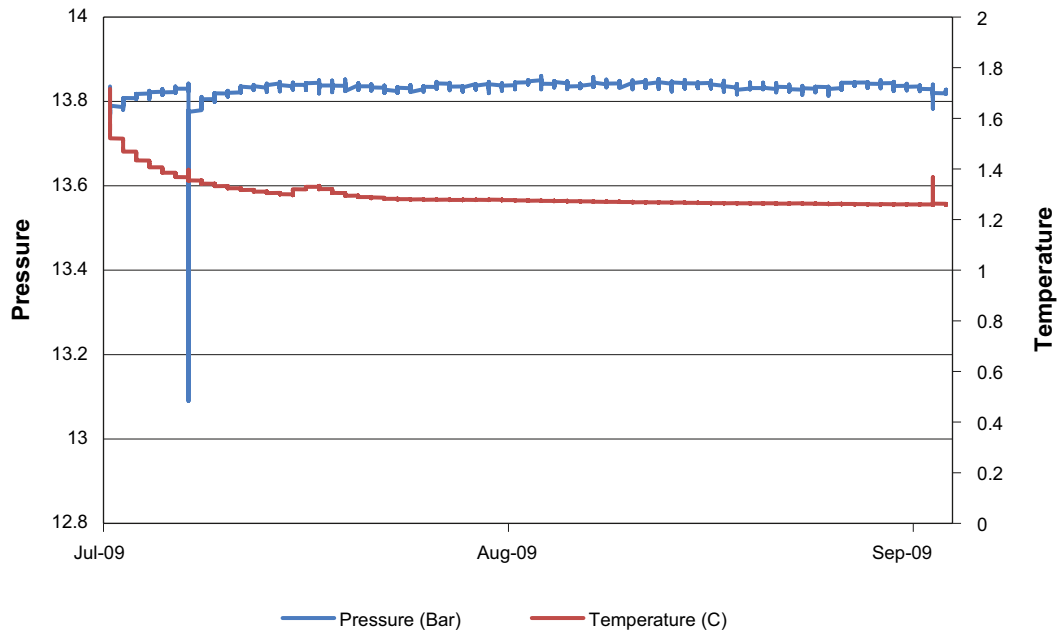


Figure 4-27. DH-GAP01 pressure and temperature over time. Logging frequency 15 minutes. No barometric pressure correction has been applied. The significant pressure drop in the beginning of July coincides with water sampling. Note the positive temperature peak and coinciding pressure drop in September, which coincides with several repeated small volume purges.

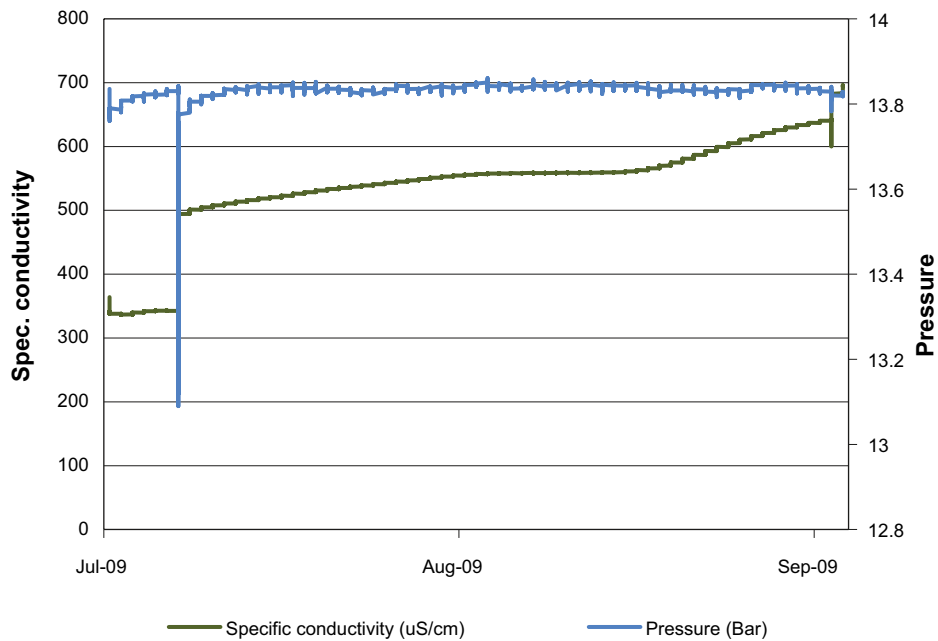


Figure 4-28. DH-GAP01 pressure and specific conductivity changes over time. Logging frequency 15 minutes. No barometric pressure correction has been applied. The significant pressure drop in the beginning of July coincides with water sampling. The significant increases in specific conductivity coincide with water sampling.

Since the Aqua TROLL is equipped with a non-replaceable battery, it was decided to change the logging frequency to every 6 hours, to allow for a longer monitoring period. The logging frequency was change to every 6 hours on 7 September 2009.

Table 4-11 shows the final reading carried out in DH-GAP01 in 2009 and the comparison with the first reading carried out in June. These results clearly show (e.g. increase in TDS and conductivity) that the borehole is recovering from drill water contamination and that formation water is entering the borehole.

4.5.2 DH-GAP03 P/T/EC sensors

Due to problems arising during the instrumentation of DH-GAP03, it was not possible to instrument this borehole with a U-tube system. Instead the borehole was instrumented with an Aqua TROLL together with a DTS cable (see Section 4.2.5) and two heating cables. Testing of the Aqua TROLL was carried out before deployment. The Aqua TROLL, DTS and heating cables were lowered by hand to a depth of 329 metres (309 metres vertical depth). Once the Aqua TROLL was in place and it was connected to a PC and the Win Situ software, a reading was taken and the instrument's depth was checked. The pressure beneath the packer measured 27.58 bar, equivalent to a vertical depth of 281.32 metres. The Aqua TROLL was set to log every 135 minutes. Table 4-12 shows the results from three readings taken directly after deployment on 6 July 2009, as well as the final reading for 2009 taken on 7 September 2009.

To monitor the variations in air temperature and barometric pressure a pressure/temperature logging station was installed next to the DH-GAP03 station during the fieldwork in September. However, post-correction to account for barometric pressure variations from July to September was not possible since the P/T logging station was installed in September.

Table 4-11. First and final recorded readings for 2009 from Aqua TROLL (S/N 138643) installed in DH-GAP01.

Date and time	28 June 2009, 13:58	7 September 2009, 19:58	Change from first to final reading
Pressure (Bar)	14.08	13.77	-0.31
Temperature (C)	3.31	1.26	-2.06
Actual conductivity ($\mu\text{S/cm}$)	155.65	388.406	+232.756
Specific conductivity ($\mu\text{S/cm}$)	265.741	712.42	+446.679
TDS (ppt)	172.731	436.075	+263.344

Table 4-12. First three and final readings from Aqua TROLL (S/N 138684) installed in DH-GAP03. Logging frequency 135 minutes.

Date and time	6 July 2009, 21:07	6 July 2009, 23:22	7 July 2009, 01:37	7 September 2009, 18:06
Pressure (Bar)	27.99	27.98	27.90	19.96
Temperature (C)	4.68	4.78	4.71	17.61*
Actual conductivity ($\mu\text{S/cm}$)	229.295	353.997	347.229	0
Specific conductivity ($\mu\text{S/cm}$)	374.678	576.722	566.952	0

* suspected malfunction

In September, two month's worth of data was recovered from the Aqua TROLL. It was initially not possible to connect the Aqua TROLL to the PC, *i.e.* no signal from the sensors. However, connection was established after a few retries. Figure 4-29 shows the variations in pressure, temperature and specific conductivity over time. It became obvious very soon that something was erroneous with the Aqua TROLL. The primary indicator of this error was the bottom temperature reading ($\sim 17.5^{\circ}\text{C}$). As can be noted from Figure 4-29 the pressure displays an overall decrease, whereas temperature displays an initial drop followed by a continuous increase with a drastic increase around mid July. Specific conductivity is scattered and displays dramatic and sudden increases and decreases. From July 17 the specific conductivity was recorded as zero. Several attempts to reset the Aqua TROLL were made without any improvements. After communication with the manufacturer (in situ), it became clear that the Aqua TROLL had experienced some internal failure. The last reading indicates that the pressure is 19.96 Bar, recalculated to a depth of 198.80 m (Aqua TROLL depth) and that the water density is 0.9987 g/cm^3 . However, the actual vertical depth of the Aqua TROLL position is 309 m. One possible explanation for the failure of the sensors is that since the drilling did not go through the base of the permafrost but came very close. It is likely that the Aqua TROLL is located in a zone of "slush" (semi-frozen water), which has made the sensors freeze and collapse. Due to the ~ 300 metres of ice in the borehole, it was not possible to replace the Aqua TROLL.

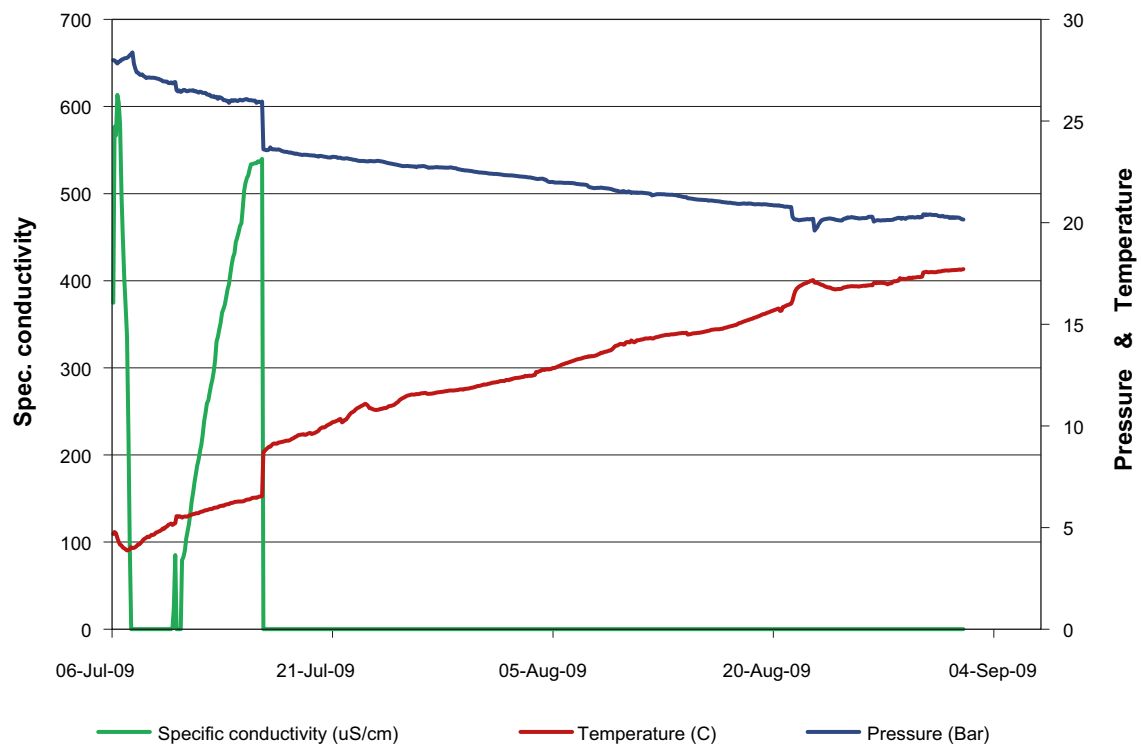


Figure 4-29. DH-GAP03 pressure and temperature variations over time. The logging frequency was 135 minutes. No barometric pressure correction has been applied.

4.6 Distributed temperature sensing (DTS)

The Distributed Temperature Sensing (DTS) system utilizes a passive optical fiber acting as temperature sensor, which allows for the monitoring of exact temperature profiles along the optical cable. The DTS-measurement is based on the proven Raman-Optical Time-Domain-Reflectometry technique. An optical laser pulse propagating through the fiber receives scattered light back to the transmitting end, where it is analyzed. By measuring accurately the difference in the signal intensity of the backscattered light, an accurate temperature measurement can be made along the whole length of the optical fiber (Figure 4-30).

GTK's Agilent DTS device from AP Sensing is applied for the investigations in the GAP-project (Figure 4-31). The accuracy for the temperature measurements is one metre spatial resolution and 0.1°C temperature resolution. To get this accuracy a minimum time of 15 min per measurement is required. To get the real temperature the device also has to be calibrated with a known external temperature source, e.g. an ice-bath, for every measurement (Figure 4-32).

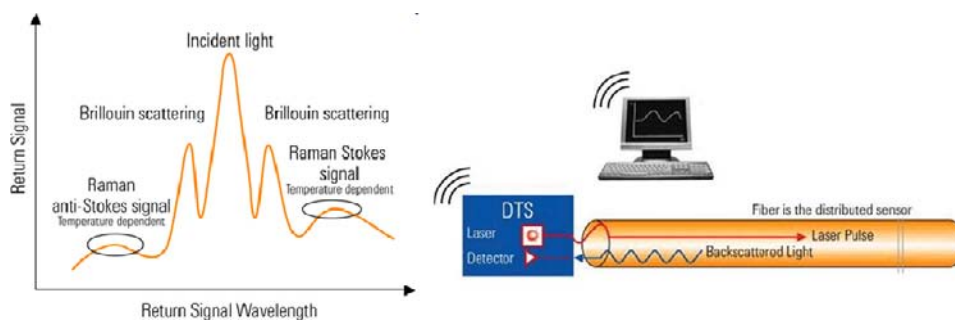


Figure 4-30. The DTS-technique is based on the Raman-Optical Time-Domain-Reflectometry technique, where an optical laser pulse is propagating through an optical fiber and gets scattered light back to the transmitting end, where it is analyzed (© AP Sensing).



Figure 4-31. Ongoing DTS-measurement at borehole DH-GAP01. The DTS-device is located under the Toughbook computer. Photo by Jon Engström.



Figure 4-32. Loop of fibre optical cable is immersed into an ice-bath in order to obtain a reference temperature for the DTS-measurements. Photo by Emily Henkemans.

4.6.1 DTS measurements in DH-GAP01 and DH-GAP03

Both boreholes were equipped with a steel coated optical BRUsteel FRNC cable with dual fibers specifically designed for harsh environments. The DTS-cable at DH-GAP01 was lowered together with the sampling device thus it is located above the packer at 0–150 m of borehole length. The acquired temperature data represents a profile down to 130 m of vertical depth. The Aqua TROLL device is located just beneath the packer at 140 m of vertical depth. It provides an independent temperature reference point 10 m below the lowest point of the DTS-cable.

DTS measurements in DH-GAP01 were performed at several occasions after the installation. The first measurement was conducted one day after the installation. This measurement shows distinct temperature peaks at several locations along the profile. Reason for these peaks is still not confirmed, but one possibility is that the backflow of hot drilling water from fractures would induce these temperature peaks. This theory is supported by the measurement performed one week later indicating clearly lower temperatures and smoother peaks than before (Figure 4-33).

The coupling of the fracture frequency to temperature peaks is a challenging task. Although fracturing is observed at the locations where most of the peaks occur, in order to know exactly which fracture is tied to a certain peak is complicated. In principle it is also possible that there is some systematic shift in the depth readings of the DTS due to reasons related to the DTS unit or its software, or more likely, to the true location of the cable in the borehole.

The measurements carried out in September show a steady state for the temperature profile, and indicate a permafrost boundary at 20 m of borehole length. This confirms that DH-GAP01 penetrates to a talik below the lake (Figure 4-33). The transition from frozen to unfrozen ground is located right at the shoreline of the lake. It is expected to move further towards the lake during winter, when the shallow waters freeze down to bottom. A heating test was performed in September where the borehole was heated with a heating cable for 3 hours time. DTS measurements were carried out during the heating and cooling periods. The temperature of the whole borehole was raised approximately 1°C, although it seems to be less in the frozen area probably due to the phase change. The effect of the heating can be clearly seen in the temperature profiles. The temperature in the borehole recovered to its initial state approximately 2 hours after the heating was stopped (Figure 4-34). This confirms that the installed heating cable in DH-GAP01 works as expected.

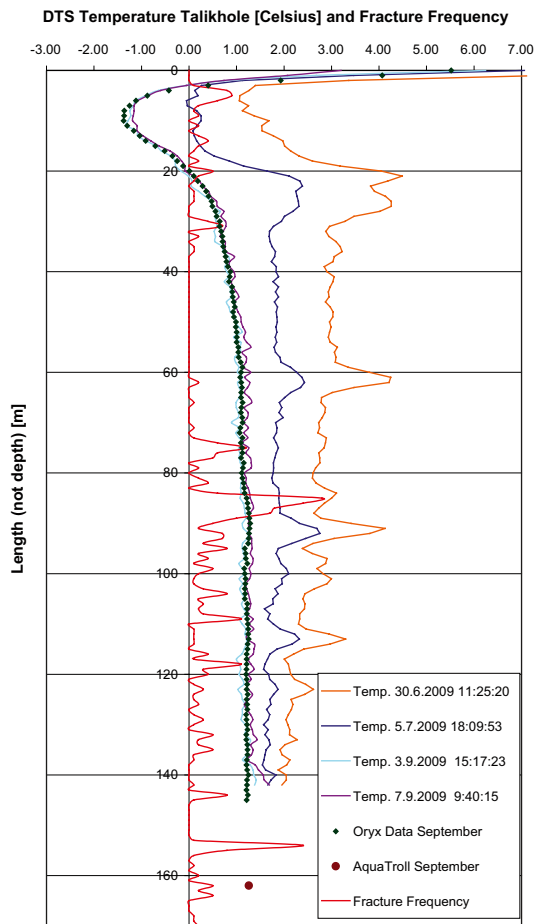


Figure 4-33. Chart showing temperature profiles in DH-GAP01. Aqua TROLL provides an independent reference temperature at 162 m (140 m of vertical depth). The orange and blue lines demonstrate the cooling after hot-water drilling. Heterogeneous cooling is evident and it is assumed that the peaks are related to leaking fractures. The steady state was reached in September. Fracture frequency per metre is also given. Note that the depth is borehole length.

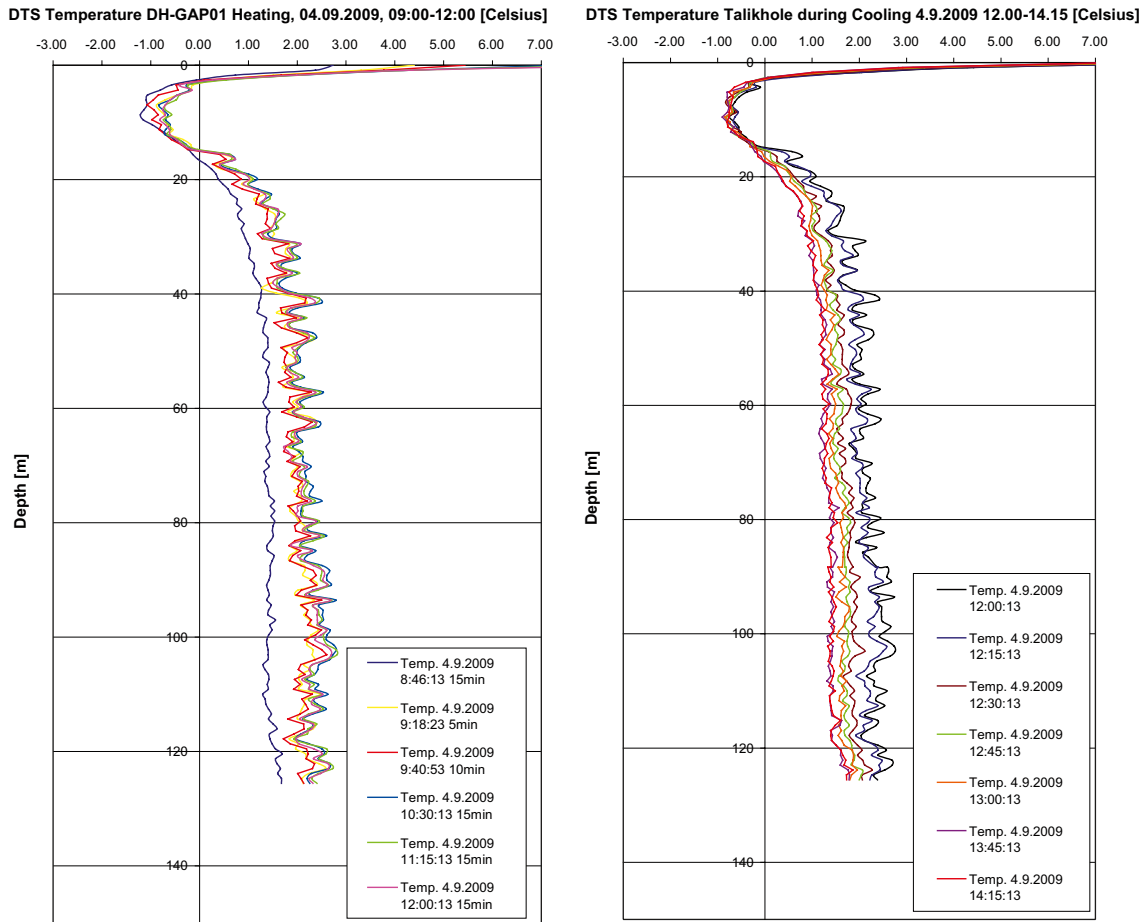


Figure 4-34. Charts showing temperature profiles in DH-GAP01, during heating and cooling. The profiles on the left provide trends during heating between 09:00–12:00 and on the right hand side is given the cooling trends cooling between 12:00–14:15. Note that vertical depth is given instead of borehole length.

In September 2009 we also carried out a depth/temperature profile of the Talik Lake along a traverse roughly coinciding with the trace of the borehole. The measurements were done with an Antares temperature probe, with a resolution of 0.01°C. The probe was attached to a measuring tape thus giving the depth while measuring temperature (Figure 4-35). The measurements were done at every 20 m along the traverse giving in total 13 measurement points. The deepest part of the lake in this area was 13 m. The end of DH-GAP01 is located just beneath the ‘central basin’. The temperature measurements indicate that the lake water is mixed very well with a temperature difference of 1.7°C. The coldest temperature, 8.87°C, measured was at the deepest point, 13.2 m, while the warmest temperature, 10.53°C, was at the shallowest point, 0.2 m.

The DTS-cable at DH-GAP03 was lowered successfully together with the Aqua TROLL device to the vertical depth of 309 m. Unfortunately, since the Aqua TROLL installed in DH-GAP03 is not functioning properly, it was not possible to obtain a down hole reference temperature and therefore only an ice-bath at the surface was applied for the purpose. One successful measurement was done in July 2009 and as we had some problems with the reference ice-bath, the calibration for that measurement is done by averaging the offset from other measurements. This measurement was performed the next day after the installation and it shows that the hole is frozen just below 40 m of vertical depth (Figure 4-36).

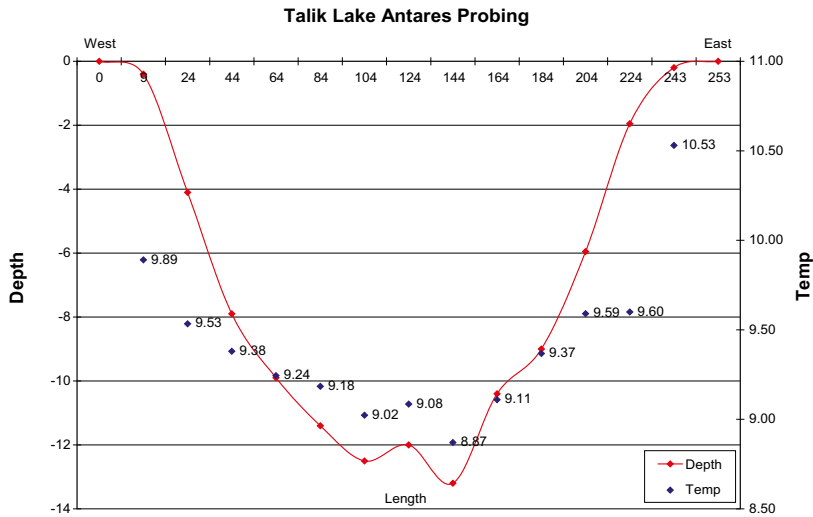


Figure 4-35. Chart showing the temperature/depth traverse over the Talik Lake. The deepest point is at ca. 13 m depth with a temperature of approximately 8.9°C.

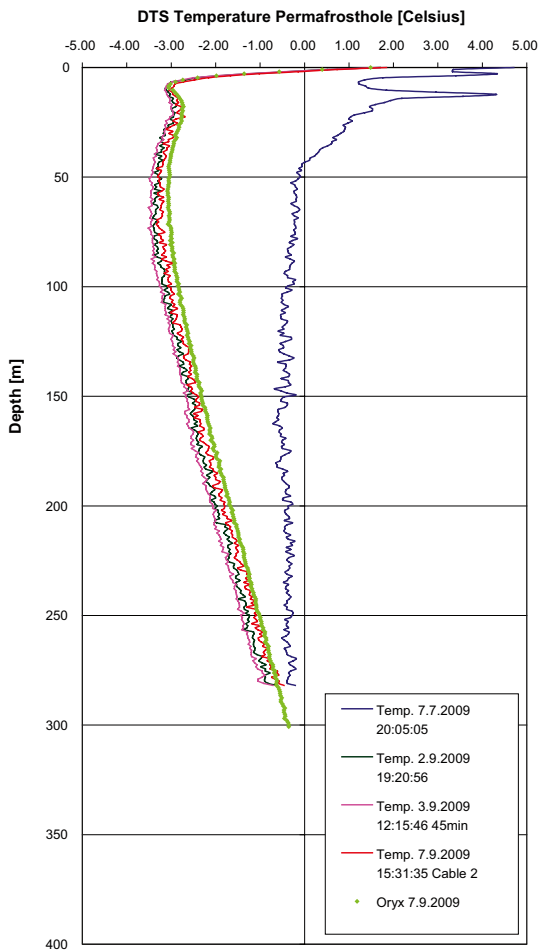


Figure 4-36. Temperature profiles in DH-GAP03. Note that vertical depth is given instead of borehole length.

Two measurements were conducted in September 2009, the first just after our arrival and the other just before our departure. These measurements give the steady state for the temperature profiles in DH-GAP03. The temperature at 309 m is -0.5°C , which means that the borehole did not penetrate the permafrost (Figure 4-36). An approximation from the slope indicates that the base of permafrost is at ~ 335 m of vertical depth. This exceeds by about 100 m the reported permafrost thickness measured from the Paakitsoq borehole located 275 km north from Kangerlussuaq /Kern-Hansen 1990/. In order to confirm the results obtained using the Agilent DTS unit, measurements were done in September 2009 using another type of DTS device. Victor Bense from the University of East Anglia, UK, carried out the measurements with Oryx Sensornet. The results obtained using the Oryx DTS unit confirmed the Agilent DTS results.

4.6.2 Modelling of the temperature observations in DH-GAP01 and DH-GAP03

Numerical heat transfer modelling of the borehole temperature observations was done with the aim to understand the thickness of the permafrost and to investigate the taliks under the lakes. The following results are preliminary and provide a general overview of the permafrost conditions at the study site.

The temperature logs obtained in the two holes are shown in Figure 4-33 and Figure 4-36. The data has considerable noise in the logs but the general characteristics are observed. There is a dramatic difference between the two holes. The “permafrost hole” (DH-GAP03) shows temperatures well below freezing, an inversion of temperature gradient in the uppermost 100 m which is attributed to recent warming, and a stable gradient beneath. The data directly indicates that the base of permafrost is at about 330 m below surface at the drilling site. On the other hand, the “talik hole” (DH-GAP01) shows temperatures above zero at depth exceeding 20 m. The temperatures increase from 20 m depth to about 60 m depth and then remain constant to the lowest measuring point at about 145 m.

The differences in temperature profiles between DH-GAP01 and DH-GAP03 are probably due to different average ground temperatures in the permafrost and talik, and the heat transfer which is not 1-dimensional under the talik-permafrost transition zone. We investigated the heat transfer in bedrock by 2D conductive models using the simulation code *Processing Schemat* (Figure 4-37). Different average ground surface temperature values were assigned to permafrost (-4°C) and talik ($+4^{\circ}\text{C}$) terrains. The other applied thermal parameter values (conductivity, basal heat flow) are only estimates, but probably representative for the study area. Basal heat flow of 38 mWm^{-2} and thermal conductivity of medium $3 \text{ Wm}^{-1}\text{K}^{-1}$ were used. Porosity was assumed to be 0%. The talik temperature was varied between $+2$ and $+4^{\circ}\text{C}$ in the models. These values were based on the fact that the lakes do not annually freeze to the bottom, and a layer of water always exists beneath the ice cover.

The modelling suggests that the talik generates a distinct anomaly in the temperature isolines. Temperature isolines show that the transition zone between permafrost and talik extends several hundred metres from the terrain boundary, *i.e.* from the jump in constant surface temperature value.

Figure 4-37 indicates how the boreholes would be located in the model. The model suggests that holes in permafrost and located sufficiently far from lakes should have temperatures which are close to a homogeneous half-space situation. Holes located on the boundary between surface temperature domains, such as the talik hole, should have temperature profiles deviating strongly from homogeneous half-space conditions. Even approximately isothermal conditions in the borehole may be observed if the hole happens to be appropriately located and oriented. These modelling results are in a good agreement with observations in the drill holes.

To sum up, permafrost conditions in the research area would therefore seem to be represented by thick permafrost (more than 300 m) in areas which are located more than about 500 m from big lakes. Permafrost thins towards lakes and disappears below the lakes. Beneath very small lakes or ponds there is probably a continuous layer of permafrost, but lakes more than approximately 100 m wide probably support taliks. Therefore, the overall permafrost distribution in the area can be described as discontinuous (“emmental cheese model”) where larger lakes have taliks beneath. Viewing a topographic map of the area will likely give a good approximation of the permafrost/talik distribution.

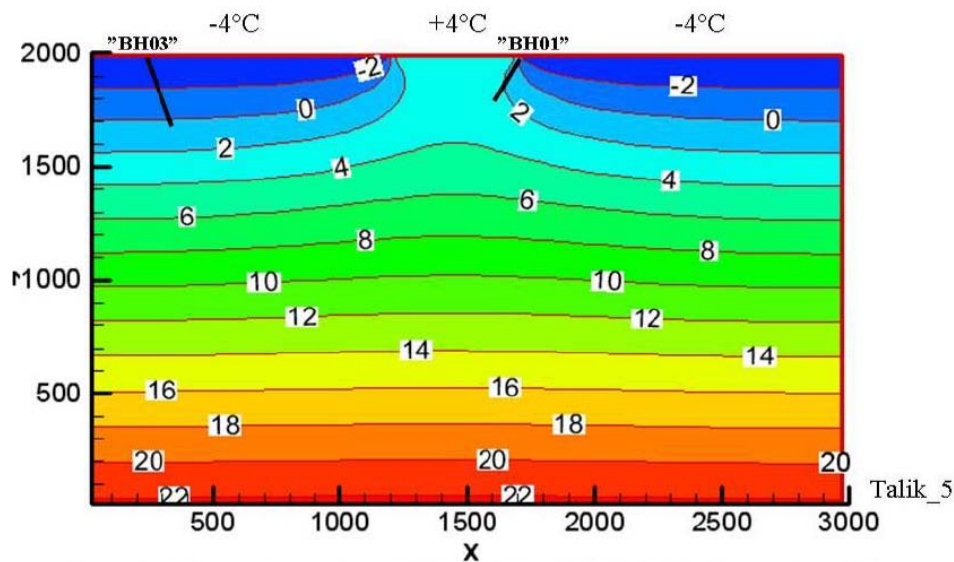


Figure 4-37. 2-dimensional steady-state conductive heat transfer model of a 500 m wide talik (lake). Surface temperature in permafrost is -4°C , and $+4^{\circ}\text{C}$ in talik, respectively. Basal heat flow is 38 mWm^{-2} and thermal conductivity of medium is $3\text{ Wm}^{-1}\text{K}^{-1}$. Porosity is assumed to be 0%.

The present modelling results are the first and only preliminary results. In further studies, time-dependent calibrated conductive forward models need to be constructed. To this end we need background information on the Holocene palaeotemperatures and ice cover history of the area, meteorological time series data on the air, ground and soil temperatures as well as lab measurements of rock thermal properties of the drill cores. Additionally, the recent ground surface temperature history during the last hundred years can be estimated from the permafrost hole data. Finally, coupled conductive-advective flow modelling could also be constructed.

4.7 Hydrogeochemistry of DH-GAP01 and surface waters

One of the important purposes of SPC is to understand how groundwater flow and geochemistry are affected by a continental ice sheet. Previous research on groundwater and geochemistry during the last ice age has focused mainly on large scale modelling and leaves a lack of physical data with which to calibrate these models. A great deal is still unknown about groundwater in deep crystalline rocks under glacial conditions. The main objective of SPC is to get better understanding of pressures and flow paths of groundwater in crystalline rock during glacial advance and retreat.

4.7.1 Preliminary preparations of DH-GAP01

The drill hole at the ‘Talik Lake’ (DH-GAP01) was flushed while drilling with approximately 40,000 litres of heated surface water with an average sodium fluorescein concentration of $221\text{ }\mu\text{g/L}$ as a tracer. DH-GAP01 was outfitted with a U-tube sampler at a vertical depth of 130 m /Freifeld et al. 2005/ and samples were obtained from the drill hole in June/July 2009 and again in September 2009. For the technical description of the sampler see Section 4.5. The sampling section was 150–221 m (borehole length), i.e. section between the packer and the bottom of the hole. A pressure of about 350 PSI was applied for purging samples. After the sample was obtained both the inlet and outlet lines should be detached from the nitrogen cylinder. Failure to detach both lines from the gas cylinder in September resulted in a very slow refill time for the sampler, because over-pressure conditions were maintained in the sample reservoir. In June/July the groundwater sampling section was purged 28 times before sampling and in September it was purged a total of five times.

4.7.2 Instrumentation of the Pingo Spring area

The Pingo Spring found on the till plain in front of Leverett glacier provides an opportunity unique to the area to study the groundwater flow system without drilling as it has been described as an open system pingo by /Scholz and Baumann 1997/. Open system pingos are created and maintained by groundwater flow.

In the summer of 2009 the Pingo Spring was instrumented with four drive-point piezometers. These piezometers consist of a stainless steel, screened end with a sharp tip (Figure 4-38). Polyethylene tubing (1/4" OD) is attached to the piezometer which is also threaded for 3/4" schedule 80 pipe designed to protect the tubing. A sledge hammer and T-bar were used to hammer the assembled drive-point piezometers into the bed of the pingo at 4 locations. One (#1) was positioned near where gas and water are observed to be upwelling and another (#4) was positioned at the pingo outflow. The remaining two were installed based on testing with a rod to see where stones and ice would allow the drivepoint to penetrate into the bottom sediment (Figure 4-39).

A sample was taken from Piezometer 1 after installation. Piezometers were then given 9 days to recover from installation before being sampled. Piezometers were then flushed using water (Lake 0013, Figure 4-41) for which isotope and inorganic geochemistry is known. The piezometers were then sampled again in September 2009 after recovery from flushing. Sampling was conducted using a vacuum hand pump outfitted with narrow tubing to fit down the piezometers tubing and attached to a filter flask to collect the sample.

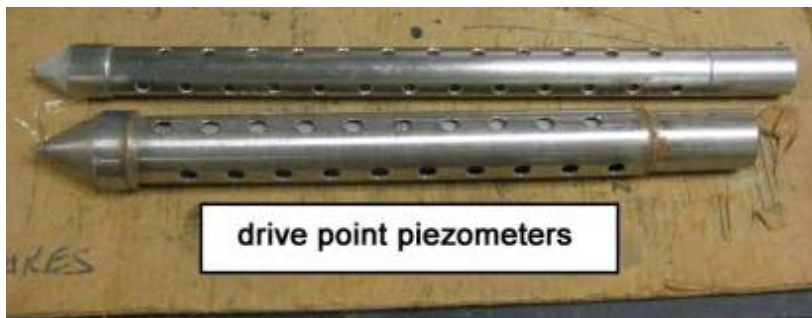


Figure 4-38. Drive point piezometers.



Figure 4-39. Location of the drive-point piezometers in the Pingo Spring. Photo by Emily Henkemans.

4.7.3 Sampling and analysing methods

A YSI 600 QS probe with a YSI 650 hand unit was used to measure field parameters: conductivity, salinity, pH, temperature, dissolved oxygen, oxidation-reduction potential and depth of measurement. The metre was calibrated initially for conductivity, daily for dissolved oxygen and depth measurements and every second day for pH. Lake profiles were accomplished from a zodiac using the YSI probe which was equipped with a 30 m cable.

The first geochemical samples from DH-GAP01 were collected with a groundwater sampler (0.45 µm membrane) under nitrogen atmosphere. However, the sampler equipment did not have an over pressure release system and therefore was not suitable to use with the gas regulator. Cation and anion samples were filtered through 0.45 µm sterile disposable filters at the field site. Anion samples were collected into Nalgene plastic bottles with no treatment. Cation samples were collected in acid washed Nalgene plastic bottles. Cation and Sr, B, U and Li samples were preserved against bacterial growth, oxidation reactions and precipitation using super pure HNO₃ (nitric acid) added to the samples until a pH > 2 was reached. Geochemical analyses were performed by Teollisuuden voima (TVO) laboratory in Olkiluoto. Isotope samples (¹⁸O, ²H and ³H) were collected in 1 L Nalgene plastic bottles and were not filtered. Analyses were conducted at the University of Waterloo Environmental Isotope Laboratory. All the samples were kept in refrigerator before delivering to laboratory.

The gas sample from the Pingo Spring was collected using a large funnel into glass bottles with Teflon septum caps. Gas analyses were performed at the University of Waterloo Organic Geochemistry Lab.

4.7.4 Drill hole and surface water sampling

Five water samples were taken from the DH-GAP01/150–221 m (borehole length) in June/July and September 2009. δ¹⁸O, δ²H and ³H isotopes were analyzed as well as the inorganic chemistry and sodium fluorescein concentrations. The first (taken on 30 June 2009) and second (1 July 2009) samples from DH-GAP01 were sent from Kangerlussuaq to Olkiluoto, Finland. The last sample collected during the summer fieldtrip on 8 July 2009 and both samples from September fieldwork were sent with the field crew returning to Olkiluoto.

Sampling of surface waters began in the summer of 2008 with 27 lakes sampled for isotopic and geochemical analyses (Aaltonen et al. 2010). In 2009 sampling was expanded to include several other lakes and several of the lakes initially sampled in 2008 were re-sampled. In 2009 a total of 20 samples were taken for isotopic analyses (δ¹⁸O, δ²H and ³H), 12 samples were taken for geochemical analyses and 1 sample was taken for gas analyses.

Surface water sampling in 2009 was directed towards two goals: to (a) examine possible groundwater connection between the ice sheet, and the Pingo Spring and blue lakes in front of the glacier (Figure 4-40) and (b) look for evidence of groundwater discharge into lakes located along fault lines where increased fracture density may provide a conduit for glacial recharge.

With the hypothesis that groundwater entering the Pingo Spring and/or till plain lakes will have parameters such as pH, conductivity and temperature that are different from those of the surface water body, the Pingo Spring and three of the large till plain lakes (lakes 0013W, 0028W and 0029W) were profiled. Using a zodiac boat, field parameters were recorded from the surface to the lake bed. Samples for isotopic and geochemical analyses were taken from each profiled lake. For Lake 0013 W, samples were taken at 3 depths while for Lakes 0028W and 0029W, a single sample was taken from close to the lake bed (Figure 4-41).

The possibility that groundwater may flow preferentially along fault lines was tested by sampling 4 lakes along the major fault that runs from Russell's Glacier to Kangerlussuaq. This included the previously sampled Lake 0013W as well as 3 additional lakes: 0032W (FL2), 0033W (FL3) and 0034W (FL4), (Figure 4-42, lower left). Lake 0032W (FL2) was sampled only for isotopic analyses. The Talik Lake was also sampled as it is located along a lineament.



Figure 4-40. View from the Leverett till plain. The ice margin is located to the left of the image. The Pingo Spring stained with iron precipitates is distinct from the numerous blue lakes and ponds in the area. Photo by Timo Ruskeeniemi.



Figure 4-41. Locations of the Lakes 0013W, 0028W and 0029W relative to the Pingo Spring and the Leverett Glacier. Photo by Emily Henkemans.

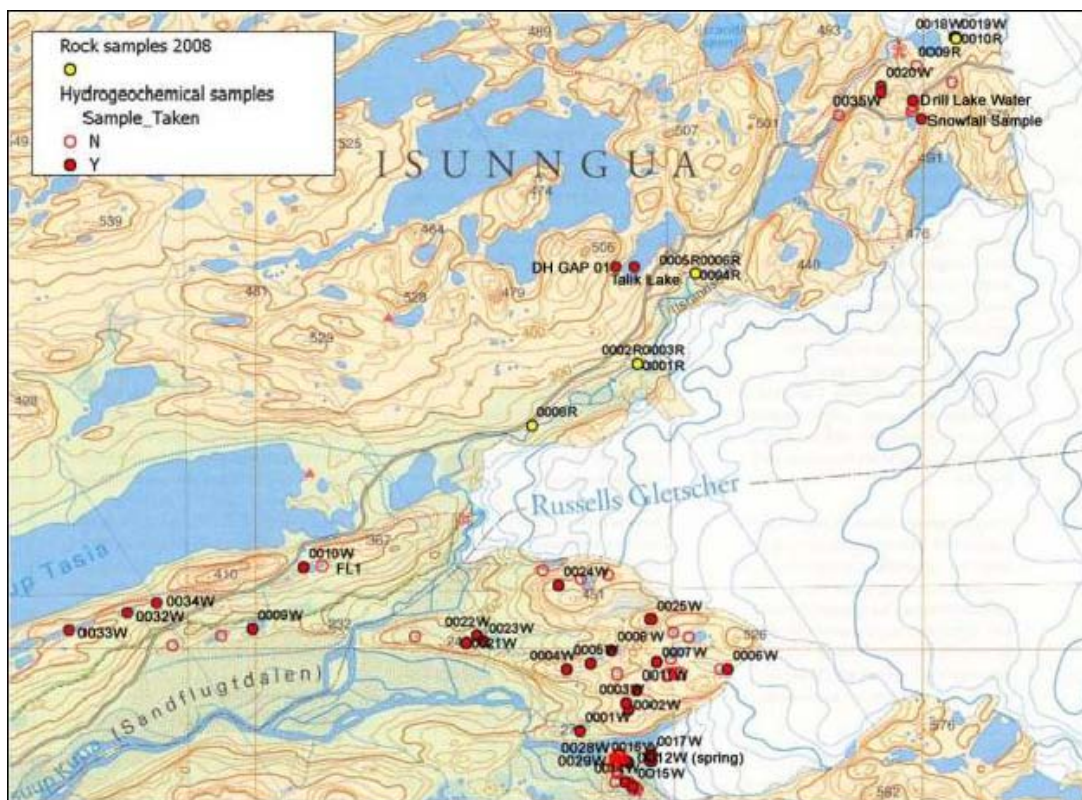


Figure 4-42. Map of sample locations including both 2008 and 2009 hydrogeochemical samples and locations where field parameters were measured but no sample was taken.

4.7.5 Drill hole DH-GAP01 and surface water results

No significant changes in any parameter measured by the YSI probe were noted for any depth in either the till plain lakes or the Talik Lake. This is also true for the transect along the borehole line in the Talik Lake.

Lakes sampled along the Kangerlussuaq fault line did not show any characteristic that might distinguish them from other surface waters sampled. It is likely that any groundwater input present is too minimal to imprint the bulk surface water with a measurable geochemical or isotope parameter that would characterize the sample as groundwater, such as significantly higher EC or lower ^3H than other surface water bodies.

The first sample from the DH-GAP01 was taken after 7 rounds of purging and the sodium fluorescein concentrations was still high (Figure 4-43), as expected being close in time to the drilling. Seen from the concentration of dye, all June /July samples are dominated more by drill water rather than by natural groundwater. The last sample that was taken on 7th September is more representative of groundwater composition. Sodium fluorescein concentration has decreased remarkably over the sampling period whereas main ions and TDS concentrations have increased (Figure 4-43). The chemistry and isotopes of the borehole water are distinct from the Talik Lake water used for the drilling. The borehole water (talik water) is chemically more evolved and can be referred to as groundwater especially due to a lack of nuclear bomb test induced tritium in talik water, which indicates that water recharged at least 50 years ago. In addition, the higher conductivity in talik water in September ($711 \mu\text{S}/\text{cm}$) compared to lake water ($171 \mu\text{S}/\text{cm}$) indicates more dissolved components in it. These results suggest longer water-rock interaction and residence times.

A progression in $\delta^{18}\text{O} - \delta^2\text{H}$ composition of DH-GAP01 samples from similar to the lake water used for drilling toward more depleted values falling closer to the global meteoric water line indicates that drill water was almost completely flushed from the system by September (Figure 4-43a). This is supported by the decrease in concentration of the sodium fluorescein tracer from the drill hole water from 120 to $35 \mu\text{g}/\text{L}$ over the same time period (Figure 4-43).

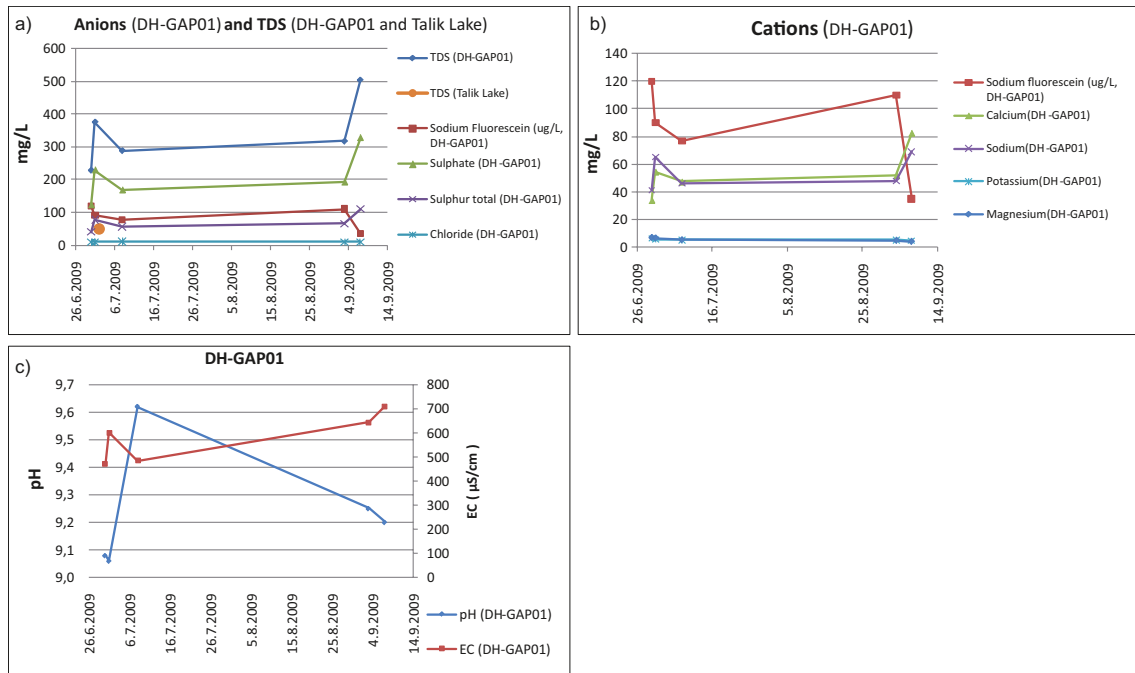


Figure 4-43. a) Main anion, b) cation concentrations and c) pH and electrical conductivity in the DH-GAP01 samples taken in June/July and September 2009.

The Pingo Spring water was found to be 3 degrees colder in Sept. 2009 than in the summer of 2008, /Aaltonen et al. 2010/, likely as a response to the cold, late summer in 2009. Isotopic analyses revealed that the spring water was also more depleted in oxygen-18 and deuterium in autumn of 2009 and tritium went from low levels (1.5 TU) in 2008 to non-detect in 2009. The isotopic shift may represent a decrease in tritiated meteoric input to the Pingo Spring in 2009. The pingo spring is producing bubbles, and gas and water samples have been taken from the spring pool (see Figure 4-39) during 2008 and 2009 (see Table 4-13 for gas analyses results). The gas bubbling out of the pingo spring is a mixture of N₂, O₂, CO₂ and CH₄. How the O₂ is introduced to the system is not yet known. There are quality questions concerning the 2008 gas sample related to the sampling procedure. However, the sample taken in 2009 was considerably better. It is possible that compositions are somewhat modified by oxidation and microbial action. However, the presence of substantial dissolved iron (6 mg/L) suggests that the pingo water contained Fe(II) and therefore the groundwater discharging at the pingo should be oxygen-free, in contradiction with the observed gas analyses. Moreover, oxygen combined with Fe(II) in groundwater has a lifetime of a few hours at most, depending on e.g. pH /Stumm and Morgan 1996/. Additional and better quality samples will be collected in the future.

In the Pingo piezometers a noticeable change occurred from the summer to fall sampling events. The summer samples are all clustered closely around the isotopic composition of the Pingo Spring while in the autumn the piezometer samples show distinct isotopic signatures with variation greater than the analytical error (Figure 4-44b). For the fall samples there is a trend of enrichment in oxygen-18 and deuterium with depth. A potential explanation is that in the summer there is an upward gradient that causes mixing and all the piezometers plot close together. In the fall the upward gradient forced by the ice sheet is cut off when melting ceases. The more enriched water may then be entering the system laterally from the other lakes, some of which are at a higher elevation than the Pingo Spring,

Table 4-13. Gas analysis results from the Pingo Spring in 2009.

	% Oxygen	% Nitrogen	%CO ₂	% Methane	Total %
Pingo 2008	10.96	85.52	0.36	ND	96.83
Pingo 2009 (average)	1.26	92.29	0.92	0.11	94.59

ND= no data

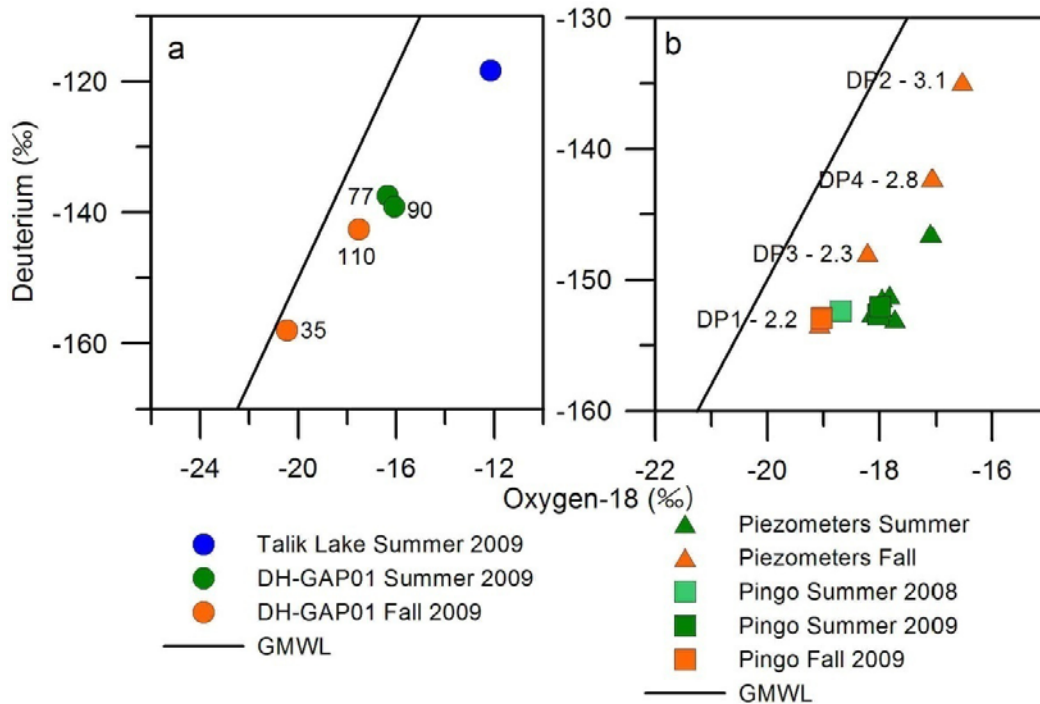


Figure 4-44. (a) Evolution of talik waters from summer to fall sampling with corresponding concentrations of sodium fluorescein tracer concentration ($\mu\text{g/L}$). (b) Pingo Spring and Pingo piezometers from summer to fall sampling. Depths of piezometers (m) are labelled for fall sampling event.

or from storage in the till plain sands. These waters would be isotopically enriched due to evaporation. If this was the case then the shallower piezometers would have a signature closer to that of the pingo pond and the deeper piezometers the more enriched isotopic signature of the lakes and/or sands. Continued monitoring of the spring and the addition of more precise age dating tools for the pingo water (e.g. CFCs, $^3\text{H/He}$, ^{14}C , ^{129}I and ^{36}Cl) will help further understanding of this system.

4.8 Concluding remarks and the plans for 2010

Based on the outcome of the 2009 field season the following conclusions can be drawn:

- Diamond drilling in permafrost applying only hot water for flushing without any added antifreeze chemicals is technically feasible. To gain sufficient time for down hole investigations the temperature of the flushing water should be heated to 60°C . The experience from 2009 showed that in felsic bedrock the drilling of 67 hours with 40°C water keeps the borehole unfrozen for 24 hours after drilling stops.
- The U-tube type sampler, where the water sample is purged using N_2 head seems to be a good approach. Elastic PA or comparable plastic instead of steel tubing should be applied for the deployment string to minimize the irregular bending of the string. Preferentially the string length should be such that it is possible to operate from a spool of transportable size. Power requirement and the capacity of the heating cable to melt ice from the sampling tubes have not been tested in practice. However, the heating/cooling tests conducted in DH-GAP01 demonstrate that it is possible to increase the borehole temperature rather quickly by using a 7 kW generator.
- The resolution of the down hole P/T/EC sensors applicable for boreholes up to several hundreds of metres deep is good. The internal data logger provides recording opportunities for extended time periods. The system can be further developed to operate via a radio link, which would allow data retrieval without field trips. However, there is always durability problems as the failure in DH-GAP03 showed. Unfortunately, no obvious reason for the malfunction has been found. The durability versus resolution becomes an issue when deeper boreholes are considered.

- Geologically the bedrock seems to be comparable to the metamorphic sites in Scandinavia. Fracture frequencies and fracture patterns are analogous also in vertical cross-section. No obvious features possibly attributed to freezing/thawing or to the oscillation of ice margin have been identified so far. Special attention should be paid to the identification of lineaments, since they can cause severe difficulties for the drilling. Fracture infillings in the drill cores are relatively scarce. However, the preliminary mineralogical investigations showed that there is some complexity in the fluid history *e.g.* indications of redox fronts and different mineral generations reflecting different formation conditions.
- The adopted DTS method for temperature profiling is ideal for the permafrost investigations. However, the good quality of acquired data requires experience in field measurements and in data processing. Also independent temperature references are necessary for the calibration. The reference can be achieved by additional temperature probes or by applying a section of the DTS cable under known temperature conditions (*e.g.* ice bath).
- Permafrost at the ice margin is thicker than was assumed based on the literature data. The shape of the temperature profile in DH-GAP03 shows that the lowest bedrock temperatures, slightly below -3°C , are actually observed around the depth of 100 m. This implies that the climate has been cooler than present in the past when the growth of permafrost has been in active phase. It is obvious that shallow monitoring boreholes (< 100 m) will underestimate the permafrost depth. It should be noted that the collected information to date does not give much grounds for evaluating the permafrost conditions beneath the ice sheet.
- The drilling and combined DTS monitoring confirmed the existence of a talik beneath the investigated lake. The water basin is 1,200 m long, 300–400 m wide and up to 40 m deep. The bedrock temperature at 140 m of vertical depth is 1.26°C and the transition from frozen to unfrozen ground is located at the shoreline of the lake. Geothermal modelling supports the idea that the investigated lake is a through talik penetrating the whole section of 330 m of frozen ground. There are numerous other lakes in the area, which are likely to support taliks as well.
- Groundwater samplings from the talik borehole indicate that there is a water reservoir chemically distinct from surface waters. So far the hydraulic monitoring of the sampling interval has not given indications of elevated pressures or other signs of vertical flow along the talik. Nor have studies on lineament-related surface waters given clear evidence of discharging melt or groundwaters. The only exception is the Pingo Spring at the foreground of the Leverett glacier. The system is related to a major fault, which provides conduits through the frozen ground. Like the talik water, the pingo water is chemically evolved and there is also significant amount of gas. Tritium was non-detected in samples taken from the drive-point piezometers demonstrating a limited role of present meteoric waters.

Plans for 2010

The research work in 2010 will be broadly divided in two categories: a) continuation of the investigations with the pilot drill holes and at the Leverett site, and b) preparations for the deep bedrock drillings in 2011.

a) Two field trips will be conducted in 2010. The first one will take place in early May aiming to retrieve data and water/gas sampling representing winter conditions and restricted melting of the ice sheet. Physico-chemical data recorded by the Aqua TROLL in DH-GAP01, as well as, the temperature and pressure data from the drill hole weather stations will be collected. The temperature profiles in the talik hole DH-GAP01 and in the permafrost hole DH-GAP03 will be measured. Some temperature profiling will be carried out in the Talik Lake. New data will be used to update the geothermal model describing the talik situation.

The second field trip will be scheduled for the first week of September. The sampling and consequent analytical program depends on the outcome of the first sampling in May. As a combination of these two campaigns a full characterization of the talik water in DH-GAP01 will be obtained. The drive-point piezometers at the Leverett moraine field will be monitored and sampled. Possibly, the pressure and temperature stations at DH-GAP01 and 03 will be supplemented with ground temperature sensors.

b) In order to start the detailed planning of the deep drill hole(s) the specific aims of the drilling needs to be decided. As soon as a reasonable level of planning is achieved, the tender documentation will be produced and invitations should be sent to potential drilling contractors preferentially during the fall 2010. The next step is to start the design of the down hole sampling and monitoring instrumentation. This task will be managed and implemented by Posiva and SKB and their consultants.

4.9 Supporting modelling: Regional groundwater flow model

Within the framework of the GAP project, a regional groundwater flow model under ice sheet conditions was developed by /Jaquet et al. 2010/. This chapter summarizes the aim and outcome of the flow modelling. The model created by /Jaquet et al. 2010/ integrates the currently available data and information related to topography, ice thickness, talik location and ice margin position as well as analogue data for boundary conditions, hydraulic parameters, permafrost distribution and deformation zones derived from previous studies. Figure 4-45 illustrates the conceptual model of the groundwater flow system. Figure 4-46 shows the location of the modelled domain, where the longest dimension of the model extends about 200 km on the ice sheet and ca. 50 km downstream of the ice margin. Since most of the data are not yet available, some scoping calculations are performed using the program DarcyTools in order to evaluate the current conceptual model for groundwater flow under ice sheet conditions, as well as to provide some guidance to the field investigations.

For this first modelling phase, coupled processes are not considered for the modelling of the groundwater flow system under ice sheet conditions; e.g. density driven flow, thermal and geomechanical effects as well as coupling with a dynamical ice sheet model are not considered, but may be investigated in the following phases.

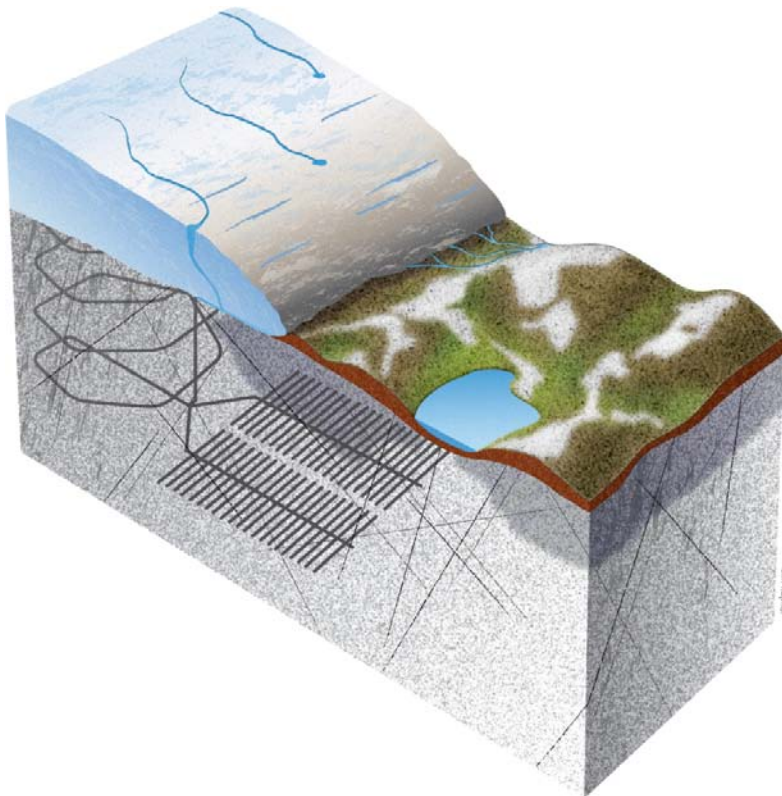


Figure 4-45. Conceptual model for the groundwater flow system under ice sheet conditions, with talik and permafrost (in dark grey). Illustration, Jan Rojmar.

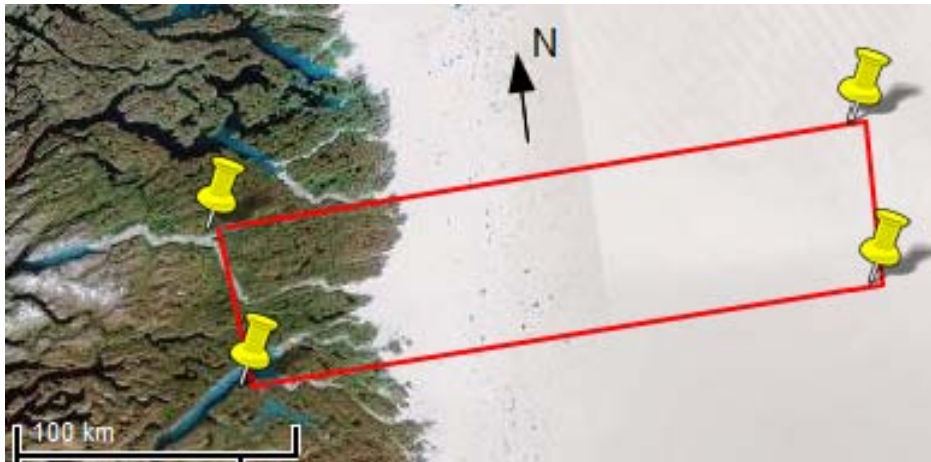


Figure 4-46. Location of the model domain (red rectangle) with a domain surface of about $250 \times 60 \text{ km}^2$.

Conceptually, the groundwater flow system is considered to be governed by infiltration of glacial melt water in heterogeneous faulted crystalline rocks in the presence of permafrost and taliks. The geological medium with conductive deformation zones was modelled as a 3D continuum with five hydrogeological units whose hydraulic properties were described using a stochastic simulation method. Based on glaciological concepts, a stochastic model was proposed for describing the sub glacial permafrost distribution in correlation with bed elevation. Numerical modelling of groundwater flow was performed at regional scale under steady state conditions for various sensitivity cases that included variations in boundary conditions and permafrost distribution.

These scoping calculations constitute a first step towards data integration and groundwater flow system understanding under realistic ice sheet conditions in Greenland. It may serve as a well founded base for future modelling issues, providing solutions to further questions.

The modelling results of the sensitivity analysis demonstrate the importance of the following factors with major impacts on the groundwater flow system:

a. Ice-bedrock boundary conditions

The boundary conditions at the ice-bedrock interface govern the groundwater flow system. Due to lack of knowledge, large uncertainty remains for these boundary conditions. The pressure variability likely to occur within the ice sheet needs to be investigated; the foreseen borehole campaign within the GAP project will provide new data that should enable to reduce the uncertainty related to these boundary conditions.

b. Permafrost distribution

For the land outside of the ice sheet, permafrost was distributed everywhere with a constant thickness, except a talik location. For the sub glacial permafrost, a middle way scenario was selected between all melting and all frozen conditions. Due to its low hydraulic conductivity, permafrost distribution has a major influence on groundwater flow patterns; in particular, it affects travel time and penetration depth of glacial melt water. The spatial variability of permafrost in 3 dimensions requires further assessments.

c. Taliks

Only three taliks were considered for the modelling; their role is of prime importance, as the taliks represent the only discharge zones located West of the ice margin. Therefore, all potential taliks will need to be considered by further investigations for the studied domain.

d. Deformation zones

For the deformation zone, a simple generic model was applied due to the small amount of data available. The deformation zones, presenting higher hydraulic conductivities than the surrounding rock domain, are likely to constitute preferential flow paths towards the surface. Their geometrical and hydraulic parameters are associated with significant uncertainties. The characterisation of the deformation zones requires the development of a model that integrates local knowledge and all data. Such a model will improve the description of the hydraulic conductivity field; especially in terms of deformation zone connectivity.

e. Topography

The bed elevation under the ice sheet as well as the (surface) elevation west of the ice margin, control surface boundary conditions. The applied ice DEM is of coarse resolution (5 km); the availability of new topographic data would improve surface description and lead to improvements in the characterisation of groundwater flow patterns.

Based on these preliminary results it is suggested that the deep borehole to be drilled close to the ice margin by SPC in 2011 should aim at reaching a depth close to 1,000 m in order to reach hydraulic conditions that are governed by the ice lying above. Pressure measurements and tracer tests will allow improved understanding of prevailing flow conditions required for numerical modelling. In addition, important data related to permafrost conditions and hydraulic parameter variability will be obtained in terms of depth. And, if deformation zones were to be intersected, crucial information could be delivered with respect to water origin; i.e. geochemistry of melt water versus groundwater. Regarding the boreholes drilled through the ice in SPB, they should provide data at regional scale of pressure variability at the ice-bedrock interface. If possible, these boreholes should be positioned along directions approximately parallel and perpendicular to the main ice flow direction in order to capture regional gradients.

Regarding future modelling work, the following topics are relevant with respect to performance assessment issues:

- 1. GAP deformation zone model.* This model is needed for improving the characterisation of heterogeneity in relation to the hydraulic parameters. The parts that would benefit most from additional deformation zone data are located: (a) in front of the ice margin (e.g. talik zones), (b) in the vicinity of ice margin and (c) under the ice sheet, downstream of the ELA. For assessment issues, it would be mostly valuable to obtain deformation zone data, at major locations in terms of inflow and outflow in relation to the groundwater flow system under ice sheet conditions.
- 2. Integration of new GAP data:* (a) DEM and geophysical data for bed elevation and ice thickness, (b) borehole data for improving boundary conditions; i.e. using pressure data measured at depth and at the ice-rock interface, and (c) location and extension of all potential taliks situated West of the ice margin.
- 3. Permafrost characterisation.* The permafrost characterisation in terms of extent and depth variability needs to be improved; i.e. by integration of actual measurements carried out within the GAP project and the latest modelling results of permafrost taken from /Vidstrand et al. 2010/. In addition, the availability of topographic data at higher resolution will allow including anisotropic effects likely to occur in the spatial variability of sub glacial permafrost.
- 4. Transient boundary conditions.* The use of results provided by a dynamic ice sheet model will enable the integration of transient melt water rates as input for the groundwater flow model. The applied temporal resolution is likely to be at a yearly level, under the assumption of acceptable run-times for ice sheet modelling.
- 5. Water geochemistry.* The development of a transport model in presence of glacial effects will allow the characterisation of the space-time distribution of melt water and groundwater at repository depth.

5 Summary

The preliminary results of the investigations carried out within the GAP project during 2009 have been described in this report. All three GAP sub-projects have been active both in and out of the field. Since 2009 is the first official GAP year, major parts of the activities have involved preparatory work, testing of equipment, reconnaissance work, establishment of monitoring networks in the field and preliminary data processing. A summary of the activities carried out in the GAP during 2009 are presented below. In addition to the fieldwork activities, regional groundwater flow modelling under ice sheet conditions has been carried out.

5.1 Sub-project A activities

Three field campaigns were carried out in SPA during 2009. These campaigns focused on: 1) deployment and maintenance of AWS and GPS stations and to test the deep-look radar equipment; 2) investigating the hydrological processes and feedbacks and testing of passive seismic equipment; 3) downloading of weather station data and GPS data and winterizing the equipment. An extensive archive of real-time satellite remote sensing datasets has been obtained to be able to better constraint the surface elevation and dynamics of basal hydrological mechanisms. From this archive it has been possible to obtain Russell Glacier Catchment (RGC)-wide constraints on annual, seasonal and specific temporal snapshots of surface speed, initial lake and moulin distribution, drainage and network connections along with the temporal-development and drainage characteristics of supraglacial lakes.

The GAP project and SPA has placed three AWS stations east of Kangerlussuaq in the melt zone in an east-west section. These stations complement the weather station transect monitored by the IMAU group in the Netherlands. As a result, the Kangerlussuaq part of the Greenland Ice Sheet has the highest density of weather stations, which allow high detailed temporal surface mass budget variability studies. The three weather stations have performed well since the installation and have provided 100% temporal data coverage. Future AWS work includes mass budget modelling, which is necessary to calculate the surface melt water production, and maintenance of the weather station network.

SPA manages a GPS network covering the RGC including 14 GPS stations including a base station situated in front of the Russell Glacier. The majority of these stations have been running since 2007. Since the installation of these stations, power and memory capacity problems have led to some data acquisition interruptions. During 2010 these problems will be addressed through station upgrading and power management regulation. Data processing of the GPS velocity data indicates that velocity increases tend to coincide with the timing of the peak melt. Future work will involve data processing and revamping of the RGC GPS network. During fieldwork 2010, a temporary network will be installed over the summer to support the hot water ice drilling carried out by SPB and the Ice2Sea project.

In order to obtain ice thickness information to be able to identify englacial hydrological features and characterize the basal hydrological conditions, the deep-look radar system was tested in the field during 2009. Besides obtaining data, the trial field run was also carried out to test the mode of transport and safety. The results from the radar campaign indicate that the measured ice thicknesses range from ca 700 to 1,150 m, and that the thickness increases as expected. A lot of time was also spent to upgrade, improve and modify existing radar systems so that these can be deployed during the 2010 field campaigns. Future work in 2010 involves the deployment of three different radar systems including: 1) a low-frequency impulse radar system to be used for catchment-scale mapping of bed properties and bed elevation; 2) a continuously logging radio-echo sounding system to be used for studying the temporal evolution of basal hydrology; and 3) an FMCW radar system for detailed high resolution studies around supraglacial lakes and moulins.

In 2010 SPA and the Swansea University plan to carry out passive and active seismic investigations in order to identify and characterize: 1) englacial hydraulic processes; 2) sub glacial hydraulic transients; 3) basal motion triggered by the ingress of surface meltwaters to the glacier bed; and 4) deeper seismic activity related to tectonic processes in the geosphere. The obtained data will form important support for numerical models on ice sheet hydrology and the rheological controls on melt water routing. The aim with the seismic fieldwork during 2009 was to test the equipment and different installation approaches to allow for optimal preparations for the 2010 field season. An extensive data set was obtained from the test experiments and this has yet to be analyzed. However, the preliminary results indicate that passive seismic data has the potential to reflect the coupled hydrological-mechanical mechanisms that are targeted in this study.

Dye and tracer studies carried out in the RGC at distances from 2 to 23 km up on the ice margin reveals routed and pressurized englacial and sub glacial conduits. Further work is needed to constrain the hydrological flow paths for melt water draining in this area.

5.2 Sub-project B activities

SPB aims at making in situ measurements of the sub glacial hydrological conditions of the Greenland Ice Sheet and to conduct numerical modelling experiments focused on ice-sheet and basal conditions. SPB has focused on preparing for the hot water ice drilling that will commence in 2010. For this purpose a field reconnaissance of the ice drilling sites was carried out in the spring of 2009, during which ice penetrating radar data was also collected. Measured ice depths range from 100 to 190 metres and the ice depth generally displayed an increase with distance from the margin. However, it was demonstrated that the basal topography displays amplitude variations, which may have some implication on the bottom depth of the bedrock borehole that SPC will drill during 2011. SPB aims at drilling as close as possible to the ice margin during 2010 so that the ice boreholes intersect the bed above the bedrock borehole to be drilled by SPC in 2011. From the radar campaign carried out by SPB in May, 2009, it is suggested that the ice is wet based in the area of planned ice drilling. During the reconnaissance SPB also discovered that due to the ice surface topography in the near margin area the ice drilling operations will be slow.

SPB has acquired all available radar data from CReSIS airborne radar, but the coverage of Isunnguata Sermia is scarce. However, the data suggest that a deep trough exists in the area where 2010 ice drilling is planned. SPB has also discussed with the NASA IceBridge project to fly over the GAP area of interest during 2010, where both radar and surface laser measurements will be carried out.

Substantial time was been spent modifying Dr. Harper's and Dr. Humphrey's Alaskan ice drill rig to be able to operate in the Greenlandian ice conditions. Besides the ice drill modifications, a number of mechanical devices had to be constructed. All the primary and secondary down hole sensors were also developed and tested. Moreover, substantial effort has been put into the logistical planning of the ice drilling operations.

Some published modelling studies suggest that the centre of the Greenland Ice Sheet is cold-based whereas the margin is warm-based, other modelling work suggests that the entire ice sheet is at the pressure melting point at the bed. However, field results from ice drilling (i.e. GRIP and GISP) show that the bed is partly frozen. SPB has started a modelling project with the aim of clarifying this issue and to investigate the basal thermal conditions in more detail within the Greenland Ice Sheet study area. SPB has also completed 3D geometry and flow field ice sheet scale models of the Greenland Ice Sheet and collected multiple data sets to be able to constrain boundary conditions.

5.3 Sub-project C activities

The main aim of the SPC during 2009 was to collect a suite of information supporting the planning of the deep drilling to be carried out in 2011 including groundwater information.

SPC drilled two cored boreholes with hot water drilling in 2009 with the aim of: 1) obtaining knowledge about the permafrost conditions close to the ice margin; 2) demonstrating the presence of a talik under a lake; 3) collecting core material for geological and fracture studies; and 4) providing groundwater sampling and hydraulic testing opportunities.

The “talik borehole” (DH-GAP01) measured 191 metres vertical and the “permafrost hole” (DH-GAP03) measured 320 m vertical. The talik borehole was instrumented with a U-tube system and a DTS-cable which allowed for water sampling and P/T/EC monitoring. Due to problems with freezing of the borehole, the permafrost borehole was only equipped with a DTS-cable and a pressure/temperature/EC probe. Unfortunately the P/T/EC probe in the latter hole failed and the only working equipment in DH-GAP03 is the DTS-cable. Results from the down hole probes suggest that the “talik” borehole water is significantly different compared to the lake water, which was used as drilling fluid. Moreover, the results indicate that the borehole is recovering from drill water contamination and that formation water is entering the borehole. The analytical results of the groundwater samples from the talik borehole suggest that a chemically distinct reservoir exists under the Talik lake.

The DTS investigations enabled temperature profiling of the two boreholes. Steady state temperature profiles were obtained from both boreholes during the fall. These profiles confirm that the talik borehole penetrates a talik and that the permafrost borehole did not penetrate the permafrost but that the depth of permafrost at the DH-GAP03 site is close to 335 metres. In order to understand the thickness of the permafrost and to investigate the existence of taliks under lakes, the DTS temperature data was fed into a 2D numerical heat transfer model. From the modelling work it can be concluded that the permafrost in the field area is thick (more than 300 m) and that lakes with a diameter greater than 100 metres likely support taliks.

Logging of the two borehole cores reveal that the dominant rock types in the area are feldspar-rich gneisses interlayered with mafic-, amphibole-rich gneisses and pegmatites, suggesting that the bedrock appears comparable to the metamorphic sites in Scandinavia and Canada. Fracture mineralogical samples were collected from the cores and focus is being given to the measurement of Ca isotopes as these can contribute to interpreting the source waters of fracture minerals, which will aid the understanding of the hydrogeochemistry of the glacial system.

A pingo spring is located on the sediment plain next to the Leverett Glacier. This spring was instrumented with drive-point piezometers to allow for head monitoring and water sampling. The pingo system provides a conduit through the frozen ground and the analytical results suggest that the pingo water is chemically evolved.

During 2010 SPC will focus on continued investigations of the talik- and permafrost boreholes and prepare for the deep bedrock drilling in 2011. Detailed planning of the bedrock drilling involves outlining drilling targets and needs, tender invitations and designing of the down hole sampling and monitoring instrumentation.

6 References

SKB's (Svensk Kärnbränslehantering AB) publications can be found at www.skb.se/publications

- Aaltonen I, Douglas B, Frapé S, Henkemans E, Hobbs M, Klint K E, Lehtinen A, Claesson Liljedahl L, Lintinen P, Ruskeeniemi T, 2010.** The Greenland Analogue Project, Sub-Project C; 2008 Field and Data Report. Posiva Working report 2010-62. 136 p.
- Al-Assam II, Taylor B E, South S, 1990.** Stable isotope analysis of multiple carbonate samples using selective acid extraction. *Chemical Geology* 80: 119–125.
- Blyth A R, Frapé S, Ruskeeniemi T, Blomqvist R, 2004.** Origins, closed system formation and preservation of calcites in glaciated crystalline bedrock: evidence from the Palmottu natural analogue site, Finland. *Applied Geochemistry*, 19, 675–686.
- Blyth A R, Frapé S K, Tullborg, E L, 2009.** A review and comparison of fracture mineral investigations and their application to radioactive waste disposal. *Applied Geochemistry* 24(5): 821–835.
- Burn C R, 2002.** Tundra lakes and permafrost, Richards Island, western Arctic coast, Canada. *Canadian Journal of Earth Sciences*, 39, 1281–1298.
- Campbell T, 2007.** Aqua TROLL 200 Operator's Manual. In-Situ Inc., Fort Collins, USA, 1–89.
- Das S B, Joughin I, Behn M D, Howat I M, King M A, Lizarralde D, Bhatia M P, 2008.** Fracture propagation to the base of the Greenland Ice Sheet during supraglacial lake drainage. *Science* 320, 778–7819.
- Freifeld B M, Chan E, Onstott T C, Pratt L M, Johnson A, Stotler R, Holden B, Frapé S, Pfiffner S M, DiFurio S, Ruskeeniemi T, Neill I, 2008.** Deployment of a deep borehole observatory at the High Lake Project Site, Nunavut, Canada. In: *Proceedings of the Ninth International Conference on Permafrost*, University of Alaska, Fairbanks, June 29–July 3, 2008. Fairbanks: University of Alaska, 469–474.
- Freifeld B M, Trautz R C, Kharaka Y K, Phelps T J, Myer L R, Hovorka S D, Collins D J, 2005.** The U-tube: a novel system for acquiring borehole fluid samples from a deep geologic CO₂ sequestration experiment. *Journal of Geophysical Research*, v. 110, B10203, doi: 10.1029/2005JB003735.
- Gamlin J D, Clark J F, Woodside G, Herndon R, 2001.** Large-scale tracing of groundwater with sulphur hexafluoride. *J. Environmental Engineering* 121, 171–174.
- Greve R, 2005.** Relation of measured basal temperatures and the spatial distribution of the geothermal heat flux for the Greenland ice sheet. *Annals of Glaciology* 42, 424–432.
- Huybrechts P, 1996.** Basal temperature conditions of the Greenland ice sheet during the glacial cycles. *Annals of Glaciology*, 23, 226–236.
- Jaquet O, Namar R, Jansson P, 2010.** Groundwater flow modelling under ice sheet conditions: scoping calculations. SKB R-10-46. Svensk Kärnbränslehantering AB.
- Kern-Hansen C, 1990.** Data basis for permafrost studies in Greenland. In *Proceedings of Polartec'90*, 635–644.
- King M, 2004.** Instruments and Methods: Rigorous GPS data-processing strategies for glaciological applications. *Journal of Glaciology*, 50, 601–607.
- Leick A, 2004.** *GPS Satellite Surveying*, John Wiley and Sons Ltd, Hoboken, New Jersey, Third Edition.
- Macharet Y Y, Moskalevsky M V, Vasilenko E V, 1993.** Velocity of radio waves in glaciers as an indicator of their hydrothermal state, structure and regime, *Journal of Glaciology*, 39, (132), 373–384.

- Mackay J R, 1992.** Lake stability in an ice-rich permafrost environment: examples from the western Arctic coast. *In* Aquatic ecosystems in semi-arid regions: implications for resource management (eds. R.D. Robarts and M.L. Bothwell). National Hydrology Research Institute, Environment Canada, Saskatoon. Symposium Series 7, 1–26.
- Makahnouk W R M, 2004.** Factors that influence and affect the solubility of the iron end-members of Columbite and Tantalite phases in granitic melts. Unpubl. B.Sc. Thesis, Univ. Waterloo, Ontario, Canada.
- Nienow P W, Hubbard A, Hubbard B, Chandler D M, Mair D W F, Sharp M J, Willis I C, 2005.** Hydrological controls on diurnal ice flow variability in valley glaciers. *Journal of Geophysical Research* 110, F04002, doi:10.1029/2003JF000112.
- Roedder E, 1984.** Reviews in Mineralogy, Fluid Inclusions. Mineralogical Society of America, Vol. 12.
- Rutt I C, Hagdorn M, Hulton N R J, Payne A J, 2009.** The Glimmer community ice sheet model, *J. of Geophysical Research*, VOL. 114, F02004, doi:10.1029/2008JF001015.
- Scholz H, Baumann M, 1997.** An ‘open system pingo’ near Kangerlussuaq (Søndre Stromfjord), West Greenland. *Geology of Greenland Survey Bulletin* 176: 104–108.
- Seaberg S Z, Seaberg J Z, Hooke R, Le B, Wiberg D W, 1988.** Character of the englacial and subglacial drainage system in the lower part of the ablation area of Storglaciären, Sweden, as revealed by dye-trace studies. *Journal of Glaciology*, 34 (117), 217–227.
- Shepherd A, Hubbard A, Nienow P, King M, McMillan M, Joughin I, 2009.** Greenland Ice Sheet motion coupled with daily melting in late summer. *Geophysical Research Letters* 36, doi:10.1029/2008GL035758.
- Stotler R L, Frappe S K, Ruskeeniemä T, Ahonen L, Paananen M, Hobbs M Y, Lambie K E, Zhang M, 2009.** Hydrogeochemistry of groundwaters at and below the base of the permafrost at Lupin: report of phase III. NWMO TR-2009-10. Toronto: Nuclear Waste Management Organization. 76 p.
- Stuart G, Murray T, Brisbourne A, Styles P, Toon S, 2005.** Seismic emissions from a surging glacier: Bakaninbreen, Svalbard, *Annals of Glaciology*, 42, 151–157.
- Stumm W, and Morgan J J, 1996.** *Aquatic Chemistry*. New York: John Wiley & Sons, Inc., Third Edition. 1040 p.
- van Tatenhove F G M, Olesen O B, 1994.** Ground temperature and related permafrost characteristics in West Greenland. *Permafrost and Periglacial Processes*, 5, 199–215.
- Vidstrand P, Follin S, Zügel N, 2010.** Groundwater flow modelling of the permafrost and glacial periods-SR-site Forsmark, R-09-21.
- Wadham J L, and 13 others (in review).** Observed rapid melt water drainage via channels beneath the Greenland Ice Sheet, *Science*.
- Wal Van de R S W, Gruell W, Van den Broeke M R, Reijmer C H, Oerlemans J, 2008.** Large and rapid melt-induced velocity changes in the ablation zone of the Greenland Ice Sheet. *Science* 321, 111–113.
- Wanninkhof R, Ledwell J R, Watson A J, 1991.** Analysis of sulphur hexafluoride in seawater. *JGR*. 96(C5), 8733–8740.
- Watson A J, Ledwell J R, Webb DJ, Wunsch C, 1988.** Purposefully released tracers. *Phil. Trans. Roy. Soc. A*. 325, 189–200.